UPPSALA
UNIVERSITET

IT Licentiate theses
2023-001

Modeling and Estimation of Impulsive Biomedical Systems

HÅKAN RUNVIK

UPPSALA UNIVERSITY
Department of Information Technology

UPPSALA
UNIVERSITET

Modeling and Estimation of Impulsive Biomedical Systems

Håkan Runvik
hakan.runvik@it.uu.se

June 2023

Division of Systems and Control
Department of Information Technology
Uppsala University
Box 337
SE-751 05 Uppsala
Sweden

http://www.it.uu.se/

Dissertation for the degree of Licentiate of Philosophy in Electrical Engineering with specialization in Automatic Control

ISSN 1404-5117
Printed by the Department of Information Technology, Uppsala University, Sweden

Abstract

Dynamical systems are often expressed in either continuous or discrete time. Some biomedical processes are however more suitably modeled as impulsive systems, which combine continuous dynamics with abrupt changes of the state of the system. This thesis concerns two such systems: the pharmacokinetics of the anti-Parkinson's drug levodopa, and the testosterone regulation in the human male. Despite the differences between these systems, they can be modeled in similar ways. Modeling entails not only the model, but also the methods used to estimate its parameters. Impulsive dynamics can enable simpler representations compared with using continuous dynamics alone, but may also complicate the estimation procedure, since standard techniques often cannot be used. The contributions of this thesis are therefore both in model development and parameter estimation.

Model development is the topic of Paper I. It presents a model of the multi-peaking phenomenon in levodopa pharmacokinetics, which is manifested by secondary concentration peaks in the blood concentration profile of the drug. The remaining papers focus on estimation, in a setup where a sequence of impulses is fed to a linear plant, whose output is measured. Two estimation techniques are considered. The first is presented in Paper II and uses a Laguerre domain representation to estimate the timing and weights of the impulses. The second combines estimation of the impulsive input with estimation of the plant parameters, which represent the elimination rates of testosterone-regulating hormones. This problem is particularly challenging since increasing the estimated elimination rates and the number of impulses generally improves the model fit, but only models with sparse input signals are practically useful. Paper III addresses this issue through a novel regularization method. The uncertainties in model and measurements encountered when working with clinical hormone data add another layer of complexity to the problem; methods for handling such issues are described in Paper IV.

Acknowledgments

I am grateful to many people who have supported the writing of this thesis, helped expanding my knowledge of mathematics and biology, and made my time at the division a memorable experience. Thanks to my supervisor Alexander Medvedev for help and guidance, to my co-supervisor Maria Kjellsson for fruitful discussions about pharmacokinetics and biology and research in general, and to all colleagues at SysCon. Finally, tak Marie.

This research is financially supported by the Swedish Research Council under the grant 2019-04451 and the PhD program at the Centre for Interdisciplinary Mathematics at Uppsala University.

List of Papers

This thesis is based on the following papers:

I H. Runvik, A. Medvedev and M. Kjellsson. "Impulsive feedback modeling of levodopa pharmacokinetics subject to intermittently interrupted gastric emptying". In: *2020 American Control Conference (ACC)*. Online, 2020.

II H. Runvik, and A. Medvedev. "Laguerre domain estimation of an input impulse train to a continuous linear time-invariant system". In *59th IEEE Conference on Decision and Control (CDC)*. Online, 2020.

III H. Runvik and A. Medvedev. "Input sequence and parameter estimation in impulsive biomedical models". In *2022 European Control Conference (ECC)*. London, 2022.

IV H. Runvik and A. Medvedev. "Robust one-step estimation of impulsive time series". *arXiv preprint, arXiv:2304.13394*. 2023.

Contents

1 Introduction **3**
- 1.1 Mathematical modeling . . . 3
  - 1.1.1 Hybrid systems . . . 4
- 1.2 Biomedical applications . . . 5
  - 1.2.1 Modeling approaches . . . 6
  - 1.2.2 Impulsive biomedical systems . . . 7
- 1.3 Outline . . . 8

2 Impulsive models of biomedical systems **11**
- 2.1 Hybrid systems . . . 11
  - 2.1.1 Impulsive systems . . . 12
- 2.2 Biomedical modeling . . . 12
  - 2.2.1 Goodwin's oscillator . . . 13
  - 2.2.2 The impulsive Goodwin's oscillator . . . 14
  - 2.2.3 Pharmacokinetic models . . . 15
  - 2.2.4 Endocrine modeling . . . 17

3 Identification and estimation of impulsive systems **19**
- 3.1 System identification . . . 19
  - 3.1.1 Evaluating candidate models . . . 20
  - 3.1.2 Model validation . . . 21
  - 3.1.3 Impulsive systems . . . 22
- 3.2 Parameter estimation . . . 22
  - 3.2.1 Least squares . . . 23
  - 3.2.2 Robust estimation . . . 24
- 3.3 Estimation of biomedical systems . . . 25
  - 3.3.1 Impulse train estimation . . . 25
  - 3.3.2 Impulsive time series estimation . . . 26

4 Conclusions **29**
- 4.1 Future work . . . 29

References **31**

Paper I **39**

Paper II **59**

Paper III **79**

Paper IV **97**

Chapter 1

Introduction

Most humans interact with a variety of systems on a daily basis, be it their phones, cars, houseplants, or even their own bodies. Whether man-made or naturally occurring, understanding such systems is crucial for many of the problems we are facing, both as individuals and as a society. In numerous branches of science, systems are described by models constructed with the tools of mathematics. Such mathematical models can serve various purposes. One common goal is to predict or control the behavior of a system without performing more experiments than necessary, which could be costly or dangerous. A car manufacturer, for example, may replace prototypes with fluid mechanical modeling; a medical doctor may determine drug doses from models of how a substance affects patients.

The focus of this thesis is mathematical models of two biomedical systems; one is describing how an anti-Parkinson's drug is distributed in the body, the other concerns the regulation of testosterone in men. These systems may seem quite different, but have one thing in common: both are well described by models containing both continuous dynamics and discrete impulses. To explain how these models work, and why we use them, an introduction to mathematical modeling is needed.

1.1 Mathematical modeling

Mathematical models are classified depending on various properties. The models in this thesis are dynamic, as opposed to static, which means that they describe the evolution of the state of a system over time. Other classifications include whether model variables are continuous or discrete, and whether the model is linear, which roughly means that the output scales well with the input. Models also fall on a spectrum depending on how they are derived. One extreme is first-principles modeling, where the model is based

directly on the laws of physics, the other is data-driven modeling, which is the basis of machine learning today. The terms white-, gray- and black-box models are also used to describe this spectrum.

Parametric models is a related concept. Such models are defined by a model structure and a finite number of parameters. In first-principles modeling, all parameters are essentially constants of nature, but more commonly, estimating some or all parameters from measured data is required when creating a parametric model. Non-parametric models, on the other hand, are characterized by the lack of a fixed model structure; they are instead inferred directly from data.

Dynamic models are normally expressed with either differential or difference equations, depending on whether time is considered a continuous or discrete variable. We use the letters p and q, respectively representing differentiation and time-shift, to mark this difference. Linear dynamical systems are particularly well understood, which is one reason why they are the focus of, e.g., introductory university courses in automatic control. Truly linear systems are rare in the real world, but the techniques described in the basic control courses are nonetheless applied in countless technical applications. This illustrates a general principle, where the choice of model depends both on the system itself, and the purpose of the modeling. A simple model will generally permit faster computations, and be easier to analyze and interpret than a complex one. It may therefore often be preferred, even if the complex model provides a more accurate description of the system.

1.1.1 Hybrid systems

Some systems include processes of vastly different time-scales. The injection or oral administration of a drug for example is a much faster process than the distribution and elimination of the drug in the body. Under such circumstances, the details of the fast process may be irrelevant for the overall behavior of the system, making it more useful to model such processes as discrete events. The resulting type of model, with both continuous and discrete dynamics, is called a hybrid system[1]. Such systems can be found all around us, as the following example illustrates.

Example 1.1. Consider pouring a glass of water. It can be modelled mathematically by an integrator as

$$y(t) = \int_0^t u(\tau)\ d\tau,$$

[1]Calling it a "hybrid model" would be more consistent with the presentation so far, however "hybrid system" is the established notation.

where $u(t)$ is the volumetric flow into the glass and $y(t)$ is the volume of water in the glass. The integrator is linear, since

$$\int_0^t cu(\tau)\ d\tau = c\int_0^t u(\tau)\ d\tau,$$
$$\int_0^t u_1(\tau)\ d\tau + \int_0^t u_2(\tau)\ d\tau = \int_0^t \big(u_1(\tau) + u_2(\tau)\big)\ d\tau.$$

These equations imply that if we double the water flow (letting $c = 2$), we get twice as much water in the glass, and if we pour water into two identical glasses separately, and then sum their contents, we get the same amount of water as if the combined flow was poured into one glass directly.

But the integrator is not always an accurate model of the glass of water. For example, if we keep pouring, the glass will at some point be full, after which adding more water will lead to overflow, while the volume of water in the glass remains constant. This sudden transition from one type of continuous dynamics to another indicates that the glass of water is a hybrid system. Note that this system is nonlinear; if we combine the contents of two glasses that are 60% full, the result is one glass that is 100% full, but not more. □

1.2 Biomedical applications

In this thesis, a specific class of hybrid systems where the discrete events are represented by impulses is used to model biomedical processes. Two applications are considered: the pharmacokinetics of the Parkinson's disease drug levodopa and the regulation of testosterone in the human male.

Parkinson's disease is characterized by the death of nerve cells in a region of the brain called the substantia nigra, which normally produces dopamine. The resulting dopamine deficiency leads to motor symptoms such as tremors and rigidity, which are the primary symptoms of the disease [20]. Levodopa is a precursor to dopamine which is administered to Parkinson's patients to increase the dopamine concentration in the brain, and thus reduce the Parkinsonian symptoms. Levodopa is used since it can cross the blood-brain barrier, whereas dopamine cannot, which enables oral administration of the drug [27]. However, since levodopa also can inhibit gastric emptying [40], this gives rise to a feedback loop which is the believed cause of secondary peaks in the levodopa concentration in the blood following administration.

The testosterone regulation involves the three hormones gonadotropin releasing hormone (GnRH), luteinizing hormone (LH) and testosterone (Te). GnRH is released in pulses, which stimulates the secretion of LH, which in turn stimulates the release of Te [52]. Similarly to levodopa, blood samples

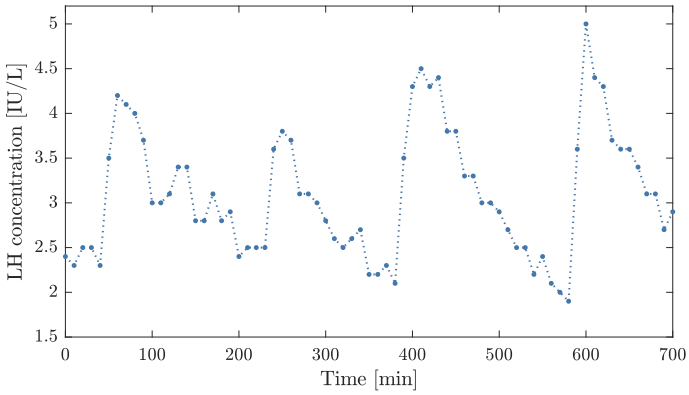

Figure 1.1: LH blood concentration sampled at 10-minute intervals from a healthy 41-year old male. Data from clinical experiments described in [28].

of LH will also display distinct peaks, when measured over time; an example concentration profile is shown in Figure 1.1.

Neither of these systems is fully understood, and they are furthermore affected by both external disturbances and internal interactions with other systems in the organism. Just one example is the circadian rhythm, which affects both the gastric emptying [17], and the testosterone level [53]. There are furthermore limitations on both the quality and the quantity of measured data.

1.2.1 Modeling approaches

When faced with complex and interconnected biomedical systems, different modeling choices can be made. The systems biology approach is to create the model by combining a large number of basic building blocks, such as models of individual cells, into networks. Such first-principles models have the benefit of a clear connection with the underlying biochemical mechanisms, but may be computationally demanding and, due to the variability inherent to these systems, hard to validate [23]. Another route, which is viable in data-rich applications, is to use machine learning to identify key features in the data, as is done with, e.g., ECG-measurements to classify cardiac arrhythmias [41]. A third alternative is to use simple models, which do not aim to describe the systems in all details, but rather capture their main dynamics.

An important question is how complex dynamic behaviors of the system are reconciled with the model. In the systems biology approach, such dynamics can form from the simple constituents of the model through emergence. In machine learning, complex behaviors can be reproduced thanks to

large and flexible models. However, even simple models can display complex dynamics, through two different routes.

The first is to incorporate stochasticity, i.e. randomness in the model. This is particularly motivated for processes where individual random events have a large impact on the overall behavior. Chemical reaction kinetics are for example often modeled with ordinary differential equations, which approximates the number of reactant species as a real number. However, if the number of species is low, this approximation is not valid, and a stochastic approach is more suitable [32].

The second concerns deterministic models; here the key to complex behavior is nonlinearity. Whereas linear differential equations can be solved analytically, and their behaviors therefore are well understood, the solutions to nonlinear dynamical systems can generally only be approximated through simulations. This makes the systems harder to predict and analyze, but also makes them more interesting mathematically. For some nonlinear systems, such as the famous Lorenz system [30], the solutions are highly sensitive to the initial conditions. Such systems are called chaotic[2], and have solutions that are completely unpredictable on a longer time-scale, even if the equations governing the system are known exactly. The Lorenz system was developed to represent atmospheric convection, but chaos can also occur in biological systems, for example, in the behavior of heart cells during cardiac arrhythmias [39].

1.2.2 Impulsive biomedical systems

Keeping the aforementioned system uncertainties and data limitations in mind, the models in this thesis are kept relatively simple; discrete impulses are combined with linear continuous and deterministic dynamics. However, this hybrid setup nonetheless results in complex behaviors and non-trivial estimation problems. An established model of this type is the impulsive Goodwin's oscillator [5], which is a closed-loop testosterone regulation model. The specified model class makes the models more white- than black-box, but the timing and weights of the impulses, as well as the parameters of the continuous part of the model, are generally unknown. An important topic in this thesis is how to determine these from concentration measurements such as those in Figure 1.1.

[2]Conditions regarding periodicity and topological mixing are also required for a proper mathematical characterization of chaos.

1.3 Outline

This thesis consists of two parts. Chapter 1–4 make up the first, which introduces concepts and provides background theory for the four papers, which are found in the second part. Chapter 2 contains descriptions of hybrid and impulsive systems in general, and of the particular impulsive biomedical models we use. Chapter 3 introduces the topics of system identification and estimation, and their application to impulsive systems. Finally, Chapter 4 presents conclusions and future research directions.

The following papers are included in the thesis:

Paper I: Impulsive feedback modeling of levodopa pharmacokinetics subject to intermittently interrupted gastric emptying

> H. Runvik, A. Medvedev and M. Kjellsson. "Impulsive feedback modeling of levodopa pharmacokinetics subject to intermittently interrupted gastric emptying". In: *2020 American Control Conference (ACC)*. Online, 2020.

Summary: In this paper we introduce a closed loop model aimed at explaining the multi-peaking phenomenon in levodopa pharmacokinetics using impulses. The resulting model is a version of the impulsive Goodwin's oscillator with several adaptions to suit this particular application.

Contribution: The idea originated from Alexander Medvedev, while I extended the setup to be suitable for the pharmacokinetic application. Both of us contributed to the technical work and the writing, with comments and feedback from Maria Kjellsson.

Paper II: Laguerre domain estimation of an input impulse train to a continuous linear time-invariant system

> H. Runvik, and A. Medvedev. "Laguerre domain estimation of an input impulse train to a continuous linear time-invariant system". In *59th IEEE Conference on Decision and Control (CDC)*. Online, 2020.

Summary: In this paper a method for estimating an input signal in the form of a sequence of impulses from the output of a linear plant is presented. The signals and the estimation problem are formulated with orthogonal basis functions, in an approach that generalizes previous work where the response of a single impulse was considered.

Contribution: The idea originated from Alexander Medvedev. I did the technical work and most of the writing, with significant mathematical guidance and support from Alexander.

Paper III: Input sequence and parameter estimation in impulsive biomedical models

> H. Runvik and A. Medvedev. "Input sequence and parameter estimation in impulsive biomedical models". In *2022 European Control Conference (ECC)*. London, 2022.

Summary: In this paper we introduce a new approach for estimating both the parameters and the impulsive input of a linear plant. The estimation is based on a parameter-dependent least squares formulation derived in a previous work, but the problem is treated more systematically here. The main contribution is a novel method for resolving the trade-off between input sparsity and fit to data.

Contribution: I came up with the idea of this paper, and I also did the technical work and the majority of the writing, with help from Alexander Medvedev.

Paper IV: Robust one-step estimation of impulsive time series

> H. Runvik and A. Medvedev. "Robust one-step estimation of impulsive time series". *arXiv preprint, arXiv:2304.13394*. 2023.

Summary: In this paper the algorithm from Paper III is refined and extended in two main directions. First, the assumptions and parameters required from the user are minimized. Second, the algorithm is adapted to work well with clinical hormone data, mainly through improved robustness against measurement errors.

Contribution: I came up with the idea of this paper, and I also did the technical work and the majority of the writing, with help from Alexander Medvedev.

The following papers are of relevance to this thesis, but not included:

> H. Runvik and A. Medvedev. "Impulsive time series modeling with application to luteinizing hormone data". In *Frontiers in Endocrinology*. Vol. 13. 2022.

> A. Proskurnikov, H. Runvik and A. Medvedev. "Cycles in impulsive Goodwin's oscillators of arbitrary order". *arXiv preprint, arXiv:2302.01364*. 2023.

Chapter 2

Impulsive models of biomedical systems

The models in this thesis have two things in common: they describe biomedical systems, and they combine continuous dynamics with discrete impulses, which means that they are instances of hybrid systems. This type of models, and the underlying biomedical systems, will be presented in this chapter.

2.1 Hybrid systems

Hybrid dynamical systems take many forms. They can represent mechanical phenomena, such as backlash or stick-slip friction. They can describe biological systems, such as the blinking of fireflies [34]. They may also be caused by discrete events that are engineered in otherwise continuous settings, such as switched control systems [35]. The diversity of hybrid phenomena makes it difficult to describe them in a unified framework. One general formulation of hybrid systems, introduced in [3], is

$$\begin{aligned} \dot{x}(t) &= F_{i(t)}(x(t), u(t)), \\ i(t) &= G(i(t^-), x(t^-), u(t)), \\ x(t) &= R(i(t^-), x(t^-), u(t^-)), \\ y(t) &= O(i(t), x(t), u(t)), \end{aligned} \tag{2.1}$$

where $t \in \mathbb{R}$ denotes time, $x(t) \in \mathbb{R}^n$ and $i(t) \in \{1, \ldots, N\}$ are the continuous and discrete states of the system, $u(t)$ and $y(t)$ are the input and output signals, each $F_{i(t)}$ is a smooth function, the map G defines the discrete state-transitions from $i(t^-)$ to $i(t)$, where $i(t^-)$ denotes left-sided limit, R is a reset map which causes jumps in the continuous states, and O is the output function. An alternative is to describe the system with constrained

differential and difference inclusions [8]. To examplify how hybrid systems are formulated, we return to the water-pouring example.

Example 2.1. Consider the model from Example 1.1, and let v denote the volume of the glass. This hybrid system can be expressed using (2.1) with

$$\begin{aligned} &F_1(x(t),u(t)) = u, && F_2(x(t),u(t)) = 0,\\ &G(1,x(t),u(t)) = \begin{cases} 2 & \text{if } x(t) = v \\ 1 & \text{otherwise} \end{cases}, && G(2,x(t),u(t)) = 2,\\ &R(i,x(t),u(t)) = x(t), && O(i(t),x(t),u(t)) = x(t), \end{aligned}$$

where the glass overflows when $i(t)$ transitions from 1 to 2. □

2.1.1 Impulsive systems

Impulsive systems are closely related to hybrid systems, and can, depending on the definitions that are used, also be seen as a subclass of hybrid systems. A common mathematical formulation of impulsive systems, given in, e.g., [14], is

$$\begin{aligned} &\dot{x}(t) = F(x(t)), \quad x(0) = x_0, && (x(t),t) \notin S,\\ &\Delta x(t) = I(x(t)), && (x(t),t) \in S, \end{aligned} \tag{2.2}$$

where F and I are continuous functions, and $S \subset [0,\infty) \times \mathbb{R}^n$ defines the resetting set. This class of systems is more restrictive than the hybrid systems, but there are also impulsive systems that cannot be written as (2.1) due to the explicit time dependence in (2.2). Only if the impulse times are intrinsic to the system, i.e., if they can be expressed as conditions of the form $x(t) \in S_x$, can an impuslive system be recast on the form (2.1). In biomedicine, the pharmacokinetics of a drug administered according to a fixed schedule is an example of externally determined impulse times, while the feedback of hormones can be modeled with intrinsic impulse times.

2.2 Biomedical modeling

Many biological systems have a set of features in common. First, they describe nonnegative quantities such as concentrations of substances or chemical energy. Second, these quantities tend to decrease towards an equilibrium, due to thermodynamic dissipation. Third, the dissipation is counteracted through a positive control mechanism, which keeps the state of the system within a normal range by replenishing the substances or energy levels. In control engineering, such feedback would typically be implemented with the goal of reaching a steady-state solution. However, examples

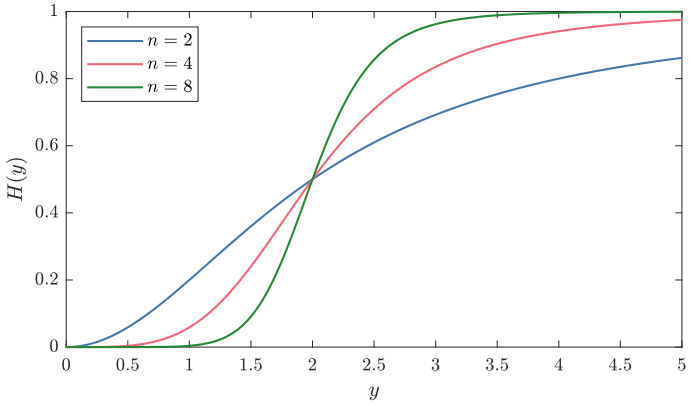

Figure 2.1: The Hill function with $K = 2$ and different values of the exponent n.

ranging from the macro-scale, such as the annual hibernation cycles of some animals, down to the metabolism, signaling and DNA synthesis of single cells [47, 36], show that oscillations are often the preferred feedback mechanism in nature.

2.2.1 Goodwin's oscillator

The Goodwin model or Goodwin oscillator was developed to describe enzyme regulation in bacteria and other cells [10, 11]. Its typical configuration consists of a third order linear continuous time plant composed of a chain of compartments, and a feedback law governed by a static, positive and bounded nonlinear function H. The model is formulated mathematically as

$$\begin{aligned}
\dot{x}_1(t) &= -b_1 x_1(t) + H(x_3(t)),\\
\dot{x}_2(t) &= -b_2 x_2(t) + g_1 x_1(t),\\
\dot{x}_3(t) &= -b_3 x_3(t) + g_2 x_2(t).
\end{aligned}$$

H is often represented by a sigmoidal Hill function of the form

$$H(y) = \frac{y^n}{K^n + y^n}$$

where the positive parameters K and n respectively determine the inflection point and the steepness of the curve (see Figure 2.1).

The Goodwin oscillator has precisely the features of positivity, dissipation and positive feedback signals described above. This has presumably contributed to its popularity as a core model for various biological systems

and as a prototypical example for theoretical investigations of biological oscillators [9]. However, to achieve oscillatory solutions, a steep nonlinear feedback is required; for the Hill function, the exponent n must be larger than 8 [12]. Such values of n are often seen as unrealistically large, at least when compared to the enzyme kinetics the original model represents. The continuous-time dynamics also make the Goodwin oscillator a less suitable model when processes with distinctly hybrid characteristics are considered. For example, the electrical behavior of neurons [19] and heart cells [13] are governed by impulses, which makes a hybrid, impulsive modeling paradigm more suitable.

2.2.2 The impulsive Goodwin's oscillator

The impulsive Goodwin's oscillator is a version of the Goodwin oscillator which was developed to capture the pulsatile nature of the feedback in endocrine systems [5]. The model contains a linear plant of the same type as the original model, but the input to the plant, rather than being a continuous signal, here consists of a train of instantaneous impulses, occurring at times τ_k with weights $d_k, k = 1, 2, \ldots$ These are determined through a feedback mechanism according to

$$d_k = F(y(\tau_k)), \quad \tau_{k+1} - \tau_k = \Phi(y(t_k)),$$

where F and Φ are bounded positive functions, which are assumed to respectively be non-increasing and non-decreasing, and are denoted the amplitude and frequency modulation functions. In analogy with the original formulation, these functions are often assumed to be Hill functions. The resulting model structure, which is illustrated in Figure 2.2, is an example of a pulse-modulated system.

It is perhaps not obvious how the impulsive Goodwin's oscillator fits into the model structures of hybrid and impulsive systems, given by (2.1) and (2.2). However, by introducing an auxillary state x_4, which is governed by

$$\dot{x}_4(t) = -1, \quad x_4(t) \neq 0; \quad \Delta x_4(t) = \Phi(y_t), \quad x_4(t) = 0,$$

and thus functions as a timer, the oscillator can be expressed in a form consistent with both (2.1) and (2.2).

In contrast with the continuous-time model, the impulsive Goodwin's oscillator has no fixed point; instead, periodic, quasiperiodic or chaotic solutions can occur. These rich nonlinear dynamics emerging from a simple model also makes it interesting from a mathematical perspective, apart from the biomedical applications. Previous work investigating properties of solutions to different versions the impulsive Goodwin's oscillator include

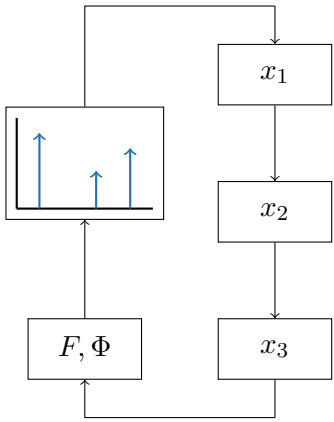

Figure 2.2: Schematic representation of the impulsive Goodwin's oscillator.

[55], which studies the effect of time delays, [46], which includes an additional feedback loop, and [33], which incorporates a circadian rhythm in the model.

2.2.3 Pharmacokinetic models

Biomedical models describing the uptake, transformations, distribution and elimination of drugs in the organism are developed in the field of pharmacokinetics (PK). Pharmacokinetic and pharmacodynamic (PD) models are often combined and denoted PK/PD models; the latter investigates the therapeutic and adverse effects of the drug on the organism. Linear compartmental models of a similar type as in the Goodwin oscillator are extensively used in compartmental PK analysis. The compartments can here represent blood, organs, or other tissues which the drug is distributed to. Impulsive input signals are also common, as the administration of bolus drug doses (both oral and through injection) conventionally are modeled as instantaneous events. Sequences of impulses, or closed-loop models, are less common in PK/PD models. However, since drugs are often administered periodically to reduce symptoms or keep a stable concentration of the active substance, it can be motivated to consider the closed-loop model. In some cases, intrinsic feedback loops can also occur.

Parkinson's and levodopa

Parkinson's disease is a common progressive neurodegenerative disorder. Both environmental and genetic factors increase the risk of developing Parkinson's disease, but its cause is still unknown. The disease is characterized

by the loss of dopaminergic neurons in the substantia nigra which leads to Parkinsonian motor symptoms, but other regions of the nervous system are also affected, and non-motor symptoms are also common [20].

Since no cure for Parkinson's disease is known, treatments are focused on symptom relief. The most efficacious drug for this purpose is levodopa, which normally is administered orally, absorbed in the small intestine, and transported via the blood into the brain, where it is converted to dopamine. The resulting increased dopamine concentration improves some, but not all Parkinsonian symptoms [27]. However, due to metabolism and dopamine conversion outside the central nervous system, the fraction of levodopa reaching the brain is small. By administering levodopa with benserazide or carbidopa, peripheral metabolism is inhibited, which leads to increased bioavailability and decreased plasma elimination of the drug [22].

The therapeutic regimen of levodopa is also complicated by several other pharmacokinetic features, such as proteins from ingested meals competing for the same facilitated transport across the intestinal mucosa and different factors affecting the gastric emptying [6]. The latter has in particular been associated with secondary peaks in the levodopa plasma concentration profile [40], where interference of the gastric emptying by dopamine results in an intrinsic feedback loop.

Pharmacokinetic modeling aims at finding models that are consistent with observed behaviors, but does not always aim to recreate the physiological mechanisms of the underlying system. For example, a double-peak concentration profile may be represented with parallel absorption compartments [7]. In contrast, Paper I models the interrupted gastric emptying with an impulsive feedback mechanism. The model structure, displayed in Figure 2.3, is similar to the impulsive Goodwin's oscillator, however an additional compartment representing the stomach is introduced to capture the total amount of the drug in the system being bounded. This modification leads to the introduction of a stable equilibrium of the system, in contrast with the original model. Comparisons against clinical data from [43] indicate that the model is feasible; however, it has two main weaknesses. First, the extension compared to the impulsive Goodwin's oscillator makes the model rather complex in relation to its descriptive power. Second, the impulsive model is not entirely consistent with the suspected cause of multi-peaking, i.e. intermittent interruptions of the gastric emptying. Sparse and large impulses in the flow through the pylorus are not supported by physiological evidence, while more frequent impulses would be averaged out on time scale of the sampled data, making it simpler to model the interruptions as reductions of an otherwise steady flow. Indeed, this has already been suggested in [37].

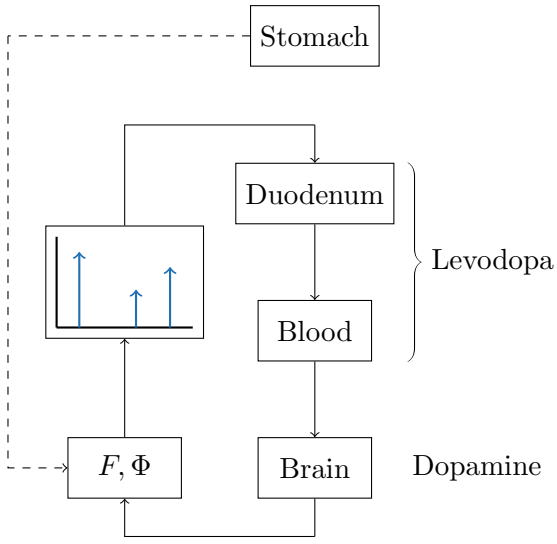

Figure 2.3: Levodopa pharmacokinetics model with feedback.

2.2.4 Endocrine modeling

The endocrine system transfers information between different parts of the body via hormones. This communication enables the regulation of the internal environment and behavior of the organism, and is therefore of critical for the normal functioning of the body. Hormones are produced in several glands and transported through the bloodstream to target cells, whose receptors interact with the hormone, resulting in modifications of the cell's function or activity [15]. Hormone activity is regulated through feedback loops, where one hormone can stimulate or inhibit the secretion of others.

Apart from being spatially distributed in the body, endocrine systems also operate over multiple time scales, which can range from tenths of seconds (e.g., the bursts of neurons) to weeks (e.g., the female ovarian cycle). As a consequence, the scope of mathematical models is often limited to specific modules or pathways in the system, and particular temporal resolutions [1].

The complexity of endocrine systems makes them challenging to model. An interdisciplinary approach is therefore recommended in [54], where the importance of the interaction between experiments and mathematical modeling is highlighted. A central topic is how to transition from high-resolution models, which accurately describe phenomena on the cellular level, to models representing the whole system. The heterogeneity of cells and the significance of this heterogeneity in their interactions make modeling strategies

based on combining large numbers of identical cell models unviable [26]. Instead, simple mathematical models can often provide valuable explanations for the complex behaviors of these systems [25, 26].

In this thesis, we consider models of entire hormone axes. Such models typically consist of a relatively low number of compartments, where hormone secretion, elimination and interaction are modeled by ordinary differential equations. The models may also include stochastic elements (see, e.g., [21]), but we will only consider deterministic formulations.

Testosterone regulation

One of the major endocrine systems in humans and other mammals is the hypothalamic-pituitary-gonadal (HPG) axis. It is primary involved in the development and regulation of reproductive systems, such as the menstrual cycle in females, but it also contributes to the regulation of other systems in the body, such as the immune system [42]. The HPG axis involves gonadotropin releasing hormone (GnRH), which is secreted from the hypothalamus gland, luteinizing hormone (LH) released from the pituitary gland, and either estrogen or testosterone (Te), respectively released from the ovaries and testes.

The endocrine models in this thesis primarily represent the male HPG axis, which also is the system the impulsive Goodwin's oscillator was designed to describe. The three states of this model thus represent the concentrations of these three hormones, and the impulsive feedback is used to capture the pulsatile nature of the secretion of GnRH, which is regulated by the testosterone concentration. This axis also includes features such as time-delays, circadian variations, and additional feedback-loops [50]. These are not included in the original impulsive Goodwin's oscillator, but corresponding modifications of the model have been investigated, as discussed in Section 2.2.2.

Since the GnRH concentration normally cannot be measured in peripheral blood, due to dilution and rapid metabolization [4], the pulsatile events can only be inferred indirectly from other hormone concentrations. How this is done mathematically will be presented in the next chapter.

Chapter 3

Identification and estimation of impulsive systems

We have so far presented a model type, and two biomedical systems it can be applied to. However, another ingredient required to build useful models is measured data, which connects the abstract model with the real world. The systematic use of data to build mathematical models is known as system identification. That is therefore the starting point of this chapter, where we explore how estimation and identification are applied to impulsive systems.

3.1 System identification

System identification is a data-driven driven approach to mathematical modeling of dynamical systems. The methods employed in this thesis differ from those traditionally used in this subject, described in, e.g., [29] or [45], but the conceptual approach of system identification is nonetheless useful to contextualize the problems we are considering.

A typical setup in system identification is depicted in Figure 3.1. It involves a system with measured inputs and outputs, that is subject to unmeasured disturbances. Discrete-time representations are used for both the system and the data which are denoted $u(n), y(n)$ for $n = 1, 2, \ldots, N$. Note that, since multiple inputs and outputs are possible, $u(n)$ and $y(n)$ may be vectors. Starting from such a system, the identification process involves four steps:

1. Design and conduct experiments on the system, and collect the data;

2. Choose a set of candidate models $\mathcal{M}$, also known as the model structure;

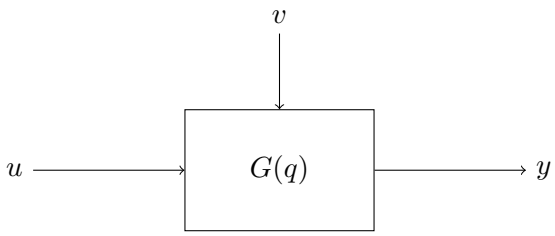

Figure 3.1: A discrete-time system $G(q)$ with input u and output y, subject to a disturbance v.

3. Use the data to select the most suitable model in $\mathcal{M}$, according to some fixed criterion;

4. Validate the model, i.e., test whether the selected model is good enough for its intended purpose.

Design of experiments and collection of data is not part of this thesis, and the chosen model structure was described in Chapter 2. The rest of this chapter will therefore focus on steps 3 and 4.

3.1.1 Evaluating candidate models

Selecting a model in $\mathcal{M}$ often means estimating the values of a set of parameters, defined by the model structure, so that the discrepancy between the output of the model, and the measured data is minimized. Common approaches to this problem include subspace methods, which identify state-space models, and methods aimed to minimize the prediction error of the model. We will use the latter to illustrate how system identification can work. The prediction of the model is its output at time n, given all measured data up to time $n-1$, and is written as

$$\hat{y}(n|\theta) = g(\theta, \mathcal{Z}^{n-1}),$$

where $\mathcal{Z}^n$ is the collected data

$$\mathcal{Z}^n = \{(y(1), u(1)), y(2), u(2)), \ldots, y(n), u(n))\},$$

and $g(\theta, \mathcal{Z}^{n-1})$ defines how the model output depend on these previous data and the parameter vector θ, which has dimension d and is assumed to belong to a set $\mathcal{D}_M \subseteq \mathbb{R}^d$. The goal of prediction error methods is to find the parameter estimate $\hat{\theta}$ that minimizes the criterion

$$V(\theta, \mathcal{Z}^N) = \frac{1}{N} \sum_{n=1}^{N} \ell(y(n) - \hat{y}(n|\theta)), \tag{3.1}$$

where ℓ is a scalar loss function, i.e.

$$\hat{\theta} = \arg\min_{\theta \in \mathcal{D}_M} V_N(\theta, \mathcal{Z}^t). \tag{3.2}$$

If the loss is chosen as

$$\ell(y(n) - \hat{y}(n|\theta) = \|y(n) - \hat{y}(n|\theta)\|_2^2,$$

where $\|\cdot\|_2$, is the Euclidean norm, we arrive at a least squares problem. This type of problems, and how to solve them, are described in Section 3.2.1.

3.1.2 Model validation

Model validation is often based on two criteria: fit to data and model simplicity. A more complex model will generally give a better fit, so there is a trade-off between these factors. A central question is whether the additional features incorporated by a more complex model are relevant to describe the system, or random disturbances in the particular set of data. By performing model validation on a data set that is separate from the estimation data, such overfitting can be detected. To prevent overfitting, regularization can be employed.

The idea of regularization is to penalize more complex models in optimization formulations such as the prediction error minimization (3.2). Model complexity is determined by the number of nonzero elements of $\hat{\theta}$, as zero elements effectively reduces the dimension of the parameter vector. LASSO (least absolute shrinkage and selection operator) is one common form of regularization, where a penalty on the 1-norm of θ is added in the minimization, so the criterion gets the form

$$V(\theta, \mathcal{Z}^N) = \frac{1}{N} \sum_{n=1}^{N} \ell(y(n) - \hat{y}(n|\theta)) + \lambda \|\theta\|,$$

where the positive parameter λ determines the degree of regularization. This free parameter can be viewed either as an advantage or a disadvantage of the method. It gives the user more control of the estimation results, but it also puts a burden on the user determine its value, and can introduce more subjectivity in the estimation.

Model selection

Model validation is closely related to the choice of $\mathcal{M}$; if the estimated model is not good enough, a different set of candidate models might be needed. To compare different model structures, statistical model selection

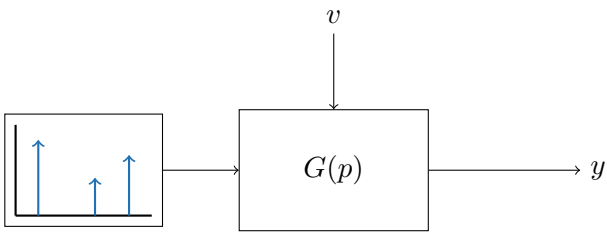

Figure 3.2: A continuous-time system $G(p)$ with impulsive input u and output y, subject to a disturbance v.

techniques can be used. They typically form a single criterion by combining the model fit with the number of parameters in the model, which enables the comparison of estimated models with different complexities. Different criteria, such as the Akaike and Bayesian information criteria have been proposed for this purpose; derivations and comparisons between these are provided in [44].

3.1.3 Impulsive systems

The impulsive system identification problems studied in this thesis are based on the open-loop setup displayed schematically in Figure 3.2. When compared with the typical system identification setup described above, two differences can be noted. First, the input signal cannot be measured, instead it is only assumed to be of a predefined class, namely a sequence of impulses. Second, although the measured data, i.e., the collection of blood samples, are in discrete time, the models are not. As a consequence, identification of these models requires other approaches than traditional system identification, but there are still similarities in the principles and underlying techniques. This identification setup also bears resemblance to time series analysis. There discrete-time signals are analyzed, often under the assumption that they are the output of a dynamic system, whose input signal is (unmeasured) white noise. The measured concentration profiles we consider, which are driven by impulses, may thus be called impulsive time series.

3.2 Parameter estimation

Parameter estimation is a central part of system identification, but statistical estimation is also a broad subject in its own right, with applications in many other areas of science and engineering. We present a few concepts from this subject here, which are of relevance for the subsequent section.

3.2.1 Least squares

In the view of statistical inference, the prediction error criterion function (3.1) is an instance of a class of estimators where a criterion function of the form

$$M(\theta) = \frac{1}{N}\sum_{n=1}^{N} m_\theta(X_n, Y_n), \tag{3.3}$$

is minimized [49, Ch. 5]. Here m_θ is a known function and $X_1, \dots X_n$ and $Y_1, \dots Y_n$ respectively are the independent and dependent variables of the problem. Such estimators are called M-estimators and also include the well-known least squares estimators, which are defined by

$$m_\theta(X_n, Y_n) = \|Y_n - f_\theta(X_n)\|_2^2,$$

where f_θ is called the model function. These estimators are attractive theoretically, through the connection with maximum likelihood estimators, and can also be efficiently computed.

Maximum likelihood

A common statistical approach to estimation is to model the observations as a sample of an unknown probability density function $p(Y;\theta)$, where

$$Y = \begin{bmatrix} Y_1^\mathsf{T} & Y_2^\mathsf{T} & \dots & Y_N^\mathsf{T} \end{bmatrix}.$$

In maximum likelihood estimation, the parameters maximizing the likelihood function $p(Y;\theta)$ are sought, however the problem is normally reformulated using the negative logarithm

$$\ell(\theta; Y) = -\log(p(Y;\theta)),$$

which results in the estimation formulation

$$\hat{\theta} = \operatorname*{arg\,min}_{\theta \in \mathcal{D}_M} \ell(\theta; Y).$$

If all estimation errors $\epsilon_n = Y_n - f_\theta(X_n)$ are assumed to have independent and identical probability density functions p_ϵ, the log-likelihood becomes

$$\ell(\theta; Y) = -\sum_{n=1}^{N} \log p_\epsilon(Y_n - f_\theta(X_n)),$$

and if p_ϵ is the Gaussian density function, the maximum likelihood and least squares estimates coincide. This connection provides an important theoretical justification for using the least squares criterion, but one should remember that the common assumption of Gaussian errors does not always hold.

Least squares solution

Least squares problems can be divided into two types. Linear least squares problems are characterized by f_θ depending linearly on the parameters θ, which results in m_θ in (3.3) being defined by

$$m_\theta(X_n, Y_n) = \|Y_n - \phi^\intercal(X_n)\theta\|_2^2,$$

where the vector $\phi(X_n)$ does not depend on θ. Such problems have the benefit that the solution can be explicitly calculated by the formula

$$\hat{\theta} = \Big(\sum_{n=1}^{N} \phi(X_n)\phi^\intercal(X_n)\Big)^{-1} \sum_{n=1}^{N} \phi(X_n)^\intercal Y_n,$$

provided that the matrix $\sum_{n=1}^{N} \phi(X_n)\phi^\intercal(X_n)$ is invertible.

If f_θ is nonlinear, iterative methods are usually required to obtain a solution. Starting from an initial guess $\hat{\theta}_0$, an update rule of the form

$$\hat{\theta}_{k+1} = \hat{\theta}_k + g_k,$$

is then repeatedly applied until convergence. One common choice for the function g_k is given by Newton's method, which can be applied if $M(\theta)$ is twice differentiable. In this method, $M(\theta)$ is approximated as a quadratic function and the update rule is based on minimizing this function, which yields

$$g_k = \big(\nabla^2 M(\hat{\theta}_k)\big)^{-1} \nabla M(\hat{\theta}_k),$$

where ∇ and ∇^2 respectively denote gradient and Hessian.

3.2.2 Robust estimation

Least squares estimators have several advantages, but they also have the weakness that their performance can be severely degraded in the presence of outliers, i.e. data points that differ significantly from other observations. This is particularly relevant for biomedical applications, where outliers can be common due to measurement errors.

Various methods have been suggested as alternatives to, and modifications of the least squares estimator, to make it more robust. A large class of these are also M-estimators. Intuitively, the problem with the least squares approach is that the criterion function grows too much when an error $|\epsilon_n|$ is large, so that a few outliers can have an outsized effect on the overall estimate. In statistical terms, the problem is that the observations do not adhere to the assumptions of the maximum likelihood estimator of identical Gaussian distributions.

Robust M-estimators are formulated with

$$m_\theta(X_n, Y_n) = \rho(Y_n - f_\theta(X_n)) = \rho(\epsilon_n),$$

where the function ρ satisfies

$$\rho(-z) = \rho(z), \quad \arg\min_z \rho(z) = 0,$$

and grows slower than quadratically for large $|\epsilon_n|$. For example, the Huber loss function [18] is defined by

$$\rho(z) = \begin{cases} \frac{1}{2}z^2 & \text{for } z < k, \\ k|t| - \frac{1}{2}z^2 & \text{for } z \geq k \end{cases},$$

and thus grows linearly for errors exceeding the constant k. The Tukey loss function [48] is instead constant for large $|\epsilon_n|$. Other approaches to robust estimation either down-weight or remove data points that are identified as outliers. M-estimators are often computed by solving weighted least squares problems, through the method of iteratively reweighted least squares [16], which illustrates how this approach is closely related to the down-weighting strategy.

3.3 Estimation of biomedical systems

There are particular challenges with working with biomedical data, such as large model uncertainties and measurement errors. But for impulsive time series, there are additional difficulties caused by the input being unknown. We will consider the estimation of only the impulsive input next, before proceeding to a combined input and parameter estimation scheme.

3.3.1 Impulse train estimation

The problem of impulse train estimation is closely related to time-delay estimation. That is a form of system identification, where the parameter Δt should be identified from the measured input and output in a setup

$$y(t) = G(p)u(t - \Delta t) + v(t),$$

where $G(p)$ is a continuous-time linear system and $v(t)$ is a noise term. In impulse train estimation, the input is not measured, and should instead be estimated. However, since it consists of a sequence of impulses, which are weighted and delayed instances of the same Dirac delta distribution, similar estimation approaches can be used for the two problems.

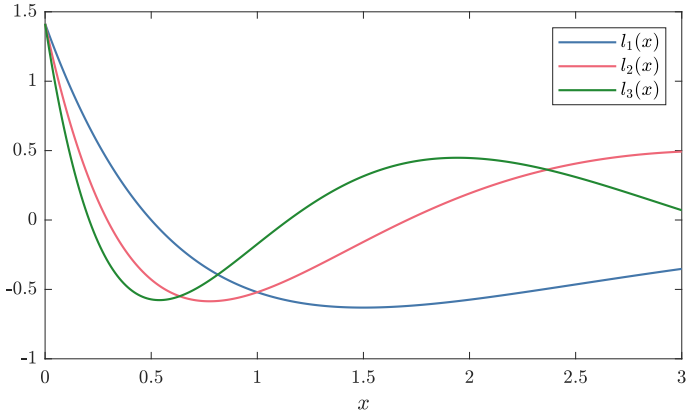

Figure 3.3: The first three Laguerre functions.

Impulse train estimation has received significantly less attention than the time-delay estimation, where a range of different delay estimation techniques have been proposed [2]. One class of methods estimates the delay by representations in specific bases; [2] lists three: time domain, frequency domain, and Laguerre domain.

In Paper II, the impulse train estimation problem is approached in the Laguerre domain, which means that signals are represented as sums of basis functions of the form of Laguerre functions. These are polynomially weighted exponential functions (see Figure 3.3), which make them suitable to represent the impulse response of a stable linear system.

3.3.2 Impulsive time series estimation

The endocrine and pharmacokinetic models presented in the previous chapter both give rise to a particular estimation problem. For a system given by

$$\begin{aligned}\dot{x}_1(t) &= -b_1 x_1(t) + \xi(t),\\ \dot{x}_2(t) &= -b_2 x_2(t) + g_1 x_1(t),\\ y(t) &= x_2(t),\end{aligned}$$

the impulsive input signal $\xi(t)$ should be estimated simultaneously with b_1 and b_2, from sampled measurements of the output signal. In the pharmacokinetic model, b_1 and b_2 are the time constants of levodopa absorption in the gut and elimination in the blood, $y(t)$ is the blood concentration of the drug, and $\xi(t)$ represents the flow through the pylorus. In the endocrine model, b_1 and b_2 instead represent the elimination rates of GnRH and LH, $y(t)$ is the LH concentration in blood and $\xi(t)$ defines the pulsatile release of GnRH.

Similar setups are studied in endocrinology, with the key difference that the input there is represented by a smooth signal, rather than a sequence of impulses. Estimation is then based on the formulation of $y(t)$ as a convolution integral

$$y(t) = \int_0^t S(z)E(t-z)\,dz,$$

where $S(z)$ is the secretion of the measured hormone, and $E(t)$ is the impulse response function, which defines the elimination of the hormone. Consequently, the estimation becomes a deconvolution problem, which can be solved if $S(t)$ is assumed to have some predefined profile. This deconvolution approach has been employed extensively since it was first suggested in [51].

The setup with an impulsive input signal enables other estimation methods for this problem. In [31], it was solved using a LASSO-regularized least squares approach, which also is employed in Paper I. The topic of Paper III and IV is a refinement of this approach, which utilizes a one-step estimation method.

One-step estimation

Two important and connected problems of the estimation problem we consider are that the number of input impulses is unknown, and that it always is possible to obtain a better fit to the data by adding more impulses. However, a solution with many impulses corresponds to a model with many parameters, and, as discussed in Section 3.1.2, such models are not desirable. Furthermore, separate data sets for validation are in general not available; validation efforts are also hampered by large variations in the impulsive input even for the same individual.

Regularization and model selection are routinely utilized when problems of this type are solved, to avoid overfitting and ensure that the sequence of input impulses is sparse. An alternative method to achieve this goal is one-step estimation. It is based on finding a preliminary estimate of the linear time constants, which generally will not be accurate, but is chosen so that the corresponding estimated input signal is sparse. As in nonlinear least squares, Newton's method is then used to improve this estimate, by approximating the residual sum of squares as a quadratic function which is minimized. However, only a single iteration is performed. The same strategy of improving a preliminary estimate with a single Newton step is also employed in the framework of M-estimators, with the purpose of obtaining an estimator with certain desirable asymtotic properties, i.e. in the limit when the number of measurements tend to infinity [49, Ch. 5.7].

A preliminary version of this method is presented in Paper III, while Paper IV contains various refinements and extensions of the approach. A

robust version of the method is in particular presented, which utilizes the robust risk minimization approach of [38]. This method greatly reduces the influence of outliers by decreasing the effective sample size, which makes the one-step method more useful for clinical data where outliers are common.

Chapter 4

Conclusions

The topic of this thesis has been the application of models with impulses to describe biomedical systems; the main contributions are a novel model describing the multi-peaking phenomenon in levodopa pharmacokinetics, and new and improved methods for estimation of impulsive systems.

Although hybrid systems is a relatively young field of research, the approach of combining discrete events with continuous dynamics to describe biological processes is not new; for example, Lapicque's integrate-and-fire neuron model [24] was developed more than a century ago. The long history of these models indicates that, although instantaneous events such as impulses are mathematical idealizations that usually are not realized in nature, the hybrid framework is a useful tool for describing biological processes in a parsimonious way. This thesis illustrate that hybrid systems also can simplify the mathematical analysis; for example, the estimation approach in Paper III and IV utilizes the simplicity of the impulse response, in a way that does not generalize to a continuous-time formulation in an obvious way.

On the other hand, hybrid dynamics may also restrict how a model can be used. Established methods in, e.g., automatic control often assume a model that is either continuous or discrete, and the non-smooth dynamics prohibits techniques that require differentiability, such as various optimization methods. It is thus recommended to both consider how well the underlying process is represented by a discrete event, and the implications for the use of the model, when deciding whether to incorporate hybrid dynamics in a model.

4.1 Future work

A promising future research direction emanating from this thesis is further developments of the one-step estimation algorithm. The method has been

shown to work well on clinical endocrine data as well as synthetic data sets. The former gives rise to a particularly challenging estimation problem due to uncertainties in the data and model, and the inherent sensitivity of the formulation; consequently, a substantial uncertainty in the estimates can be expected. A suitable direction for reducing this uncertainty would be to incorporate further constraints on the impulse estimates. Physiological limitations and feedback mechanisms could then guide the estimation procedure.

A second area worthy of more investigation is the application of this algorithm to other systems. It has so far been used on a somewhat restricted class of systems where the impulsive input is fed to a linear plant, but many other real-world systems could be represented if a more general class of linear or nonlinear plants were considered. Since the theoretical basis of the algorithm at present is limited—analytical derivations have been made in Paper IV, but the motivation for using the method is mostly empirical—such generalizations would probably require further theoretical investigations. A goal of such combined analytical and empirical work could be to find general criteria defining which systems the method feasibly can be applied to.

References

[1] R. Bertram. Mathematical modeling in neuroendocrinology. *Comprehensive Physiology*, 5(2):911–927, 2015.

[2] S. Björklund and L. Ljung. A review of time-delay estimation techniques. In *42nd IEEE International Conference on Decision and Control (IEEE Cat. No. 03CH37475)*, volume 3, pages 2502–2507. IEEE, 2003.

[3] M. S. Branicky, V. S. Borkar, and S. K. Mitter. A unified framework for hybrid control: Model and optimal control theory. *IEEE transactions on automatic control*, 43(1):31–45, 1998.

[4] H.-F. Chen, E.-B. Jeung, M. Stephenson, and P. C. Leung. Human peripheral blood mononuclear cells express gonadotropin-releasing hormone (GnRH), GnRH receptor, and interleukin-2 receptor γ-chain messenger ribonucleic acids that are regulated by GnRH in vitro. *The Journal of Clinical Endocrinology & Metabolism*, 84(2):743–750, 1999.

[5] A. Churilov, A. Medvedev, and A. Shepeljavyi. Mathematical model of non-basal testosterone regulation in the male by pulse modulated feedback. *Automatica*, 45(1):78 – 85, 2009.

[6] M. Contin and P. Martinelli. Pharmacokinetics of levodopa. *Journal of Neurology*, 257(2):253–261, Nov. 2010.

[7] K. R. Godfrey, P. A. Arundel, Z. Dong, and R. Bryant. Modelling the double peak phenomenon in pharmacokinetics. *Computer Methods and Programs in Biomedicine*, 104(2):62–69, 2011.

[8] R. Goebel, R. G. Sanfelice, and A. R. Teel. Hybrid dynamical systems. *IEEE control systems magazine*, 29(2):28–93, 2009.

[9] D. Gonze and P. Ruoff. The Goodwin oscillator and its legacy. *Acta Biotheoretica*, 69:857–874, 2021.

[10] B. C. Goodwin. Oscillatory behavior in enzymatic control processes. *Advances in enzyme regulation*, 3:425–437, 1965.

[11] B. C. Goodwin. An entrainment model for timed enzyme syntheses in bacteria. *Nature*, 209:479–481, 1966.

[12] J. S. Griffith. Mathematics of cellular control processes I. Negative feedback to one gene. *Journal of theoretical biology*, 20(2):202–208, 1968.

[13] R. Grosu, S. A. Smolka, F. Corradini, A. Wasilewska, E. Entcheva, and E. Bartocci. Learning and detecting emergent behavior in networks of cardiac myocytes. *Communications of the ACM*, 52(3):97–105, 2009.

[14] W. M. Haddad, V. Chellaboina, and S. G. Nersesov. Impulsive and hybrid dynamical systems. In *Impulsive and Hybrid Dynamical Systems*. Princeton University Press, 2014.

[15] S. Hiller-Sturmhöfel and A. Bartke. The endocrine system: An overview. *Alcohol health and research world*, 22(3):153, 1998.

[16] P. W. Holland and R. E. Welsch. Robust regression using iteratively reweighted least-squares. *Communications in Statistics-theory and Methods*, 6(9):813–827, 1977.

[17] W. A. Hoogerwerf. Role of clock genes in gastrointestinal motility. *American Journal of Physiology-Gastrointestinal and Liver Physiology*, 299(3):G549–G555, 2010.

[18] P. J. Huber. Robust estimation of a location parameter. *The Annals of Mathematical Statistics*, pages 73–101, 1964.

[19] E. M. Izhikevich. Hybrid spiking models. *Philosophical Transactions of the Royal Society A: Mathematical, Physical and Engineering Sciences*, 368(1930):5061–5070, 2010.

[20] L. V. Kalia and A. E. Lang. Parkinson's disease. *The Lancet*, 386(9996):896–912, 2015.

[21] D. M. Keenan, S. Alexander, C. H. Irvine, I. Clarke, C. Scott, A. Turner, A. J. Tilbrook, B. J. Canny, and J. D. Veldhuis. Reconstruction of in vivo time-evolving neuroendocrine dose-response properties unveils admixed deterministic and stochastic elements. *Proceedings of the National Academy of Sciences*, 101(17):6740–6745, 2004.

[22] S.-P. Khor and A. Hsu. The pharmacokinetics and pharmacodynamics of levodopa in the treatment of Parkinson's disease. *Current Clinical Pharmacology*, 2(3):234–243, 2007.

[23] P. Kohl, E. J. Crampin, T. Quinn, and D. Noble. Systems biology: An approach. *Clinical Pharmacology & Therapeutics*, 88(1):25–33, 2010.

[24] L. Lapicque. Recherches quantitatives sur l'excitation electrique des nerfs traitee comme une polarization. *Journal de physiologie et de pathologie générale*, 9:620–635, 1907.

[25] G. Leng and D. J. MacGregor. Mathematical modelling in neuroendocrinology. *Journal of neuroendocrinology*, 20(6):713–718, 2008.

[26] G. Leng and D. J. MacGregor. Models in neuroendocrinology. *Mathematical biosciences*, 305:29–41, 2018.

[27] P. A. LeWitt. Levodopa for the treatment of Parkinson's disease. *New England Journal of Medicine*, 359(23):2468–2476, 2008.

[28] P. Y. Liu, P. Y. Takahashi, P. D. Roebuck, A. Iranmanesh, and J. D. Veldhuis. Age-specific changes in the regulation of LH-dependent testosterone secretion: Assessing responsiveness to varying endogenous gonadotropin output in normal men. *American Journal of Physiology-Regulatory, Integrative and Comparative Physiology*, 289(3):R721–R728, Sept. 2005. Publisher: American Physiological Society.

[29] L. Ljung. *System identification: Theory for the user*. Prentice Hall information and system sciences series. Prentice Hall, Upper Saddle River, N.J, 2nd ed. edition, 1999.

[30] E. N. Lorenz. Deterministic nonperiodic flow. *Journal of atmospheric sciences*, 20(2):130–141, 1963.

[31] P. Mattsson and A. Medvedev. Modeling of testosterone regulation by pulse-modulated feedback: An experimental data study. In *AIP Conference Proceedings*, volume 1559, pages 333–342. American Institute of Physics, 2013.

[32] D. A. McQuarrie. Stochastic approach to chemical kinetics. *Journal of applied probability*, 4(3):413–478, 1967.

[33] A. Medvedev, A. V. Proskurnikov, and Z. T. Zhusubaliyev. Mathematical modeling of endocrine regulation subject to circadian rhythm. *Annual Reviews in Control*, 46:148–164, 2018.

[34] R. E. Mirollo and S. H. Strogatz. Synchronization of pulse-coupled biological oscillators. *SIAM Journal on Applied Mathematics*, 50(6):1645–1662, 1990.

[35] A. S. Morse. Control using logic-based switching. *Trends in control: A European perspective*, pages 69–113, 1995.

[36] B. Novák and J. J. Tyson. Design principles of biochemical oscillators. *Nature reviews Molecular cell biology*, 9(12):981–991, 2008.

[37] K. Ogungbenro, H. Pertinez, and L. Aarons. Empirical and semi-mechanistic modelling of double-peaked pharmacokinetic profile phenomenon due to gastric emptying. *The AAPS Journal*, 17(1):227–236, January 2015.

[38] M. Osama, D. Zachariah, and P. Stoica. Robust risk minimization for statistical learning from corrupted data. *IEEE Open Journal of Signal Processing*, 1:287–294, 2020.

[39] Z. Qu. Chaos in the genesis and maintenance of cardiac arrhythmias. *Progress in biophysics and molecular biology*, 105(3):247–257, 2011.

[40] D. Robertson, A. Renwick, N. Wood, N. Cross, B. Macklin, J. Fleming, D. Waller, and C. George. The influence of levodopa on gastric emptying in man. *British journal of clinical pharmacology*, 29(1):47–53, 1990.

[41] S. Sahoo, M. Dash, S. Behera, and S. Sabut. Machine learning approach to detect cardiac arrhythmias in ECG signals: A survey. *Irbm*, 41(4):185–194, 2020.

[42] H. Segner, B. L. Verburg-van Kemenade, and M. Chadzinska. The immunomodulatory role of the hypothalamus-pituitary-gonad axis: Proximate mechanism for reproduction-immune trade offs? *Developmental & Comparative Immunology*, 66:43–60, 2017.

[43] M. Senek, D. Nyholm, and E. I. Nielsen. Population pharmacokinetics of levodopa/carbidopa microtablets in healthy subjects and Parkinson's disease patients. *European Journal of Clinical Pharmacology*, 74:1299–1307, 2018.

[44] P. Stoica and Y. Selen. Model-order selection: A review of information criterion rules. *IEEE Signal Processing Magazine*, 21(4):36–47, 2004.

[45] T. Söderström and P. Stoica. *System identification*. Prentice-Hall international series in systems and control engineering. Prentice-Hall, Englewood Cliffs, 1989.

[46] H. Taghvafard, A. V. Proskurnikov, and M. Cao. An impulsive model of endocrine regulation with two negative feedback loops. *IFAC-PapersOnLine*, 50(1):14717–14722, 2017.

[47] B. P. Tu and S. L. McKnight. Metabolic cycles as an underlying basis of biological oscillations. *Nature reviews Molecular cell biology*, 7(9):696–701, 2006.

[48] J. W. Tukey. *Exploratory data analysis*. Addison-Wesley series in behavioral science. Quantitative methods. Addison-Wesley, Reading, Mass, 1977.

[49] A. W. van der Vaart. *Asymptotic statistics*. Cambridge series on statistical and probabilistic mathematics ; 3. Cambridge University Press, Cambridge, 1998.

[50] J. D. Veldhuis. Recent insights into neuroendocrine mechanisms of aging of the human male hypothalamic-pituitary-gonadal axis. *Journal of andrology*, 20(1):1–18, 1999.

[51] J. D. Veldhuis, M. L. Carlson, and M. L. Johnson. The pituitary gland secretes in bursts: Appraising the nature of glandular secretory impulses by simultaneous multiple-parameter deconvolution of plasma hormone concentrations. *Proceedings of the National Academy of Sciences of the United States of America*, 84(21):7686–7690, Nov. 1987.

[52] J. D. Veldhuis, D. M. Keenan, P. Y. Liu, A. Iranmanesh, P. Y. Takahashi, and A. X. Nehra. The aging male hypothalamic-pituitary-gonadal axis: Pulsatility and feedback. *Molecular and cellular endocrinology*, 299(1):14–22, 2009.

[53] J. D. Veldhuis, J. C. King, R. J. Urban, A. D. Rogol, W. S. Evans, L. A. Kolp, and M. L. Johnson. Operating characteristics of the male hypothalamo-pituitary-gonadal axis: Pulsatile release of testosterone and follicle-stimulating hormone and their temporal coupling with luteinizing hormone. *The Journal of Clinical Endocrinology & Metabolism*, 65(5):929–941, 1987.

[54] E. Zavala, K. C. Wedgwood, M. Voliotis, J. Tabak, F. Spiga, S. L. Lightman, and K. Tsaneva-Atanasova. Mathematical modelling of endocrine systems. *Trends in Endocrinology & Metabolism*, 30(4):244–257, 2019.

[55] Z. T. Zhusubaliyev, E. Mosekilde, A. N. Churilov, and A. Medvedev. Multistability and hidden attractors in an impulsive Goodwin oscillator with time delay. *The European Physical Journal Special Topics*, 224(8):1519–1539, 2015.

Paper I

Title

Impulsive feedback modeling of levodopa pharmacokinetics subject to intermittently interrupted gastric emptying

Authors

Håkan Runvik, Alexander Medvedev and Maria Kjellsson

Edited version of

H. Runvik, A. Medvedev and M. Kjellsson. "Impulsive feedback modeling of levodopa pharmacokinetics subject to intermittently interrupted gastric emptying". In: *2020 American Control Conference (ACC)*. Online, 2020.

Impulsive feedback modeling of levodopa pharmacokinetics subject to intermittently interrupted gastric emptying

Abstract

A novel modeling approach capturing the multiple peak phenomenon in oral levodopa administration is proposed. Multiple peaks in the blood plasma concentration of the drug are attributed to the effects caused by gastric emptying. The developed model describes the instances of interrupted gastric emptying by an impulsive feedback of the dopamine concentration in the brain acting on the pyloric sphincter. A combination of the continuous levodopa clearing dynamics and the impulsive feedback results in a hybrid model, whose solutions are positive and bounded. The stability properties of the model are studied by means of a Poincaré map describing the propagation of the continuous model states through the firings of the impulsive feedback. Model feasibility is illustrated on data sets obtained in clinical experiments.

1 Introduction

Pharmacokinetics (PK) studies what happens to substances, e.g. pharmaceutical drugs, administered to a living organism, often in terms of time excursions of blood plasma concentrations. Typically, a single oral drug administration results in a rapid increase in the drug plasma concentration until a peak value is reached, followed by an exponential decline due to the drug molecules clearing from the body. Yet, double or multiple concentration peaks have also been observed after a single oral dose of certain drugs. Causes of secondary peaks have been classified into physicochemical,

formulation, and physiological factors [3]. By effectively splitting a single bolus dose into a number of smaller doses that take action at delayed instants, the multiple peak phenomenon postpones the intended therapeutic effect. Furthermore, since the number and timing of the secondary peaks are patient-specific and depend as well on other factors, the oral way of drug administration can result in somewhat erratic treatment response.

Conventional compartmental PK models are struggling to capture secondary peaks and more advanced dynamical paradigms involving feedback are sought for, see [12]. A feasible but limiting way of portraying the double-peak phenomenon explored there is the introduction of a variable gastric emptying rate. Another approach is to use two parallel absorption compartments, which was proposed to describe the pharmacokinetics of levodopa/carbidopa microtablets in [16].

Symptomatic treatment of Parkinson's disease (PD) is based on the dopamine precursor levodopa [11]. Levodopa is normally administered together with a DDC-inhibitor, such as carbidopa, which prevents the conversion of levodopa to dopamine outside the brain. This increases the plasma level and half-life time of the levodopa [14], which allows a greater proportion of the administered dose to reach the brain.

Double-peak profiles in levodopa serum concentrations are often observed but the exact mechanism behind the phenomenon is not completely understood. Levodopa is only absorbed once it reaches the proximal part of the intestine, i.e. the duodenum. As the transit time through the small intestine is three to four hours while the plasma elimination half-life levodopa is short, gastric emptying is a major determinant for onset of symptom relief. In young and elderly healthy volunteers, single and multiple doses of levodopa have been reported to delay gastric emptying. For instance, in healthy elderly, the time to 90% gastric emptying was increased from 40 min to 65 min in the presence of levodopa, [15], and a pattern of gastric emptying consisting of 2 rapid phases separated by a plateau was present in most cases.

Gastric emptying is normally regulated by the physicochemical properties of the food through neuroendocrine control mechanisms [5]. Neural control of gastric emptying is implemented by the neurons located in the solitary nucleus of the brainstem, while the vagus nerve exerts both inhibitory and excitatory effects on the stomach and connects it to the brain (the brain-gut axis).

Hormones that regulate gastric emptying (e.g. cholecystokinin, ghrelin, leptin) are released from the intestine and pancreas [5]. They also facilitate the connection between the gastrointestinal tract function and energy metabolism, body weight, food intake, etc.

The pylorus is a complex anatomic structure controlling the flow from

the stomach to the intestines and adjusting it to physiological needs [13]. It is tightly closed only intermittently and arrests all flow out of and into the stomach. Gastric emptying is the result of numerous pulses of flow across the pylorus and delayed emptying may arise from disordered sequencing of contractions, [6].

Cholecystokinin (CCK) is a hormone synthesized in the gut and brain. The primary function of CCK is to decrease food intake but it also inhibits gastric emptying, promotes pancreatic secretions, and causes pylorus contraction [10]. There are two different subtypes of CCK receptors: CCK-1 and CCK-2. CCK-1 receptors are primarily found in the gastrointestinal tract, while CCK-2 receptors are mostly distributed in the tissues of central neural system (CNS). Stimulation of CCK-2 receptors in the brain reduces the release of dopamine. It is suggested that dopamine signaling may function as a feedback to the CNS that mediates adjustments in intake according to the caloric density of a meal, while the exact pathways are not known [4]. Biological evidence from non-primates suggests that dopamine can stimulate the secretion of CCK [1].

This paper particularly addresses the oral levodopa administration and focuses on the multiple peak phenomenon in the PK due to intermittently interrupted gastric emptying. The main contribution of the present work is twofold: First, a novel PK model for oral administration of levodopa is developed by capturing the impact of gastric emptying on the drug concentration in the blood by a pulse-modulated feedback. Second, the model parameters are fitted to patient data, thus demonstrating the model feasibility and opening up for its identification. A perspective application of the mathematical model is in smart dispensers of levodopa microtablets [7].

The rest of the paper is structured as follows. First, the model equations including the feedback mechanism are presented and motivated. Next, a Poincaré map of the model is analyzed regarding its asymptotic behavior and convergence to a fixed point. Finally, model parameter values are estimated from experimental data and the feasibility of the feedback mechanism is demonstrated.

2 Model development

On a conceptual level, the physiological process to be mathematically described can be outlined as follows. A single dose of orally administered levodopa reaches the stomach. When the dopamine concentration in the brain is low, the pylorus is open and dissolved levodopa proceeds to the duodenum, where it is adsorbed into the bloodstream. After crossing the blood-brain barrier, levodopa turns into dopamine. High concentration of

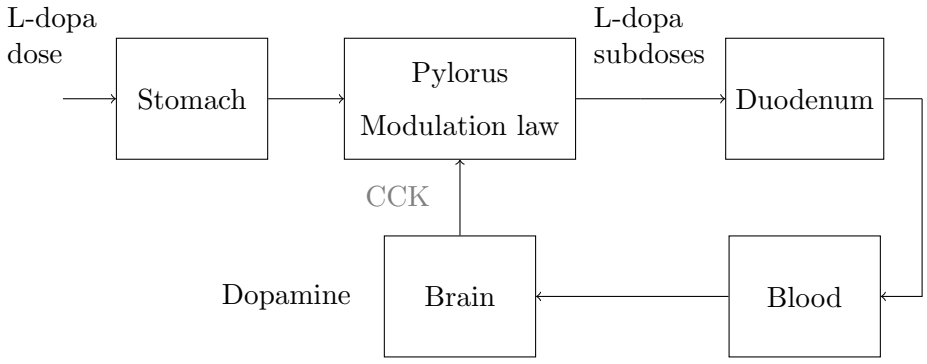

Figure 1: A schematics of the organs participating in the multiple peak phenomenon in the single-dose levodopa administration, interpreted as a pulse-modulated system.

dopamine causes an intermittent pylorus contraction, conceivably by interacting with CCK. The levodopa flow across the pylorus is then disrupted until the dopamine peak subsides and the pylorus orifice opens again. This results in the observed multiple peaks in the levodopa blood concentration.

In a model, this can be captured by interpreting the disrupted levodopa flow across the pylorus as a train of independent subdoses, whose timing and mass are modulated by the dopamine level. The process is illustrated in Fig. 1. The overall system is comprised then of a continuous plant controlled with a pulse-modulated feedback. The administered levodopa dose $d > 0$ is transferred across the pylorus as a train of subdoses $d_n \geq 0, n = 0, 1, 2, \ldots$ at times $t_n, n = 0, 1, 2, \ldots$ such that $d = \sum_{n=0}^{\infty} d_n$.

Let $r(t)$ denote the amount of levodopa in the stomach at time t. Following Fig. 1, at the point of discontinuity t_n, a subdose of levodopa flows across the pylorus. The drug content in the stomach is then instantaneously reduced by

$$r(t_n^+) = r(t_n^-) - d_n, \tag{1}$$

where the minus or plus in a superscript denotes the left-sided and right-sided limit, respectively,

$$d_n = F\left(v_{\mathrm{B}}(t_n), r(t_n)\right), \tag{2}$$

and v_{B} is the dopamine concentration in the brain. The subdose increases the levodopa concentration in the duodenum, denoted $v_{\mathrm{D}}(t)$, by

$$v_{\mathrm{D}}(t_n^+) = v_{\mathrm{D}}(t_n^-) + \frac{d_n}{\omega},$$

where $\omega > 0$ is the (constant) volume of the duodenum.

The amplitude modulation function $0 \leq F(v_{\mathrm{B}}, r) \leq r$ relates the magnitude of the jump to the current dopamine concentration in the brain and the levodopa dose left in the stomach. The function $F(\cdot, \cdot)$ is assumed to be non-decreasing in the first argument. To account for the latency in the communication between the brain and the pylorus, the next jump instant is calculated as

$$t_{n+1} = t_n + \Phi\left(v_{\mathrm{B}}(t_n)\right), \tag{3}$$

where the frequency modulation function $\Phi(\cdot)$ satisfies

$$0 < \Phi_1 \leq \Phi(\cdot) \leq \Phi_2, \tag{4}$$

and Φ_1, Φ_2 are constant parameters.

In between jumps, first-order elimination dynamics are assumed

$$\dot{v}_{\mathrm{D}} = -a_{\mathrm{D}} v_{\mathrm{D}}.$$

The model compartment for the blood is described by

$$\dot{v}_{\mathrm{C}} = -a_{\mathrm{C}} v_{\mathrm{C}} + b_{\mathrm{C}} v_{\mathrm{D}}.$$

Finally, levodopa produces dopamine in the brain, once again, according to first-order dynamics

$$\dot{v}_{\mathrm{B}} = -a_{\mathrm{B}} v_{\mathrm{B}} + b_{\mathrm{B}} v_{\mathrm{C}}.$$

The dopamine concentration v_{B} modulates the process of forming levodopa subdoses portrayed by (2) and (3).

Summing up, the complete model can be written in a state-space form as

$$\dot{x} = Ax + B\xi(t), \quad y = Cx, \tag{5}$$

where the states are given by

$$x^{\intercal} = \begin{bmatrix} v_{\mathrm{D}} & v_{\mathrm{C}} & v_{\mathrm{B}} \end{bmatrix},$$

the system matrices are

$$A = \begin{bmatrix} -a_{\mathrm{D}} & 0 & 0 \\ b_{\mathrm{C}} & -a_{\mathrm{C}} & 0 \\ 0 & b_{\mathrm{B}} & -a_{\mathrm{B}} \end{bmatrix}, B = \begin{bmatrix} \frac{1}{\omega} \\ 0 \\ 0 \end{bmatrix}, C^{\intercal} = \begin{bmatrix} 0 \\ 0 \\ 1 \end{bmatrix}, \tag{6}$$

and $\xi(t)$ defines the train of subdoses formed according to

$$\xi(t) = \sum_{n=0}^{\infty} d_n \delta\left(t - t_n\right), \tag{7}$$

where the timing of the impulses is defined by (3), the amplitudes are given by (2) and $\delta(\cdot)$ is the Dirac delta function. The initialization of the system is given by a set of initial values for the continuous states,

$$x(0)^\intercal = \begin{bmatrix} v_{\mathrm{D}0} & v_{\mathrm{C}0} & v_{\mathrm{B}0} \end{bmatrix},$$

and a fixed time $t_0 > 0$ for the first subdose.

3 Model analysis

From the fact that only a single-dose administration of levodopa is considered, and all the involved drug molecules will eventually clear out, the system described by (5) and (7) is bounded and expected to tend towards a point of equilibrium, as $t \to \infty$. However, the impulsive feedback in the model is discontinuous, which gives rise to hybrid closed-loop dynamics and complicates the analysis of the model behavior. A suitable way to circumvent this difficulty is to sample the system at the points of discontinuity and derive a Poincaré map that describes the propagation of the continuous state vector $x(t)$ through the instants $t_n, n = 0, 1, 2, \ldots$. This is possible since Φ is bounded from above and below. It is furthermore assumed that the eigenvalues of A, given by a_{D}, a_{C} and a_{B} are distinct, since they correspond to distinct biological processes; a_{D} and a_{C} describe levodopa clearing in different compartments, while a_{B} corresponds to the half-life time of dopamine in the brain.

Following previous work [2] and defining $x_n = x(t_n^-)$, a solution to (5) gives rise to the discrete map, propagating the continuous dynamics through the feedback firings

$$x_{n+1} = Q\left(x_n\right), \tag{8}$$

where

$$Q(x) = e^{A\Phi(Cx)}\left(x + F(Cx, r)B\right). \tag{9}$$

To explicitly relate the available pool of levodopa in the stomach to the subdoses produced by the impulsive feedback, (1) is written as

$$r_{n+1} = r_n - F\left(Cx_n, r_n\right), \quad r_0 = d, \tag{10}$$

where the notation $r_n = r(t_n^-))$ is introduced. The relation between r_n and d_n can then be expressed as

$$r_n = d - \sum_{i=0}^{n-1} d_i.$$

At equilibrium, the pool of levodopa in the stomach is depleted and no more drug reaches the duodenum, implying $F(Cx, r) = 0$. Thus, a fixed point x^0 of (8) satisfies

$$x^0 = e^{A\Phi(Cx^0)}x^0. \tag{11}$$

Obviously, the only type of fixed point admissible in the model at hand is an equilibrium. With a strictly positive $\Phi(x)$ and a Hurwitz A, the only solution to equation (11) is $x^0 = 0$. The equilibrium of the Poincaré map is therefore

$$x^0 = \begin{bmatrix} 0 & 0 & 0 \end{bmatrix}^\intercal,$$
$$r^0 = \{y \in \mathbb{R}^+ | F(0, y) = 0\}.$$

Notice that this equilibrium point also corresponds to the equilibrium point of the continuous part of (5). The discrete state variable of the impulsive (hybrid) model governed by (3) is unbounded.

The considered model possesses an equilibrium and admits a zero solution. Therefore, it differs greatly from the impulsive Goodwin's oscillator covered in, e.g., [2] and [17], despite the similarities in the mathematical formulation. Two distinctive features of model (5), (7) introduced by design render the solutions converging to the equilibrium. First, the amplitude modulation function allows $F(\cdot, \cdot) = 0$. Second, the closed-loop system is driven by an exogenous positive signal that asymptotically converges to zero while the impulsive Goodwin's oscillator is, in its original form, an autonomous system.

3.1 Stability analysis

To analyze the stability of the derived equilibrium point x^0, a Lyapunov function is used. This analysis is simplified by the positivity of the system. Indeed, the linear continuous part of the model in (5) is positive since A is Metzler and the initial conditions and input signals are positive, while (10) is positive by the construction of F.

Exploiting model positivity, the following linear Lyapunov function is introduced, which corresponds to the total amount of levodopa and dopamine in the system

$$V(\tilde{x}) = v_\mathrm{S} + \frac{a_\mathrm{D}}{b_\mathrm{C}} v_\mathrm{D} + \frac{a_\mathrm{D} a_\mathrm{C}}{b_\mathrm{C} b_\mathrm{B}} v_\mathrm{B} + \frac{1}{\omega} r. \tag{12}$$

where $\tilde{x} = \begin{bmatrix} x^\intercal & r \end{bmatrix}^\intercal$. When $\tilde{x}$ is restricted to be non-negative, this function is also non-negative, and zero only when $\tilde{x}$ is zero. The Lyapunov function can be applied to the Poincaré map, by evaluating the difference

$$V\left(\tilde{Q}(\tilde{x})\right) - V(\tilde{x}),$$

where $\tilde{Q}(\tilde{x}) = \left[\begin{smallmatrix} Q^\intercal(x) & r - F(Cx,r) \end{smallmatrix} \right]^\intercal$.

Theorem 1. Consider the system defined by

$$x_{n+1} = e^{A\tau_n} \left(x_n + F(Cx_n, r)B \right),$$

where $\tau_n > 0, n = 0, 1, 2, \ldots$ and the matrices A, B and C are given by (6). If the amplitude modulation function satisfies

$$0 \leq F(\cdot, \eta) \leq \eta,$$

and $F(\cdot, \eta) = 0 \iff \eta = 0$, then Lyapunov function (12) is decreasing for all $\tilde{x} \in \mathbb{R}^4_+$ and the fixed point $\tilde{x}^0 = 0$ is asymptotically stable.

Proof. See Appendix A. □

Theorem 1 can now be applied to map (9), with $\tau_n = \Phi(Cx_n)$, since the frequency modulation function is bounded according to (4), and the states x_n are (element-wise) positive. The stability of the equilibrium point of the Poincaré map means that the continuous states of the hybrid system also will tend towards this equilibrium, since the continuous trajectories in between the impulse times are bounded.

4 Model feasibility

To demonstrate model feasibility, the model fit to clinical data is discussed in this section. This work is conducted in two steps. First, the parameters of an open-loop model consisting of the states v_S and v_D, and the driving impulses, are identified from clinical data. Then a closed-loop model, corresponding to the system presented in previous sections, is created. The parameters of the modulation functions in the impulsive feedback are chosen so that the simulated levodopa blood concentration of the closed loop system is close to the corresponding open loop results.

The experimental data, described in detail in [16] and consisting of longitudinal measurements of the levodopa concentration in the blood after a single oral dose of Flexilev®, is used to estimate the impulses and model dynamics. Flexilev® is administered in the form of water dissolved tablets, containing 5 mg of levodopa and 1.35 mg of carbidopa monohydrate [9]. Maximum plasma concentrations of levodopa are reached after approximately 45 min. Each patient in the cohort was administered an individualized dose of Flexilev® constituting 150% of their normal morning dose of levodopa with blood sampled every 20 min, measuring the concentration of levodopa.

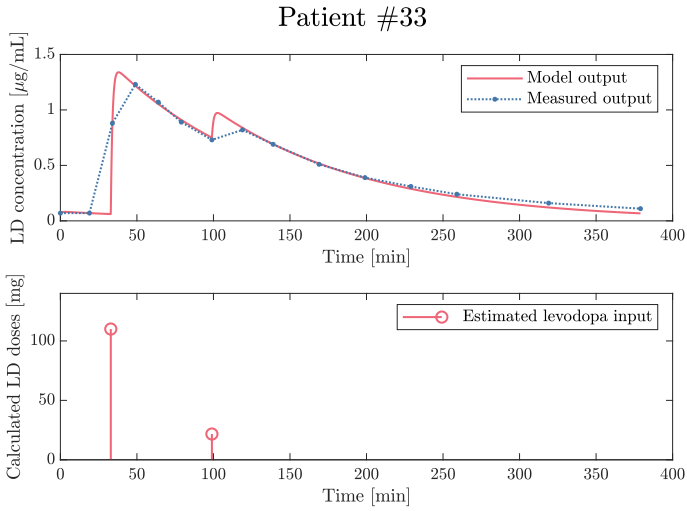

Figure 2: Double-peak levodopa blood concentration profile in clinical experiment data and simulated by an open-loop model with estimated impulses.

4.1 Subsystem estimation

Based on the available measurements, only the subsystem consisting of v_{D} and v_{C} is considered in this step. The optimization method presented in [8] is used for the estimation, utilizing a constraint on the ℓ_1-norm of the impulse amplitudes to ensure sparsity of the solution. Applied to the data set for each patient, the result of the optimization is the impulse times and amplitudes and the a_{D} and a_{C} coefficients. The parameters b_{C} and ω cannot be separately identified, but their fraction is used to scale the impulses so that the impulses sum to the entire dose. The data and the estimates for one patient, exhibiting the characteristic double-peak profile, are displayed in Fig. 2. The more pronounced peaks in the model predictions compared to the observations are caused by the undersampling of the rising fronts of the levodopa concentration profiles. This allows the optimization algorithm to select one of the model time constants very fast to maximize the fit during the rest of the data set. More frequent sampling would alleviate this problem.

Examination of the estimation results reveals that the impulses identified for the open-loop system cannot qualitatively correspond to the impulses generated by an impulsive feedback. Consider again Fig. 2, and compare this concentration profile to one with a single peak, e.g. the hypothetical case where dopamine concentration would be unaffected by the levodopa concentration. Since the total dose would be the same in both cases, the second

impulse would need to occur earlier in the single-peak case and close enough to the first impulse not to be noticed in the resulting blood concentration profile. This cannot be achieved with the proposed modulation functions where the second impulse time t_1 would be the same in both cases, since v_B would be the same at t_0. Thus, additional impulses have to be produced by the feedback to comply with the observed behavior.

4.2 Closed-loop model

A complete parameterized model with impulsive feedback can be constructed based on the estimated dynamics and impulses. The estimated model is extended for this purpose with the dynamics of the dopamine concentration in the brain and suitable modulation functions for the feedback. Notably, the applied model estimation procedure does not constitute system identification but only illustrates the model feasibility.

The estimation is performed for two patients with complex PK responses to the levodopa dose. Both patients display a distinct plateau in the decay in the concentration profile, as well a slower than exponential decay during the later part of the profile. This behavior is well explained by the multiple impulses driving the system, as shown in Fig. 3. These patients were chosen over those with simpler concentration profiles, since a profile with one or two impulses would lead to a trivial estimation task.

4.3 Modeling assumptions

As there is no measurement of the dopamine concentration in the brain, the dynamics of this state are not estimated and a fixed half-life time is assumed instead. Since the parameter b_B only acts as a scaling of v_B, which can be compensated for in the feedback, $b_\mathrm{B} = a_\mathrm{B}$ is set for simplicity.

4.4 Feedback model

The modeling constraints presented in the previous sections guide the construction of the modulation functions that define the impulsive feedback law. The functions generally need to be bounded and monotonous, which means that a nonlinear function with a sigmoidal curve is sought for. The Hill function is therefore a suitable candidate. This function, in different versions, is commonly used in pharmacometrics and can be expressed in the following way

$$f(x) = \frac{1}{1 + (x/h)^p}.$$

The parameter $p \in \mathbb{R}^+$ is termed as the Hill function order and determines the steepness of the curve, while $h \in \mathbb{R}^+$ scales the argument. A

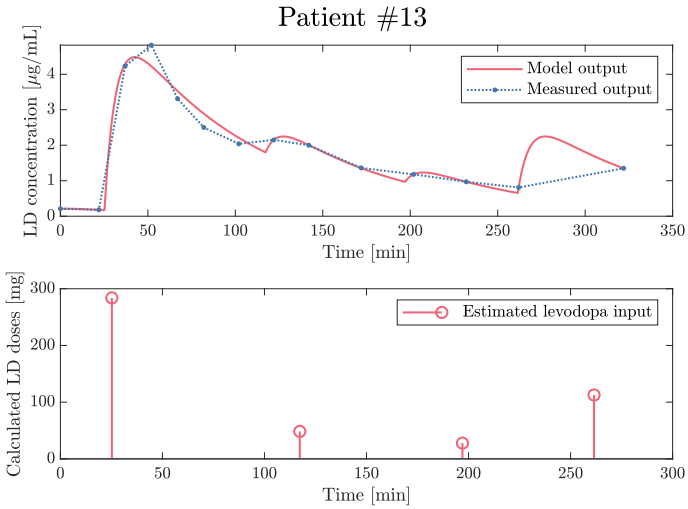

Figure 3: Multi-peak levodopa blood concentration profile in clinical experiment data and simulated by an open-loop model with multiple estimated impulses. The last impulse corresponds to an additional dose of levodopa that is not part of the experiment protocol and administered to alleviate severe symptoms in the patient at that time.

higher-order Hill function resembles a step function but is differentiable.

The frequency modulation function is chosen as a Hill function of the form

$$\Phi(v_{\mathrm{B}}) = k_1 + k_2 \frac{(v_{\mathrm{B}}/h_1)^{p_1}}{1 + (v_{\mathrm{B}}/h_1)^{p_1}},$$

where p_1, h_1, k_1 and k_2 are positive real parameters. The amplitude modulation function is composed of two factors

$$F(v_{\mathrm{B}}, r) = f(r) F_0(v_{\mathrm{B}}),$$
$$F_0(v_{\mathrm{B}}) = \frac{1}{1 + (v_{\mathrm{B}}/h_2)^{p_2}},$$

where p_2 and h_2 are positive real parameters and $0 \leq F_0 \leq 1$. The factor $f(r)$ is given by

$$f(r) = \alpha \left(\frac{-1}{4} + \frac{\left((r + \frac{3\alpha}{8})/(3^{1.5}\alpha/8)\right)^2}{1 + \left((r + \frac{3\alpha}{8})/(3^{1.5}\alpha/8)\right)^2} \right),$$

which is a Hill function that is parameterized to describe a smooth saturation function, where α is the saturation level. The saturation represents the physical limitation in transport of liquid through the pylorus. The function f satisfies $0 \leq f(r) \leq r$ by its construction.

4.5 Feedback law verification

The modulation function parameter values in Table 1 were chosen manually (i.e. without any identification algorithm) to match the estimated dynamics and impulses for two patients diagnosed with Parkinson's disease, i.e. Patient 13 and Patient 14. The estimated models driven by the corresponding impulsive feedback law are compared with the same model driven directly by the estimated impulses in Fig. 4 and Fig. 5. The results for the scenarios when the dopamine concentrations remain low and constant thus keeping the pylorus orifice open are also displayed in these plots for reference.

Table 1: Modulation function parameters.

Patient ID	p_1	p_2	h_1	h_2	k_1	k_2	α
13	2	2.5	1	2.4	3.8	95	0.65
14	4	3	5	3.9	6	133	1.4

For both patients above, the estimation results for the open-loop models contain an extra impulse toward the end of the simulation. In each case, this is due to an out-of-protocol levodopa dose, administered to alleviate severe symptoms in the patient at the time. Since both time and dose of administration is known, the last impulse can be used to verify the parametrization of the model for each patient.

To do this, the estimated impulses are first moved in time, so that they coincide with the administration times. For impulses occurring at the penultimate sampling point, this can be done without changing the estimated blood concentration at any sampling point, if the impulse amplitudes are suitably rescaled. The resulting amplitude is then compared with the value given by the amplitude modulation function, where r is given by the administered dose. The results are summarized in Table 2, where λ_{fb} denotes the impulse amplitudes from the modulation function.

Table 2: Impulse amplitudes for out-of-protocol levodopa administration.

Patient ID	λ_{sc} (mg)	λ_{fb} (mg)	Administered dose (mg)
13	71.0	62.6	100
14	48.8	130.6	150

For Patient 13, the modulation function predicts an amplitude that is similar to the estimated value. The difference is considerably greater for

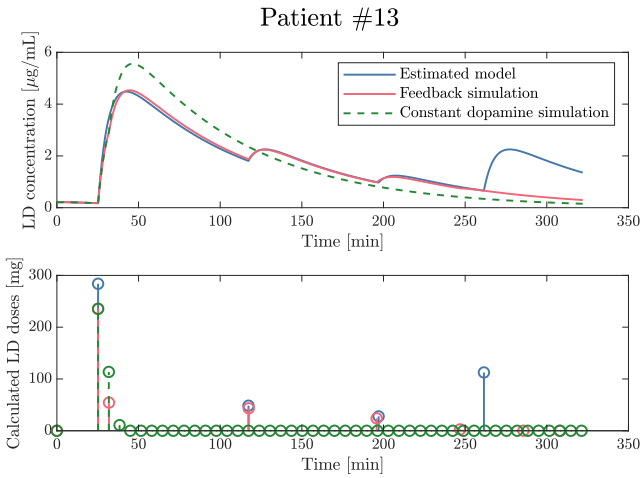

Figure 4: Levodopa blood concentration and impulses, with impulses based on estimation, dopamine feedback and constant dopamine level.

Patient 14. However, for this patient, the pre-dose blood levodopa concentration is significantly higher than one would expect after an overnight washout, indicating that unaccounted levodopa administrations might have occurred during the experiment. This could explain the poor results for the amplitude verification.

4.6 Discussion

The close similarity between the results from simulation with the feedback model and the estimated impulses driving open-loop dynamics depicted in Fig. 4 and Fig. 5 confirms that the proposed impulsive feedback model can reproduce the multi-peak behaviors observed in clinical experiments.

When, on the other hand, the feedback loop is broken and substituted with a constant dopamine level, the multi-peak behaviour does not occur. The levodopa is in this case transported to duodenum through a fast sequence of impulses, which are almost indistinguishable in the resulting blood concentration profile. This is an important result, meaning that it is specifically the neuroendocrine feedback mechanism and not the pharmacokinetics that causes the multi-peak phenomenon.

An important difference between the estimated impulse train in the open-loop model and the impulses generated by the feedback is that the feedback produces a significantly greater number of impulses throughout the simulations. The first estimated impulse is typically replaced by two smaller ones

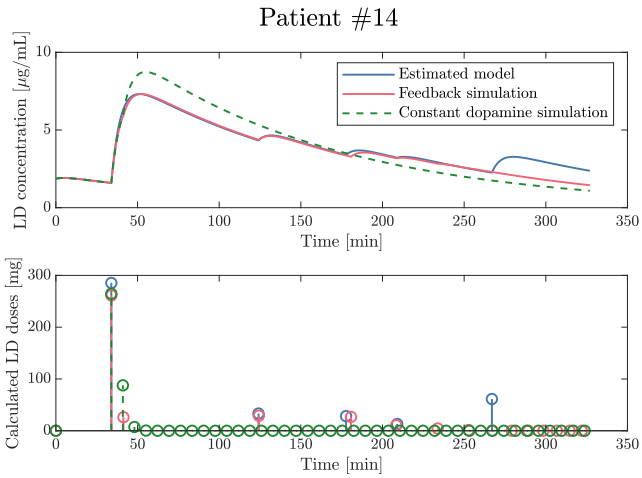

Figure 5: Levodopa blood concentration and impulses, with impulses based on estimation, dopamine feedback and fixed dopamine level.

and very low amplitude impulses are introduced at low levels of remaining levodopa. This highlights a conceptional conflict between the model estimation, where sparsity is desired in order to avoid overfitting, and the feedback mechanism, which requires more frequent and lower amplitude impulses in order to produce results that are consistent with the underlying biology. The intrinsic difficulty in distinguishing between a single impulse and several impulses close to each other that is pointed out in [8] can also clearly be seen in the results in this work. How to reconcile these different objectives in obtaining a certain output profile is a question to be addressed in future research.

A Proof of Theorem 1

Inserting (9) into (12) to evaluate the evolution of the Lyapunov function over one time step gives

$$V\left(\tilde{Q}(\tilde{x})\right) - V(\tilde{x}) = -\omega^{-1}\left(c_1(x_1 + F(Cx, r)) + c_2x_2 + c3x_3\right),$$

where c_i are given by

$$c_1 = a_{\mathrm{C}} a_{\mathrm{B}} \beta_{\mathrm{D}} \left(1 - e^{-a_{\mathrm{D}}\tau}\right) + a_{\mathrm{D}} a_{\mathrm{B}} \beta_{\mathrm{C}} \left(1 - e^{-a_{\mathrm{C}}\tau}\right) + a_{\mathrm{D}} a_{\mathrm{C}} \beta_{\mathrm{B}} \left(1 - e^{-a_{\mathrm{B}}\tau}\right)$$
$$c_2 = \frac{a_{\mathrm{D}}}{b_{\mathrm{C}} \left(a_{\mathrm{C}} - a_{\mathrm{B}}\right)} \left(a_{\mathrm{C}} \left(1 - e^{-a_{\mathrm{B}}\tau}\right) - a_{\mathrm{B}} \left(1 - e^{-a_{\mathrm{C}}\tau}\right)\right)$$
$$c_3 = \frac{a_{\mathrm{D}} a_{\mathrm{C}}}{b_{\mathrm{C}} b_{\mathrm{B}}} \left(1 - e^{-a_{\mathrm{B}}\tau}\right),$$

where

$$\beta_{\mathrm{D}} = \frac{1}{\left(a_{\mathrm{C}} - a_{\mathrm{D}}\right)\left(a_{\mathrm{B}} - a_{\mathrm{D}}\right)}, \quad \beta_{\mathrm{C}} = \frac{1}{\left(a_{\mathrm{D}} - a_{\mathrm{C}}\right)\left(a_{\mathrm{B}} - a_{\mathrm{C}}\right)},$$
$$\beta_{\mathrm{B}} = \frac{1}{\left(a_{\mathrm{D}} - a_{\mathrm{B}}\right)\left(a_{\mathrm{C}} - a_{\mathrm{B}}\right)},$$

$$\alpha_i = \prod_{\substack{j=1 \\ j \neq i}}^{3} \frac{1}{a_j - a_i}, \quad i = 1, 2, 3.$$

Now show that $c_i, i = 1, 2, 3$ are positive whenever $\tau > 0$. For c_1, we notice that $\tau = 0 \implies c_1 = 0$. It is therefore sufficient to verify the positivity of the derivative

$$\frac{dc_1}{d\tau} = a_{\mathrm{D}} a_{\mathrm{C}} a_{\mathrm{B}} \left(\beta_{\mathrm{D}} e^{-a_{\mathrm{D}}\tau} + \beta_{\mathrm{C}} e^{-a_{\mathrm{C}}\tau} + \beta_{\mathrm{B}} e^{-a_{\mathrm{B}}\tau}\right).$$

The symmetry of this expression means that we can assume $a_{\mathrm{D}} < a_{\mathrm{C}} < a_{\mathrm{B}}$. We then eliminate β_{B} to get

$$\frac{dc_1}{d\tau} = \frac{a_{\mathrm{D}} a_{\mathrm{C}} a_{\mathrm{B}}}{a_{\mathrm{D}} - a_{\mathrm{C}}} \left(\frac{e^{-a_{\mathrm{D}}\tau} - e^{-a_{\mathrm{B}}\tau}}{a_{\mathrm{D}} - a_{\mathrm{B}}} - \frac{e^{-a_{\mathrm{C}}\tau} - e^{-a_{\mathrm{B}}\tau}}{a_{\mathrm{C}} - a_{\mathrm{B}}}\right),$$

where the expressions both outside and inside the parenthesis are positive. The positivity of c_2 and c_3 is easier to verify, again by starting from $\tau = 0$ and calculating the derivative. Since $F(Cx, r))$ is positive, we get that $V(\tilde{x})$ is decreasing for $\tilde{x} \in \mathbb{R}^4_+$.

References

[1] R. Bhattacharya, D. Touroutine, B. Barbagallo, J. Climer, C. M. Lambert, C. M. Clark, M. J. Alkema, and M. M. Francis. A conserved dopamine-cholecystokinin signaling pathway shapes context-dependent Caenorhabditis elegans behavior. *PLoS genetics*, 10(8):e1004584–e1004584, Aug. 2014.

[2] A. Churilov, A. Medvedev, and A. Shepeljavyi. Mathematical model of non-basal testosterone regulation in the male by pulse modulated feedback. *Automatica*, 45(1):78 – 85, January 2009.

[3] N. M. Davies, J. K. Takemoto, D. R. Brocks, and J. A. Yanez. Multiple peaking phenomena in pharmacokinetic disposition. *Clinical Pharmacokinetics*, 49(6):351–377, June 2010.

[4] I. E. de Araujo, J. G. Ferreira, L. A. Tellez, X. Ren, and C. W. Yeckel. The gut-brain dopamine axis: A regulatory system for caloric intake. *Physiol Behav.*, 106(3):394–399, June 2012.

[5] R. K. Goyal, Y. Guo, and H. Mashimo. Advances in the physiology of gastric emptying. *Neurogastroenterology & Motility*, 31:e13546, April 2019.

[6] M. Horowitz and J. Dent. The study of gastric mechanics and flow: a Mad Hatter's tea party starting to make sense? *Gastroenterology*, 107(1):302–306, July 1994.

[7] D. Johansson, A. Ericsson, A. Johansson, A. Medvedev, D. Nyholm, F. Ohlsson, M. Senek, J. Spira, I. Thomas, J. Westin, and F. Bergquist. Individualization of levodopa treatment using a microtablet dispenser and ambulatory accelerometry. *CNS neuroscience & therapeutics*, 24(5):439–447, May 2018.

[8] P. Mattsson and A. Medvedev. Modeling of testosterone regulation by pulse-modulated feedback: An experimental data study. *AIP Conference Proceedings*, 1559(1):333–342, September 2013.

[9] Medical Products Agency. Public assessment report: Flexilev (levodopa/carbidopa). Technical report, 2011. Asp no: 2011-1568.

[10] T. H. Moran, R. Kornbluh, K. Moore, and G. J. Schwartz. Cholecystokinin inhibits gastric emptying and contracts the pyloric sphincter in rats by interacting with low affinity CCK receptor sites. *Regulatory Peptides*, 52(3):165–172, August 1994.

[11] D. Nyholm and H. Lennernäs. Irregular gastrointestinal drug absorption in Parkinson's disease. *Expert Opinion on Drug Metabolism & Toxicology*, 4(2):193–203, March 2008.

[12] K. Ogungbenro, H. Pertinez, and L. Aarons. Empirical and semi-mechanistic modelling of double-peaked pharmacokinetic profile phenomenon due to gastric emptying. *The AAPS Journal*, 17(1):227–236, January 2015.

[13] D. Ramkumar and K. S. Schulze. The pylorus. *Neurogastroenterology and Motility*, 17:22–30, July 2005. Suppl. 1.

[14] D. Robertson, N. Wood, H. Everest, K. Monks, D. Waller, A. Renwick, and C. George. The effect of age on the pharmacokinetics of levodopa administered alone and in the presence of carbidopa. *British Journal of Clinical Pharmacology*, 28(1):61–69, July 1989. Publisher: John Wiley & Sons, Ltd.

[15] D. R. Robertson, A. G. Renwick, B. Macklin, S. Jones, D. G. Waller, C. F. George, and J. S. Fleming. The influence of levodopa on gastric emptying in healthy elderly volunteers. *European Journal of Clinical Pharmacology*, 42(4):409–412, April 1992.

[16] M. Senek, D. Nyholm, and E. Nielsen. Population pharmacokinetics of levodopa/carbidopa microtablets in healthy subjects and Parkinson's disease patients. *European Journal of Clinical Pharmacology*, 74:1299–1307, October 2018.

[17] Z. T. Zhusubaliyev, A. N. Churilov, and A. Medvedev. Bifurcation phenomena in an impulsive model of non-basal testosterone regulation. *Chaos: An Interdisciplinary Journal of Nonlinear Science*, 22(1):013121, Feb. 2012.

Paper II

Title

Laguerre domain estimation of an input impulse train to a continuous linear time-invariant system

Authors

Håkan Runvik and Alexander Medvedev

Edited version of

H. Runvik, and A. Medvedev. "Laguerre domain estimation of an input impulse train to a continuous linear time-invariant system". In *59th IEEE Conference on Decision and Control (CDC)*. Online, 2020.

Laguerre domain estimation of an input impulse train to a continuous linear time-invariant system

Abstract

A novel estimation algorithm for the times and weights of a finite number of impulses constituting the input signal of a known continuous linear time-invariant system from the output signal of the latter is proposed. The intended application area is the estimation of pulsatile input in biomedical systems. The output signal is assumed to belong to $\mathbb{L}_2$ and be represented in Laguerre domain. A generalization of the Laguerre domain to distributions is utilized to incorporate Dirac δ-functions into the mathematical framework. The estimation algorithm utilizes the Laguerre parameter p to regularize an otherwise ill-conditioned problem. The viability of the method is demonstrated on simulated and experimental data exhibiting a double-peak decay in the concentration of an anti-Parkinsonian drug after a single dose administration.

1 Introduction

In biomedical applications dealing with e.g. hormone secretion in endocrine systems and the pharmacokinetics of many drugs, concentration profiles displaying a rapid increase followed by an exponential decay are often encountered. Such a profile can be mathematically described as the impulse response of a dynamical system. However, this behaviour may also repeat itself, which motivates the study of the response to an impulse train.

In many endocrine systems, hormones are released repeatedly over the day in a pulsative matter, but not periodically in mathematical sense [5].

When direct measurement (blood sampling) is impossible, deconvolution is often employed to reconstruct these pulses [18].

The impulse train model is applicable to pharmacokinetics of orally administered drugs, when a single dose of a drug produces multiple plasma concentration peaks [3]. In particular, this behavior is exhibited by the anti-Parkinsonian drug levodopa, whose pharmacokinetics can be captured by an impulsive feedback model [13].

In the present work, the estimation of the (firing) times and weights of an input impulse train from the output signal of a given dynamical system is therefore considered. The response of a system to an impulse train is seldom addressed, in contrast with single impulse response. In [9], the estimation of the impulsive input and the parameters of a linear system was performed for sampled data under a sparsity constraint. The proposed approach has been applied to endocrine data in [10]. Finite-memory observers [12] have also found application in state estimation of systems with impulsive input [11].

The matter of delay estimation is closely related to the problem under consideration. In [6], delay estimation from the response of a continuous system to a single was studied in Laguerre domain.

Laguerre functions are particularly useful for analyzing impulse responses. Being a set of polynomially weighted and normalized exponential functions [8], they offer a natural basis for capturing the signal form of solutions to linear time-invariant (LTI) differential equations.

The main contribution of this paper is an algorithm estimating the impulse times and weights from the Laguerre spectrum of the output signal of a continuous LTI system. It is, to the best of our knowledge, the first time this estimation problem has been treated in the Laguerre domain.

The rest of the paper is organized as follows. First necessary background information on the representation of signals and systems in the Laguerre domain is provided. Then the Laguerre representation of the impulse train is derived, motivating the use of the matrix pencil method to solve the estimation problem. Finally, the estimation algorithm is presented and its performance is investigated on both numerical and experimental data.

2 Laguerre domain representation

Let $L_0, L_1, \ldots$ denote the sequence of Laguerre polynomials [16]. The continuous Laguerre function of order k is then defined in time domain as

$$l_k(t) = \sqrt{2p}\, \mathrm{e}^{-2pt}\, L_k(2pt),$$

where $p > 0$ denotes the Laguerre parameter.

The Laguerre functions form an orthonormal basis in $\mathbb{L}_2[0,\infty)$ and can therefore be used to express any signal $y(t) \in \mathbb{L}_2$ as an infinite series

$$y(t) = \sum_{k=0}^{\infty} y_k l_k(t), \tag{1}$$

where the sequence of the Laguerre coefficients y_k is square summable and the coefficients are calculated as

$$y_k = \int_0^{\infty} l_k(t) y(t)\ dt. \tag{2}$$

The signal $y(t)$ is thus uniquely represented by its Laguerre spectrum, which also defines the Laguerre transform of the signal, according to $\mathscr{L}\{y\} = \{y_k, k = 0, 1, \dots\}$. The inverse Laguerre transform is then given by (1). Further, the following shorthand notation is utilized $\{y_k, k = 0, 1, \dots\} \triangleq \{y_k\}$. By analogy with Fourier transform, $\{y_k\}$ is termed the Laguerre domain representation of $y(t)$.

2.1 Linear time-invariant dynamics

Consider the continuous linear time-invariant (LTI) system

$$\begin{aligned} \dot{x}(t) &= Ax(t) + Bu(t), \quad x(0) = 0, \\ y(t) &= Cx(t), \end{aligned} \tag{3}$$

where A, B, C are the system matrices, x is the state vector and $u, y \in \mathbb{L}_2[0,\infty)$ are scalar input and output signals. In Laguerre domain, with $\{u_k\}$ and $\{y_k\}$ as the input and output, the continuous model in (3) transforms into an equivalent discrete system

$$\begin{aligned} x_{k+1} &= Fx_k + Gu_k, \quad x_0 = 0, \\ y_k &= Hx_k + Ju_k, \end{aligned} \tag{4}$$

where the system matrices are given (see [1]) by

$$\begin{aligned} &F = -(pI - A)^{-1}(pI + A), G = -\sqrt{2p}(pI - A)^{-1}, \\ &H = \sqrt{2p}C(pI - A)^{-1}, J = C(pI - A)^{-1}B. \end{aligned}$$

Note that the linearity and causality of the continuous system carry over to the Laguerre domain description. Discrete-time techniques can thus be readily applied to (4) in Laguerre domain and mapped back to the time domain through the inverse Laguerre transformation, see, e.g., [1].

2.2 Impulses and delays

As mentioned above, the Laguerre transform maps a signal in $\mathbb{L}_2$ to a square-summable sequence. However, since impulses, i.e. Dirac δ-functions, do not belong to $\mathbb{L}_2$, the transform does not apply to impulse trains. However, a generalization of the Laguerre transform proposed in [7] can be used. By replacing (2) with the Laguerre sharp transform, in the following denoted as $\mathscr{L}^{\#}\{\cdot\}$, the transform can be applied to both signals in $\mathbb{L}_1$ and finite measures. The coefficients of this transform are evaluated as

$$y_k^{\#} = \int_0^{\infty} (l_0 * y)(t) l_k(t)\ dt. \tag{5}$$

The original definition of the Laguerre sharp transform in [7] is double-sided, i.e. on the whole real line. Here, a single-sided version of the transform is utilized to enable handling initial conditions. The proposition below summarizes important properties of the transform derived in [7].

Proposition 1 ([7])**.** The set of all functions f, such that $\mathscr{L}^{\#}\{f\} \in \ell_2$, constitutes a Hilbert space $\mathbb{L}_2^{\#}$, which includes all integrable and square-integrable functions, i.e.

$$(\mathbb{L}_1 \cup \mathbb{L}_2) \subset \mathbb{L}_2^{\#}.$$

Furthermore, the following properties hold:

- If $y \in \mathbb{L}_2$ and $\mathscr{L}\{y\} = \{y_k\}$, then $\mathscr{L}^{\#}\{y\} = \{\nabla y_k\}$,
- Every finite signed measure has a Laguerre sharp transform that is unique,
- If μ_{D_τ} is a probability measure with all mass in a single point $\tau \in \mathbb{R}^+$ (i.e. a Dirac measure), $\mathscr{L}^{\#}\{y\} = \{\nabla l_k(\tau)\}$, where ∇ is the first difference operator, i.e. $\nabla l_k = l_k - l_{k-1}$, $\nabla l_0 = l_0$.

Since the generalized probability distribution of a Dirac measure at $\tau \in \mathbb{R}^+$ is the Dirac δ-function $\delta(t-\tau)$, it follows that the Laguerre sharp transform of a unit impulse is given by the difference between Laguerre functions evaluated at the time of the impulse. In particular, the following applies to a unit impulse at time zero.

Corollary 1. Let δ_k denote the Kronecker delta. Then

$$\mathscr{L}^{\#}\{\delta(t)\} = \sqrt{2p}\delta_k.$$

Proof. Follows from $l_k(0) = \sqrt{2p}$ for all k. □

The first difference relations that result from the Laguerre sharp transform justify the formal use of the traditional Laguerre transform, even for impulses. Evaluating the transform of $\delta(t-\tau)$ to $\{l_k(\tau)\}$ still produces a one-to-one mapping between the time and Laguerre domain and any operation performed on this sequence has an equivalent one defined on the first difference of it. In what follows, Laguerre spectra and Laguerre coefficients will therefore refer to the traditional transform, to unify the notation.

The spectra of impulses shifted in time can be obtained from the Laguerre domain description of delay systems. In [2], it is shown that a pure (point) continuous time delay of duration τ between the output y and input u relates the Laguerre spectra according to

$$y_k = \mathrm{e}^{-\kappa/2}\left(\sum_{j=1}^{k} L_j^{(-1)}(\kappa)u_{k-j} + u_k\right). \tag{6}$$

Here $\kappa = 2p\tau$ and $L_k^{(-1)}$ denotes the associated Laguerre polynomial $L_k^{(\alpha)}|_{\alpha=-1}$ [16]. If the input signal is an impulse at time $\nu > 0$, so that the output impulse is delayed to time $\tau + \nu$, the relation

$$L_k(2p(\tau+\nu)) = \sum_{j=0}^{k} L_j^{(-1)}(2p\tau)L_{k-j}(2p\nu)$$

is obtained and, if furthermore $\nu = 0$, the result is

$$L_k(2p\tau) = \sum_{j=0}^{k} L_j^{(-1)}(2p\tau). \tag{7}$$

2.3 Impulse train

Consider now a finite sequence of impulses, i.e.

$$u(t) = \sum_{i=1}^{n} \lambda_i \delta(t-t_i), \tag{8}$$

where $\{\lambda_i\}$ is the set of the (real) impulse weights and $\{t_i\}$ is the ordered set of the positive impulse times. In the intended application areas, the impulse weights are normally non-negative, but this is not assumed in what follows. The Laguerre spectrum of (8) is given by

$$u_k = \sum_{i=1}^{n} \lambda_i l_k(t_i). \tag{9}$$

Introduce the following vector comprised of the coefficients

$$U_r^\intercal = \begin{bmatrix} u_0 & u_1 & \dots & u_r \end{bmatrix}.$$

This vector can be decomposed as

$$U_r = \Lambda_r W, \tag{10}$$

where

$$\Lambda_r = \begin{bmatrix} L_0(2pt_1) & L_0(2pt_2) & \dots & L_0(2pt_n) \\ L_1(2pt_1) & L_1(2pt_2) & \dots & L_1(2pt_n) \\ \vdots & \vdots & & \vdots \\ L_r(2pt_1) & L_r(2pt_2) & \dots & L_r(2pt_n) \end{bmatrix},$$

$$W^\intercal = \begin{bmatrix} w_1 & w_2 & \dots & w_n \end{bmatrix},$$

and

$$w_i = \sqrt{2p}\, \mathrm{e}^{-pt_i}\, \lambda_i.$$

The matrix Λ_r can be factorized in terms of the Vandermonde matrix

$$V_r = \begin{bmatrix} 1 & 1 & \dots & 1 \\ 2pt_1 & 2pt_2 & \dots & 2pt_n \\ \vdots & \vdots & & \vdots \\ (2pt_1)^r & (2pt_2)^r & \dots & (2pt_n)^r \end{bmatrix},$$

and the following lower triangular matrix with rows given by the Laguerre polynomial coefficients:

$$\Pi_r = \begin{bmatrix} c_0^0 & 0 & \dots & 0 \\ c_0^1 & c_1^1 & \dots & 0 \\ \vdots & \vdots & & \vdots \\ c_0^r & c_1^r & \dots & c_r^r \end{bmatrix},$$

where c_k^i is the coefficient of term k of Laguerre polynomial i. This leads to

$$U_r = \Pi_r V_r W,$$

where Π_r is known in advance. The matrix Π_r is also invertible since the diagonal elements, corresponding to the leading coefficients of the Laguerre polynomials, are always nonzero. This fact, together with the form of the matrices V_r and W, enables the calculation of $\{\lambda_i\}$ and $\{t_i\}$ from the elements of U_r by the matrix pencil method.

3 Estimation algorithm

3.1 The matrix pencil method

The matrix pencil method [20] is an estimation technique that can be applied to extract information from signals with an underlying matrix pencil structure. The method is based on the following matrix construction that enables the transformation of the estimation problem to a generalized eigenvalue problem.

Let $D_w = \operatorname{diag}(W)$, $D_\alpha = 2p \operatorname{diag}(T)$, where

$$T^\intercal = \begin{bmatrix} t_1 & t_2 & \dots & t_n \end{bmatrix},$$

and consider the pair of matrices

$$X_0 = V_{r-L-1} D_w V_{L-1}^\intercal, \quad X_1 = V_{r-L-1} D_w D_\alpha V_{L-1}^\intercal,$$

where $L \in \mathbb{N}$ is the so-called pencil parameter. If $n \leq L \leq r - n$, the non-zero generalized eigenvalues of the matrix pair X_1, X_0 are precisely the elements of D_α. The matrices X_0 and X_1 can furthermore be constructed from the vector $\tilde{U}_r = \Pi_r^{-1} U_r$. Denoting its elements

$$\tilde{U}_r^\intercal = \begin{bmatrix} \tilde{u}_0 & \tilde{u}_1 & \dots & \tilde{u}_r \end{bmatrix},$$

the i:th row and j:th column entries of X_0 and X_1 are respectively given by $\tilde{u}_{i+j-1}$ and $\tilde{u}_{i+j}$. It is therefore theoretically possible to determine the delay times $\{t_i\}$ by solving the generalized eigenvalue problem, and the weights $\{w_i\}$ by solving linear equation (10).

3.2 Related problems

The applicability of the matrix pencil method to the Laguerre domain impulse train estimation highlights the similarity between the problem at hand and other problems where the matrix pencil method is shown to be helpful. These typically involve sums of complex exponentials, e.g. in electromagnetic applications [17]. The connection to these problems can be further appreciated by considering the asymptotic relation (given in e.g. [16]) of Laguerre polynomials to trigonometric functions

$$L_k(z) = \frac{e^{\frac{z}{2}}}{\pi^{1/2}(kz)^{1/4}} \cos\left(2\sqrt{kz} - \frac{\pi}{4}\right) + O\left(\frac{1}{k^{3/4}}\right), \tag{11}$$

which holds as $k \to \infty$. The considered estimation problem can thus also be interpreted as the problem of finding the weights and frequencies of a sum of sinusoidals, albeit with frequencies and amplitudes that depend on k. One can in particular see a similarity to the problem of super-resolution, described in [4]. There, sparse data, in the form of an impulse sequence, are extracted from a frequency-limited Fourier transform of the signal.

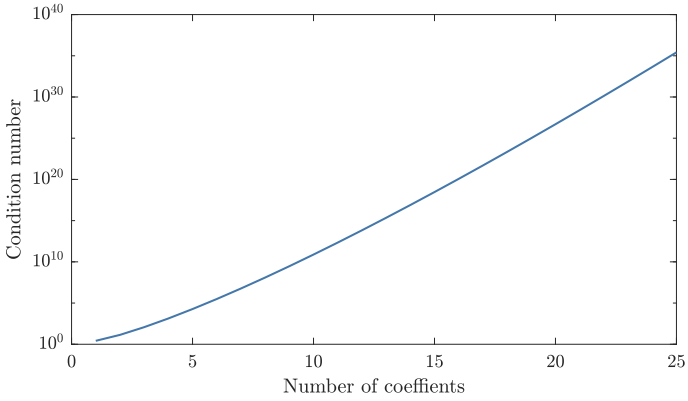

Figure 1: Condition number of Π_r as a function of r in logarithmic scale.

3.3 Numerical considerations

The following two observations regarding the numerical properties of the proposed method can be made:

1. The magnitude of the leading Laguerre polynomial coefficient decreases rapidly with the polynomial order, causing Π_r to be poorly conditioned.

2. If $t_i \approx t_k, i \neq k$, both Λ_r and V_r are poorly conditioned.

The first point is illustrated in Fig. 1. The condition number growth is faster than exponential, which makes numerical implementations sensitive to noise and limits the number of Laguerre coefficients that can be used in practice. The second point will be addressed later in this paper.

3.4 Impulse train estimation

Consider the problem of estimating the input impulse train given by (8), i.e. the sets $\{\lambda_i\}$ and $\{t_i\}$, along with their cardinality n, from the output $y(t)$ of (3). In the absence of uncertainty, the cardinality of the sets can be evaluated by the technique outlined in Section 3.1, since the number of non-zero generalized eigenvalues of the pair X_0, X_1 is the same as the number of impulses in the input train [20].

Following [20], uncertainty can be handled by utilizing a rank-truncated More-Penrose pseudo-inverse when the eigenvalue problem is solved. A singular value decomposition of X_0 is used for this purpose. Finding the number of impulses then becomes a matter of choosing a suitable threshold, under which singular values are discarded. However, the observed conditioning

problems of the matrices involved in the input impulse train estimation make this approach infeasible in the present case. Even with minimal noise levels, the thresholding method often fails to identify the correct generalized eigenvalues. A significant complication arises as the means of determining both the number of essential eigenvalues and which eigenvalues to choose to perform the estimation are missing.

To address the ill-posedness, an algorithm that utilizes the Laguerre parameter to regularize the problem and estimates the number of eigenvalues as well as their values is proposed. The Laguerre parameter is frequently used for this purpose, as the conditioning of Laguerre domain estimation problems generally depends on the parameter value, see, e.g., [19].

The method is outlined in Algorithm 1. It is based on an empirical observation that many Laguerre parameter values yield good estimates of t_i, but these estimates do not necessarily correspond to the largest singular values of X_0. Therefore, the Laguerre input and output spectra are evaluated, and the corresponding t_i are estimated, for different Laguerre parameter values. The algorithm then proceeds by identifying the t_i that most Laguerre parameter values have in common, and terminating the search once the similarity of the remaining t_i is too low.

4 Results

Algorithm 1 is applied to two types of data. First, analytically calculated Laguerre spectra of impulse trains corrupted by additive noise are utilized to generate synthetic data. Then the estimation is performed on a levodopa blood concentration profile from a clinical experiment. The same parameters for the estimation algorithm are used in both cases, see Table 1.

Table 1: Estimation parameters.

L	r	$p_{\min}$	$p_{\max}$	t_{tol}	α
7	13	0.04	5	0.02	0.3

4.1 Synthetic data

The Laguerre spectrum of two impulses with unitary weight, at times $t_1 = 1$, $t_2 = 1.5$, was analytically generated by means of (9). The low number of impulses is motivated by simplicity. White Gaussian noise was then added to the spectrum, with a standard deviation of 1% of the mean Laguerre

Algorithm 1 Laguerre impulse train identification

Set the following:
  Feasibility region R for delay times
  Minimal ratio α
  Delay time tolerance t_{tol}
Setup Laguerre parameter grid P of length m
for each p_i in P **do**
  Calculate output Laguerre spectrum
  Solve generalized eigenvalue problem
  Calculate corresponding delay time
  Let E_i include these times
end for
Discard delay times not in R
Sort remaining delay times in an array S
Let $n = 0$, $b =$ **true**
while b **do**
  $n = n + 1$
  Let S_n be the longest sequence in S, such that they are all equal within the tolerance t_{tol}
  if length of $S_n > \alpha m$ **then**
    Remove S_n from S
    Find all indices i such that no element of E_i is in S_n
    Remove all elements of E_i from S
  else
    Let $b =$ **false**
  end if
end while
for all i such that an element of E_i is in S_n **do**
  Find the elements of E_i that are in S_j, $1 \leq j \leq n$
  Solve for delay times and weights using these elements
end for

coefficient magnitude, and then Algorithm 1 was applied to recover the impulse times and weights.

The estimation results are illustrated in Fig. 2, where the estimation errors are plotted as function of p. The algorithm recovers the delay times and weights correctly, with a notable performance improvement for higher values of p. The uncertainties in both the delay time and the weight estimates are decreasing and a greater proportion of the Laguerre parameter values produce estimates within the prescribed tolerance. The result makes sense in view of (11), as a larger value of p yields a greater separation of the frequencies in this approximation.

Experiments where α and t_{tol} were changed were also performed at this point; α does not impact the estimation results significantly, while a smaller t_{tol} decreases the estimation errors, but increases the number of estimation fails.

The effect of the time separation between impulses was investigated next. The estimation was performed repeatedly with different values of t_2 such that $t_1 = 1 \leq t_2 \leq 1.5$. The results for different noise levels are presented in Fig. 3. In Fig. 4, the estimation result as function of impulse separation and Laguerre parameter value is displayed, with 1% noise. The ability to distinguish the delay times is clearly dependent on the noise level. Interestingly, the algorithm does not fail completely when the separation is too low, instead a single impulse between the true signals is identified. Although not being mathematically accurate, such merging estimate behavior is desirable in practice, where the effect of two impulses can be well approximated with a single one. There is however a transition region where neither one nor two impulses are estimated, which grows with the noise level. As demonstrated in [10], the sampled response of a linear system to two impulses is indistinguishable from the response to a single impulse, when the separation between the impulses is sufficiently small.

4.2 Experimental data

The levodopa plasma concentration measured in a patient diagnosed with Parkinson's disease was used in this estimation. The data come from a clinical experiment where a single dose of levodopa was administered orally after an overnight wash-out, as described in [15]. The concentration profile have been modified by removing a fixed offset caused by a low but non-zero initial levodopa plasma concentration of the patient. The dynamics are modelled as a linear second-order system driven by an impulse train as in [13]. The finite-dimensional model was identified using the least-squares-based algorithm from [10]. A corresponding Laguerre domain model was calculated and deconvolution with the estimated Laguerre spectrum of the

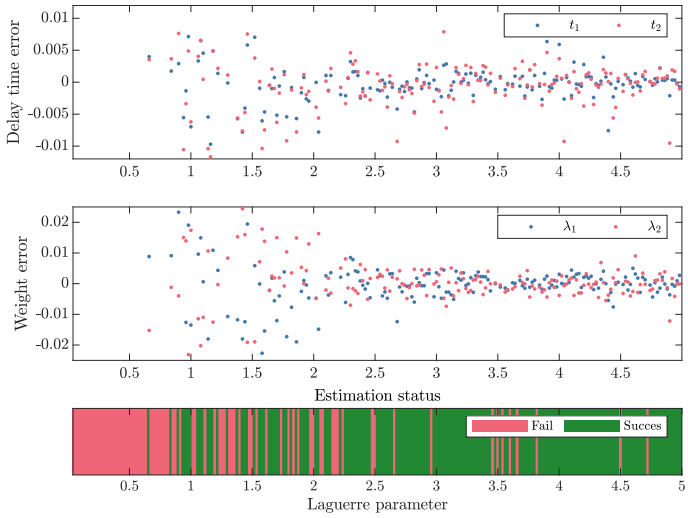

Figure 2: Errors of estimated impulse times and weights, and estimation status, as function of the Laguerre parameter p, for an impulse train with 1% additive noise.

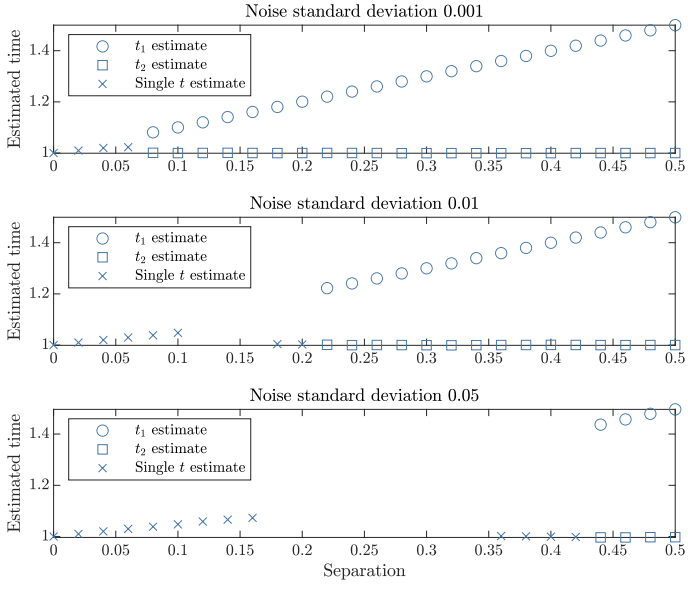

Figure 3: Estimated impulse times for different impulse time separations with 0.1%, 1% and 5% noise.

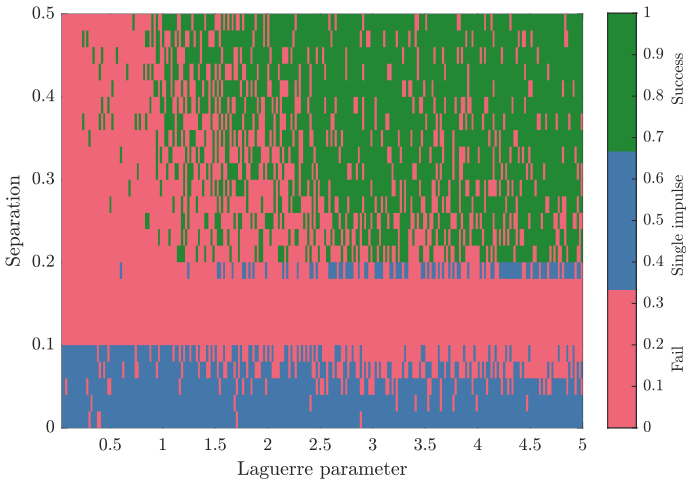

Figure 4: Estimation result as function of Laguerre parameter and impulse separation.

output was used to approximate the Laguerre spectrum of the impulse train.

Deconvolution is generally an ill-posed problem, with various regularization techniques suggested in literature to robustify solutions, see, e.g., [14]. In this work, the system

$$Y_r = \Theta U_r,$$

where Y_r is the output spectrum and

$$\Theta = \begin{bmatrix} J & 0 & \dots & 0 \\ HG & J & \dots & 0 \\ \vdots & & & 0 \\ HF^{r-1}G & HF^{r-2}G & \dots & J \end{bmatrix},$$

was solved directly for U_r, since a relatively low number of Laguerre coefficents is considered.

Algorithm 1 was then executed, yielding the delay time and weight estimates depicted in Fig. 5. There it can be seen that four impulses are identified in an interval of Laguerre parameter values. Fig. 6 shows that simulation of the estimated model gives a close resemblance between the results and the data, and the variations in the weight estimates produce negligible changes in the results. In Fig. 7, the estimated Laguerre spectra for the output and impulse train, for $p = 3.5$, are depicted.

This experiment highlights again the difficulty in differentiating between impulses with little separation in time. Here, two impulses rather than four

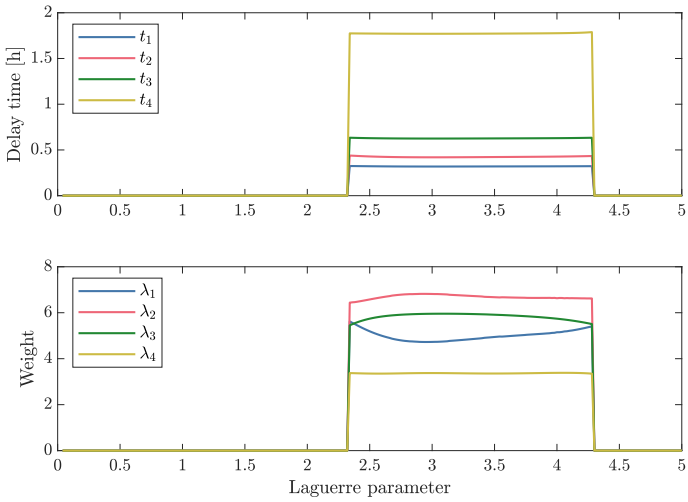

Figure 5: Estimated impulse times and weights as function of the Laguerre parameter p, for the levodopa data. The estimates are set to zero if they are outside the error tolerance.

would be intuitively expected, given the shape of the concentration profile. The three impulses used for the first peak is most likely a result of the linear interpolation of the rising front in the concentration profile, which cannot be well reproduced as the response of a single impulse.

5 Conclusions

A Laguerre domain approach to the problem of impulse train estimation from the output of an LTI system has been presented. Results from simulated and experimental data show that the proposed algorithm works as intended, and opens up for future research in this area. This includes improving the theoretical foundation of the algorithmic approach, further investigations of the observed impact of the Laguerre parameter value on the estimates, and possible extensions of the algorithm to allow for other classes of input signals.

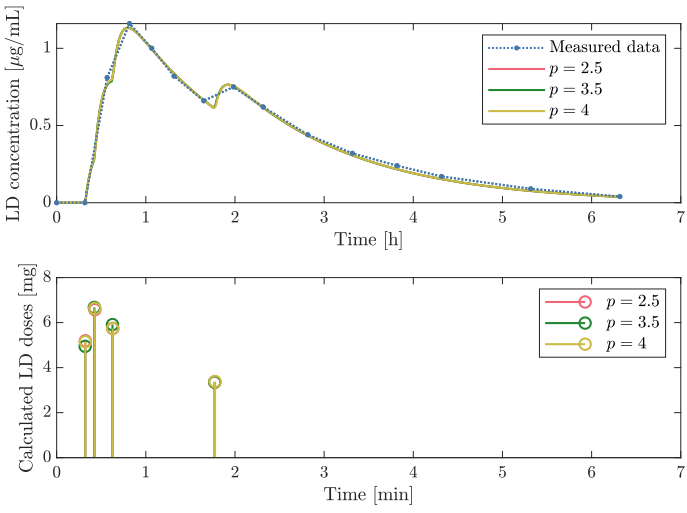

Figure 6: Comparison between simulated system and actual data, and the estimated impulses, for three Laguerre coefficients.

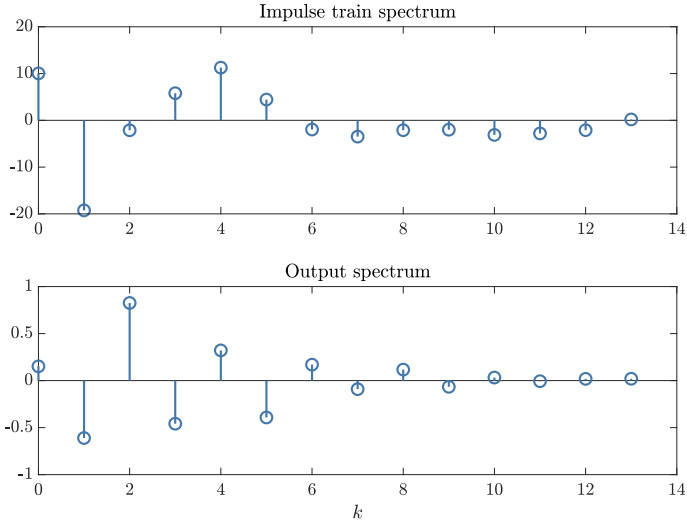

Figure 7: Estimated impulse train and output Laguerre spectra when $p = 3.5$.

References

[1] B. R. Fischer and A. Medvedev. Laguerre shift identification of a pressurized process. In *Proceedings of the 1998 American Control Conference. ACC (IEEE Cat. No.98CH36207)*, volume 3, pages 1933–1937 vol.3, 1998.

[2] B. R. Fischer and A. Medvedev. l_2 time delay estimation by means of Laguerre functions. In *Proceedings of the 1999 American Control Conference (Cat. No. 99CH36251)*, volume 1, pages 455–459 vol.1, 1999.

[3] N. M. Davies, J. K. Takemoto, D. R. Brocks, and J. A. Yanez. Multiple peaking phenomena in pharmacokinetic disposition. *Clinical Pharmacokinetics*, 49(6):351–377, 2010.

[4] D. L. Donoho. Superresolution via sparsity constraints. *SIAM Journal on Mathematical Analysis*, 23(5):1309–1331, 1992.

[5] M. L. Hartman, A. C. Faria, M. L. Vance, M. L. Johnson, M. O. Thorner, and J. D. Veldhuis. Temporal structure of in vivo growth hormone secretory events in humans. *American Journal of Physiology-Endocrinology and Metabolism*, 260(1):E101–E110, 1991. Publisher: American Physiological Society.

[6] E. Hidayat and A. Medvedev. Laguerre domain identification of continuous linear time-delay systems from impulse response data. *Automatica*, 48(11):2902–2907, 2012.

[7] J. Keilson and U. Sumita. A general Laguerre transform and a related distance between probability measures. *Journal of Mathematical Analysis and Applications*, 113(1):288–308, 1986.

[8] Y. W. Lee. *Statistical Theory of Communication.* John Wiley & Sons, Inc., New York, 1960.

[9] P. Mattsson and A. Medvedev. Estimation of input impulses by means of continuous finite-memory observers. In *2012 American Control Conference*, Montreal, Canada, 2012.

[10] P. Mattsson and A. Medvedev. Modeling of testosterone regulation by pulse-modulated feedback: An experimental data study. *AIP Conference Proceedings*, 1559(1):333–342, 2013.

[11] P. Mattsson and A. Medvedev. State estimation in linear time-invariant systems with unknown impulsive inputs. In *European Control Conference*, Zurich, Switzerland, 2013.

[12] A. Medvedev. Continuous least-squares observers with applications. *IEEE Transactions on Automatic Control*, 41(10):1530–1537, 1996.

[13] H. Runvik, A. Medvedev, and M. Kjellsson. Impulsive feedback modeling of levodopa pharmacokinetics subject to intermittently interrupted gastric emptying. In *2020 American Control Conference*, pages 1323–1328, 2020.

[14] S. M. Riad. The deconvolution problem: an overview. *Proceedings of the IEEE*, 74(1):82–85, 1986.

[15] M. Senek, D. Nyholm, and E. Nielsen. Population pharmacokinetics of levodopa/carbidopa microtablets in healthy subjects and Parkinson's disease patients. *European Journal of Clinical Pharmacology*, 74:1299–1307, 2018.

[16] G. Szegő. *Orthogonal polynomials*. American Mathematical Society, Providence, Rhode Island, 1975.

[17] T. K. Sarkar and O. Pereira. Using the matrix pencil method to estimate the parameters of a sum of complex exponentials. *IEEE Antennas and Propagation Magazine*, 37(1):48–55, 1995.

[18] J. Veldhuis, D. Keenan, and S. Pincus. Motivations and methods for analyzing pulsatile hormone secretion. *Endocrine Reviews*, 29(7):823–864, 2008.

[19] M. Verhaegen, D. Westwick, and R. Kearney. The use of a bilinear transformation of the shift operator in subspace model identification. *IEEE Transactions on Automatic Control*, 40(8):1422–1428, 1995.

[20] Y. Hua and T. K. Sarkar. Matrix pencil method for estimating parameters of exponentially damped/undamped sinusoids in noise. *IEEE Transactions on Acoustics, Speech, and Signal Processing*, 38(5):814–824, 1990.

Paper III

Title

Input sequence and parameter estimation in impulsive biomedical models

Authors

Håkan Runvik and Alexander Medvedev

Edited version of

H. Runvik and A. Medvedev. "Input sequence and parameter estimation in impulsive biomedical models". In *2022 European Control Conference (ECC)*. London, 2022.

Input sequence and parameter estimation in impulsive biomedical models

Abstract

A hybrid model for biomedical time series comprising a continuous second-order linear time-invariant system driven by an input sequence of positively weighted Dirac delta-functions is considered. The problem of the joint estimation of the input sequence and the continuous system parameters from output measurements is investigated. A solution that builds upon and refines a previously published least squares formulation is proposed. Based on a thorough analysis of the properties of the least squares solution, improvements in terms of accuracy and ease of use are achieved on synthetic data, compared to the original algorithm.

1 Introduction

Signals exhibiting slow, dissipative dynamics that are interrupted by multiple rapid bursts occur in many biological systems. Common examples are found in, e.g., endocrinology, since pulsatility is recognized as a fundamental property in the secretion of most hormones [9]. In pharmacokinetics, multi-peaking phenomena in drug concentration [2] can also display such characteristics. There is no generally accepted approach to mathematical modeling of these behaviors. In the endocrine case, a popular construct features a linear plant to portray the hormone elimination fed with an input signal that represents the secretion episodes. For instance, a Gaussian input signal shape is assumed in [6], which enables deconvolution-based input estimation.

To avoid additional assumptions, a pulsatile time series is modeled by a linear plant with impulsive input in this work. In closed loop, this setup

was developed for modeling testosterone regulation in [1], while a similar model was employed for pharmacokinetic applications in [4]. The estimation of the input sequence and continuous plant parameters is treated. Least squares (LS) methods were previously used to address this hybrid identification problem [5], [7], while a Laguerre domain approach was employed for the input estimation in [3]. The present work is based on the same optimization formulation as [7], where LASSO (least absolute shrinkage and selection operator) regularization was used. Yet, a more rigorous estimation procedure is achieved based on a comprehensive analysis of the underlying optimization problem. The main contribution is in the optimization problem analysis that underpins the theoretical foundation of the identification approach. Further, the resulting estimation method does not require user-defined data-dependent parameters and displays better performance as well as ease of implementation.

The rest of the paper is organized as follows. First, the model and estimation problem are formulated. Then, an analysis of the parameter-dependent characteristics of the LS solution is performed and shown to enable an efficient estimation of the parameters in the noise-free case. Finally, the method is generalized to account for noise and uncertainties and experimental results for synthetic data are presented.

2 Estimation problem

2.1 Model description

Consider the impulsive sequence

$$\xi(t) = \sum_{k=0}^{\infty} d_k \delta\left(t - \tau_k\right), \tag{1}$$

where $\delta(\cdot)$ is the Dirac delta function and d_k and τ_k determine the positive impulse weights and times. It is fed into a linear time-invariant compartmental state-space model

$$\dot{x} = Ax + B\xi(t), \quad y = Cx, \quad x = \begin{bmatrix} x_1 & x_2 \end{bmatrix}^\mathsf{T}, \tag{2}$$

where

$$A = \begin{bmatrix} -b_1 & 0 \\ g_1 & -b_2 \end{bmatrix}, \quad B = \begin{bmatrix} 1 \\ 0 \end{bmatrix}, \quad C = \begin{bmatrix} 0 \\ 1 \end{bmatrix}^\mathsf{T}, \tag{3}$$

with positive parameters b_1, b_2, g_1. Defining the Heaviside step function as $H(t)$ and assuming the initial state $x(t_0) = x_0$, the output of the system can

in a straightforward manner be calculated as

$$y(t) = C\Big(e^{A(t-t_0)}x_0 + \int_{t_0}^{t} \mathrm{e}^{A(t-\tau)}\, B\xi(\tau)\, \mathrm{d}\tau\Big)$$
$$= Ce^{A(t-t_0)}x_0 + \sum_{k=0}^{\infty} g_1 d_k z(b_1, b_2, t-\tau_k),$$

where

$$z(b_1, b_2, t) = \frac{\mathrm{e}^{-b_2 t} - \mathrm{e}^{-b_1 t}}{b_1 - b_2} H(t).$$

2.2 Estimation problem formulation

Let the output of (2) be sampled, possibly irregularly, over a finite horizon and result in the measurements $y(t_k)$, where $k = 1, \ldots, K$ and $t_k < t_{k+1}$, thus yielding the vector

$$Y = \begin{bmatrix} y(t_1) & \ldots & y(t_K) \end{bmatrix}^{\mathsf{T}}.$$

Since an impulse in between two sampling times cannot be distinguished in the sampled output from a pair of impulses that occur at the sampling times [7], the impulses are without loss of generality restricted to occur at the sampling times. Then it holds that

$$Y = \Phi(b_1, b_2)\theta, \tag{4}$$

where

$$\Phi(b_1, b_2) = \begin{bmatrix} \varphi(b_1, b_2, t_1) & \ldots & \varphi(b_1, b_2, t_K) \end{bmatrix}^{\mathsf{T}},$$

$$\varphi(b_1, b_2, t_i) = \begin{bmatrix} \mathrm{e}^{-b_2(t_i - t_1)} \\ z(b_1, b_2, t_i - t_1) \\ \vdots \\ z(b_1, b_2, t_i - t_K) \end{bmatrix},$$

$$\theta = \begin{bmatrix} x_2(t_1) & d_1 & \ldots & d_{K-1} \end{bmatrix}^{\mathsf{T}}.$$

Notice that $\Phi(b_1, b_2)$ is square and that the state $x_2(t_1)$ is included in the formulation rather than x_0, since $x_2(t_1)$ and d_1 uniquely determine the state of the system for $t > t_1$.

Further, the combined impulse and parameter estimation in system (2) is treated, i.e. the parameters $d_k, k = 1, \ldots, K$ and $b_i, i = 1, 2$ are sought. Notice that $g_1 = 1$ can be assumed, as changing this parameter corresponds to scaling of the impulses. Furthermore, assume that $b_1 < b_2$.

An LS optimization formulation introduced in [7] is employed to the problem in hand. In the estimation, $b_i^*, i = 1, 2$ denote the true parameter values while b_i represent the parameters in the LS formulation

$$\hat{\theta}(b_1, b_2) = \arg\min_{\theta} \|Y - \Phi(b_1, b_2)\theta\|^2, \tag{5}$$

where $\|\cdot\|$ is the Euclidean vector norm. The parameter-dependent objective function makes the setup resemble a multi-parametric programming problem (see, e.g., [8]). We also use the notation d_k^* for the true impulse weights while d_k represent their estimates for given parameter values b_1 and b_2 (we suppress the dependency for ease of notation).

In the noise-free case, the optimization formulation is unconstrained. The estimate of θ can therefore be calculated via a matrix inversion (the invertibility of Φ is shown in [7]). In the presence of noise or uncertainties, the impulse weights are restricted to be non-negative, which results in a constrained LS problem.

2.3 Estimation principle

In the noise-free case, the estimation is based on the following properties of the optimization problem in (5), which are given in Proposition 1.

- If $b_1 + b_2 > b_1^* + b_2^*$ and $b_1 > b_1^*$, all impulse estimates solving (5) have positive weights;
- If $b_1 + b_2 < b_1^* + b_2^*$ and $b_1 < b_1^*$, all impulse estimates solving (5) that do not correspond to true impulses have negative weight.

The properties above give rise to the division of the parameter space depicted in the left subplot of Fig. 1. The idea is to utilize the structure of this space to identify b_1^* and b_2^*. A problem arises in the regions marked as unknown, where the signs of the impulse weights solving the optimization problem vary depending on the data. However, theoretical reasoning regarding simplified cases (see Section 3.1) indicates that the parameter space will be divided qualitatively according to the right subplot of Fig. 1. This is also observed in numerical experiments. The quantitative behavior (i.e. the slopes of the curves) depends on the values of b_1^*, b_2^* and the distribution of impulses and sampling instances. This refined partitioning enables navigation in the parameter space to the point (b_1^*, b_2^*), as described in Section 3.2.

When noise or uncertainties are present, the parameter space is no longer divided in well-defined regions, as impulses of both signs typically appear in most of the parameter space. However, it is still possible to estimate the boundary of the region with positive impulses, which we denote γ_P. If the noise level is low enough, it is also possible to find an approximation of the true parameter values.

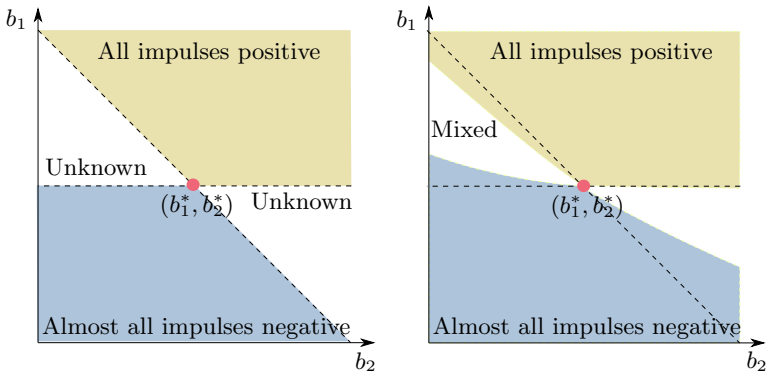

Figure 1: The division of the b_1-b_2 parameter space, relative to the true parameter values (b_1^*, b_2^*), in terms of the solutions to (5). Left: regions with guaranteed signs of impulse weights. Right: region boundaries according to the analysis in Section 3.1 and numerical experiments. "Mixed" indicates that both positive and negative impulses are present.

3 Noise-free estimation

We will first show how the b_1-b_2 parameter space is divided into the regions indicated above. The analysis is based on the following lemma.

Lemma 1. Let $y(t)$ be the response of system (2) to the input $d_1\delta(t - t_1)$ with $x_0 = \begin{bmatrix}0 & 0\end{bmatrix}^\mathsf{T}$. Denote the response of an estimate of (2) with the parameters $\hat{b}_1$, $\hat{b}_2$ to the input $\hat{d}_1\delta(t - \hat{t}_1)$ as $\hat{y}(t)$. Assume that $\hat{b}_1 + \hat{b}_2 > b_1 + b_2$, $\hat{b}_1 > b_1$ and $\hat{b}_1 > \hat{b}_2$. Then, there exist at most two $\tau > \max\{t_1, \hat{t}_1\}$ such that $y(\tau) = \hat{y}(\tau)$.

Proof. See Appendix A. □

Provided that the impulse sequence is sparse (i.e. that the set S below is nonempty), the result above can be used to characterize the properties of the solution to (2) in two cases, where the estimated system is either faster or slower than the true dynamics. These are defined in the following proposition.

Proposition 1. Consider LS problem (5) with the initial condition $x_2(t_1) = 0$. Assume that the noise-free measurements Y are produced by (2) and let $S = \{k \in \{1, \dots, K\} \mid d_k^* = 0\}$. If $b_1 + b_2 > b_1^* + b_2^*$ and $b_1 > b_1^*$, then $d_k > 0$ for $k = 1, \dots K$. If $b_1 + b_2 < b_1^* + b_2^*$ and $b_1 < b_1^*$, then $d_k < 0$ for $k \in S$.

Proof. See Appendix B. □

Note that Lemma 1 and Proposition 1 apply only when the initial state is zero, while the optimization formulation in (5) allows a nonzero initial value for x_2 (a nonzero initial x_1 can be represented by an impulse and is thus not included in the estimation). However, since the contribution from the initial state tends to zero exponentially, the proposition is expected to hold in the case of nonzero initial conditions too.

3.1 Boundaries of the sign-definite impulse regions

The proposition above does not provide information about the region which is marked as unknown in the left subplot of Fig. 1. To gain understanding of the behavior in this region, consider a simplified case of three sampled measurements of the response to a single impulse at time $t = 0$. Denote it as $y^*(t)$ and assume that it is generated by (2) with the parameter values b_1^*, b_2^*. Let $y(t)$ be the response of the same system but with parameters b_1, b_2. The boundary between solutions with positive and negative impulse weights is then defined by the case when $y(t)$ intersects $y^*(t)$ precisely at the sampling times (i.e. no additional positive or negative impulses are required to explain the behavior). If the curves intersect at the times τ, ν, μ, the relation between b_1, b_2 and b_1^*, b_2^* is given by a solution to the equation

$$(\chi^\tau - \psi^\tau)(\omega^\mu - \omega^\nu) + (\chi^\nu - \psi^\nu)(\omega^\tau - \omega^\mu) + (\chi^\mu - \psi^\mu)(\omega^\nu - \omega^\tau) = 0, \quad (6)$$

where $\chi = \mathrm{e}^{b_1 - b_2^*}$, $\psi = \mathrm{e}^{b_1 - b_1^*}$ and $\omega = \mathrm{e}^{b_1 - b_2}$. Note that equation (6) has $b_1 = b_2$ as another, infeasible solution. By solving (6) for ω, an expression for b_2 would be obtained. However, since solving (6) algebraically for ω is not possible in a general case, only equidistant sampling, i.e. $\nu = \tau + c, \mu = \tau + 2c$, where $c > 0$, is considered. The feasible solution then becomes

$$b_2 = b_1 - \ln(\omega) = b_1 - \frac{1}{c} \ln\Big(\frac{\chi^{\tau+c} - \chi^{\tau+2c} - \psi^{\tau+c} + \psi^{\tau+2c}}{\chi^\tau - \chi^{\tau+c} - \psi^\tau + \psi^{\tau+c}}\Big) \triangleq b_1 - \frac{1}{c} \ln\Big(\frac{\omega_1}{\omega_2}\Big),$$

where the solution naturally is $b_2 = b_2^*$ if $b_1 = b_1^*$. Taking the derivative with respect to b_1 yields

$$\frac{db_2}{db_1} = -1 + (\chi^{\tau+c} - \psi^{\tau+c})\Big(\frac{1}{\omega_1} - \frac{1}{\omega_2}\Big).$$

Since $b_1 < b_2$, it follows that $\chi < \psi$ and $0 < \omega_1 < \omega_2$. That leads to the inequality

$$-\infty < \frac{db_2}{db_1} < -1.$$

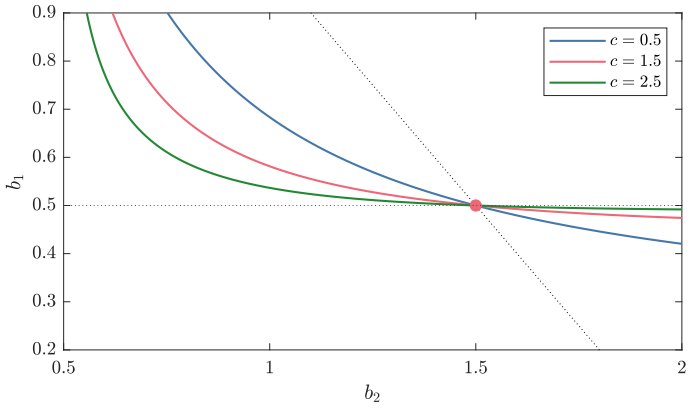

Figure 2: The pairs of estimates b_1, b_2 resulting in intersections between $y(t)$ and $y^*(t)$ at times $1, 1+c, 1+2c$ for different values of c and $b_1^* = 0.5$, $b_2^* = 1.5$. The dotted lines represent the theoretical limits for the borders given in Proposition 1.

The second derivative, given by

$$\frac{d^2 b_2}{db_1^2} = c\big(\chi^{\tau+c} - \psi^{\tau+c}\big)\Big(-\frac{1}{\omega_1} - \frac{1}{\omega_2} + \big(\chi^{\tau+c} - \psi^{\tau+c}\big)\Big(\frac{1}{\omega_1^2} - \frac{1}{\omega_2^2}\Big)\Big) > 0,$$

shows that the derivative changes monotonously. Finally, if the samples are shifted in time relative to the impulse, b_2 changes according to

$$\frac{db_2}{d\tau} = \frac{1}{c}(b_1 - b_2)\psi^{\tau+c}(1-\psi^c)\big(\frac{1}{\omega_2} - \frac{1}{\omega_1}\big).$$

If $b_1 < b_1^*$, then $\psi < 1$, which makes the expression positive, while $b_1 > b_1^*$ makes it negative, i.e. a shift in time causes a pivot of the curve around the point (b_1^*, b_2^*). The resulting curves are illustrated in Fig. 2.

If more than three measurements are considered, each triplet of measurements generates a separate b_2-boundary. For a non-equidistant triplet, the qualitative behavior of the corresponding solution to (6) appears to be similar to that of the equidistant case in numerical experiments. Since a solution with only positive impulses requires that parameter estimates are above all these boundaries, the limiting case, which defines the curve γ_P, corresponds to the largest value of b_2 for a given b_1. For solutions with almost all impulses being negative, the converse holds. Adding more impulses does not alter this behavior. As all boundaries intersect at $b_1 = b_1^*$, $b_2 = b_2^*$, and triplets with different time shifts produce different slopes according to the above discussion, this explains the non-smoothness of the boundaries at

this point illustrated in Fig. 1. Note that the presented analysis only is valid if the impulses are sufficiently sparse, i.e. there are instances with at least three sampling times in between two impulses.

3.2 Estimation algorithm

The following procedure is suggested to solve the estimation problem in the absence of noise. Let $d(c)$ denote the distance between the pair of points where the boundaries of the positive and negative impulse regions (see Fig. 1) intersect with the line $b_1 = 2b_2 + c$. Since the boundaries meet at the point (b_1^*, b_2^*), minimization of $d(c)$ with respect to c recovers the values of b_1^* and b_2^*. The points of intersection which determine $d(c)$ can be calculated with the bisection method, by considering the signs of the estimated impulse weights obtained from solving (5) at points along the line $b_1 = 2b_2 + c$. Once b_1^* and b_2^* are calculated, Algorithm 1 in [7] is used to calculate the impulse times and weights.

No further details on this algorithm are provided, as only estimation under uncertainties is relevant in applications.

4 Estimation under uncertainty

4.1 Estimation of b_1 and b_2

To represent noise or model uncertainty, we consider the modification of (4)

$$Y = \Phi(b_1, b_2)\theta + \epsilon,$$

where ϵ is a zero-mean noise vector. The parameter space is then no longer divided as in Fig. 1, since the region of mixed impulse weights then covers a larger area and, in particular, includes (b_1^*, b_2^*). A non-negativity constraint for the impulse weights is for this reason added to (5). In the absence of noise, this would leave the region above γ_P unaffected, while rendering the residual sum of squares

$$\|Y - \Phi(b_1, b_2)\hat{\theta}(b_1, b_2)\|^2 \triangleq g(b_1, b_2) \tag{7}$$

nonzero in the rest of the parameter space. In particular, for a fixed value $b_2 = \bar{b}_2$ such that $(\bar{b}_1, \bar{b}_2)$ is on γ_P, $g(b_1, \bar{b}_2)$ is expected to be decreasing in b_1 when $b_1 < \bar{b}_1$. In the noisy setting, the qualitative behavior tends to be similar, but the residual sum is nonzero even for $b_1 > \bar{b}_1$. We will utilize this property to estimate γ_P using the following result.

Lemma 2. Let $f(x) = c_1(x - x^*)^2 + c_2$, where $c_1, c_2 > 0$. Define $N_f(x)$ and $\hat{x}$ by

$$N_f(x) = -\frac{f(x)}{df(x)/dx},$$

$$\begin{aligned} \hat{x} &= \arg\min_x N_f(x) + \min_x N_f(x), \\ \text{s.t. } & \min_x N_f(x) > 0. \end{aligned}$$

Then $\hat{x} = x^*$.

Proof. Straightforward minimization. □

The minimization problem stated in the lemma is applied to the residual sum of squares $g(b_1, \bar{b}_2)$, i.e. the function is assumed to be approximately quadratic, somewhat similarly to Newton's method in optimization. The point of this technique is that the objective function only is required to be quadratic below γ_P, so the optimization can be performed even though $g(b_1, \bar{b}_2)$ does not have a unique minimum close to γ_P.

Generalizing to incorporate both b_1 and b_2 in the formulation, and constraining the permitted number of impulses (mimicking the effect of the constraint on $\min N_f$ above), we arrive at the formulation

$$\begin{aligned} (\hat{b}_1, \hat{b}_2) &= \arg\min_{b_1,b_2} N_g(b_1, b_2) + \min_{b_1,b_2} N_g(b_1, b_2), \\ &\text{s.t. } \#\{d_k > d_{\min}\} \leq \Pi, \end{aligned} \tag{8}$$

where

$$N_g = \frac{-g(b_1, b_2)}{\partial g(b_1, b_2)/\partial b_1},$$

Π is the maximal permitted number of impulses, $d_{\min}$ is the threshold for counting an impulse and # denotes cardinality. It should be noted that the cost function, together with the impulse number constraint, constitute a nonconvex optimization problem which admits multiple local minima.

It is however not obvious that a solution to (8) approximates (b_1^*, b_2^*), and not some other point on γ_P. Indeed, the numerical experiments in the next section demonstrate that the estimation works well with relatively low levels of noise and a frequent sampling, but with a higher noise level, only an estimate $\hat{\gamma}_P$ of this boundary can be found. The corresponding optimization formulation then becomes

$$\begin{aligned} \bar{b}_1 &= \arg\min_{b_1} N_g(b_1, \bar{b}_2) + \min_{b_1} N_g(b_1, \bar{b}_2), \\ &\text{s.t. } \#\{d_k > d_{\min}\} \leq \Pi, \end{aligned} \tag{9}$$

where $(\bar{b}_1, \bar{b}_2)$ is the intersection between $\hat{\gamma}_P$ and $b_2 = \bar{b}_2$.

4.2 Estimation algorithms

As the optimization problems (8), (9) are non-convex, we use gridding to solve them, utilizing the finite difference over the grid points to approximate the derivative in N_g. That means that, in the low-noise case, the parameter combination in the grid which minimizes N_g is used in the calculation, while in the high-noise case, for each b_2-grid point, the minimizing b_1 is used. Finally, to determine the location and weights of the impulses, all impulses below a user-defined threshold are removed and adjacent impulses are merged. The resulting procedure is summarized in Algorithm 1.

Algorithm 1 Impulse and time constant estimation

1: Calculate $(\hat{b}_1, \hat{b}_2)$ from (8) (low noise) *or* solve (9) for $\bar{b}_1 = \hat{b}_1$ for a given $\bar{b}_2 = \hat{b}_2$ (high noise)
2: Calculate $\hat{\theta}(\hat{b}_1, \hat{b}_2)$ from (5)
3: Let $S = \{k \in \{1, \ldots, K\} \mid \hat{d}_k < d_{\min}\}$
4: Solve (5) with all d_k with $k \in S$ constrained to be zero
5: Merge adjacent non-zero impulses according to Algorithm 1 in [7]

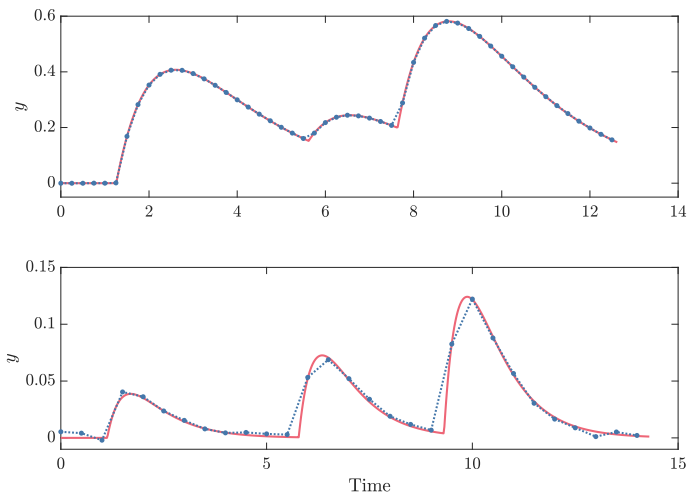

Figure 3: Examples of sampled synthetic data with low (top) and high (bottom) levels of additive measurement noise.

5 Numerical experiments

The proposed estimation technique is evaluated on synthetic data consisting of the response to three impulses with additive zero-mean Gaussian measurement noise. Two Monte Carlo experiments with 100 realizations were performed; one with low noise variance (experiment A) and one with a more realistic (i.e. higher) noise level (experiment B). In the former case, a comparison is made with the implementation in [7]. The parameters of the experiments are specified in Table 1, while examples of data realizations are shown in Fig. 3. The parameter values of the estimation algorithms are given in Table 2.

Table 1: Monte Carlo experiment parameter distributions (left) and fixed values (right). $U_{[\cdot,\cdot]}$ denotes uniform distribution, $\Delta\tau_i$ and Δt_i are the time separation between consecutive impulses and samples respectively, σ is the noise standard deviation and τ_{end} is the time between the last impulse and the end of the time horizon.

b_1^*	$U_{[0.4,1.4]}$
$b_2^* - b_1^*$	$U_{[0.3,1.3]}$
d_i^*	$U_{[0.1,1]}$
$\Delta\tau_i$	$U_{[1,5]}$

	A	B
σ	2×10^{-4}	0.0015
Δt_i	0.25	0.5
τ_{end}	5	5

Table 2: Estimation algorithm parameters. Δb is the distance between the grid points and $\bar{d}$ denotes the mean impulse weight.

b_1 range	$[0.5b_1^*, 0.5(b_1^* + b_2^*))$
b_2 range	$[0.5(b_1^* + b_2^*), 1.5b_2^*]$
Δb	0.02
$d_{\min}$	$0.05\bar{d}$
Π	$0.5K$

5.1 Estimation from low noise data

The low-noise version of Algorithm 1 was used on synthetic data with additive measurement noise of low variance. The results are compared with the ℓ_1-constrained estimation algorithm in [7], implemented with the same b_1-b_2-grid. To account for the regularization that is required in that method,

gridding was also performed over possible values of the regularization parameter $\lambda_{\max}$, and the Akaike information criterion was used to determine its value. As displayed in Table 3, the current implementation performs better.

Table 3: Root mean squared errors for parameters estimated using Algorithm 1 ($A1$) and regularized LS [7] ($A2$).

	$A1$	$A2$
b_1	0.0105	0.0234
b_2	0.0255	0.0582
d_i	0.0164	
τ_i	0.0745	

The estimated input was also evaluated. In 78% of the realizations, a correct number of impulses were estimated whereas the remaining had an average of 1.77 extra impulses caused by the noise. The impulses corresponding to the true input sequences were identified, and the resulting estimation errors are given in Table 3. Both the timing and weights of the impulses are estimated with satisfactory accuracy.

5.2 Estimation from realistic data

Here the high-noise version of Algorithm 1 was employed on data with a higher noise level, and less frequent sampling than the previous case, over a grid of b_2-values. In Fig. 4, the estimate $\hat{\gamma}_P$ for one data set is displayed, together with the true parameter values and γ_P. The resulting average Euclidean distance between $\hat{\gamma}_P$ and (b_1^*, b_2^*) over all realizations is 0.0122. The curve evidently tends to be close to the true parameters, but a strategy to obtain the best estimate along this curve has not been found.

6 Conclusions

A novel estimation technique for a class of continuous second-order systems with impulsive input has been presented. It builds upon previous work [7], but outperforms that method on synthetic data with low noise and also has the advantage of not requiring any data-dependent user-defined parameters. Under strong uncertainty, only an implicit relation between the plant parameters can be determined. It is hypothesized that under such circumstances, unique parameter values generally cannot be reliably estimated. A more thorough analysis of this issue, and its implications on estimations from clinical data, are possible future research directions.

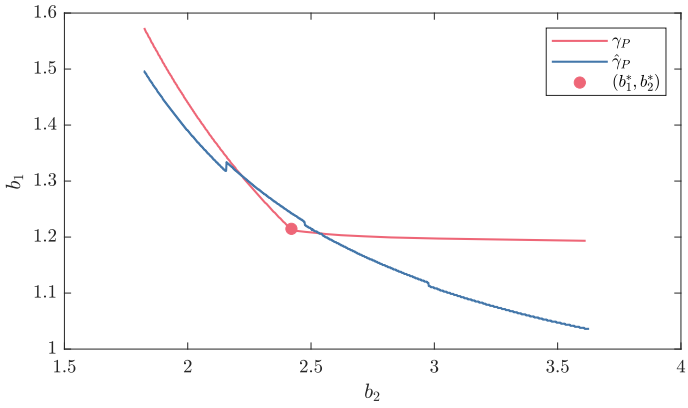

Figure 4: The γ_P-boundary, its estimate $\hat{\gamma}_P$ generated using Algorithm 1 (with a higher grid resolution for improved visual appearance), and the true parameter values for one synthetic data realization.

A Proof of Lemma 1

Let $\hat{x}_i, i = 1, 2$ denote the states of the estimated system. First, consider the case of the two outputs being tangent for some $\tau > \max\{t_1, \hat{t}_1\}$, i.e. $x_2(\tau) = \hat{x}_2(\tau)$ and $\dot{x}_2(\tau) = \dot{\hat{x}}_2(\tau)$. The dynamics for x_2 and $\hat{x}_2$ then gives

$$\hat{x}_1(\tau) = x_1(\tau) + (\hat{b}_2 - b_2)x_2(\tau), \tag{10}$$

which is used to calculate second derivative:

$$\begin{aligned} \ddot{\hat{x}}_2(\tau) - \ddot{x}_2(\tau) &= \dot{\hat{x}}_1(\tau) - \hat{b}_2\dot{\hat{x}}_2(\tau) - \dot{x}_1(\tau) + b_2\dot{x}_2(\tau) \\ &= (b_1 - \hat{b}_1 + b_2 - \hat{b}_2)x_1(\tau) + (b_2 - \hat{b}_1)(\hat{b}_2 - b_2)x_2(\tau). \end{aligned} \tag{11}$$

Two separate cases establish the sign of this expression:

- If $\hat{b}_2 - b_2 \leq 0$ then $(b_2 - \hat{b}_1)(\hat{b}_2 - b_2) \leq 0$, so $\ddot{\hat{x}}_2(\tau) - \ddot{x}_2(\tau)$ is negative since $(b_1 - \hat{b}_1 + b_2 - \hat{b}_2) < 0$;
- If $\hat{b}_2 - b_2 > 0$, then (10) implies $\hat{x}_1(\tau) > x_1(\tau)$ and thus $\dot{\hat{x}}_1(\tau) = -\hat{b}_1\hat{x}_1(\tau) < -b_1x_1(\tau) = \dot{x}_1(\tau)$. Applying this to the first row of (11) gives $\ddot{\hat{x}}_2(\tau) - \ddot{x}_2(\tau) < 0$.

It follows that $\hat{x}_2(t) \leq x_2(t)$ in a neighborhood of τ.

Now assume that $x_2(\nu) = \hat{x}_2(\nu)$, for some $\nu \neq \tau$ and that there are no intersections between $x_2(t)$ and $\hat{x}_2(t)$ for t between τ and ν (otherwise use that intersection to define ν). Using (10) and the dynamics of the first states

$$x_1(t) = d_1\,\mathrm{e}^{-b_1(t-t_1)}, \quad \hat{x}_1(t) = \hat{d}_1\,\mathrm{e}^{-\hat{b}_1(t-\hat{t}_1)},$$

an expression for $\dot{\hat{x}}_2(\nu) - \dot{x}_2(\nu)$ can be calculated as

$$\begin{aligned}\dot{\hat{x}}_2(\nu) - \dot{x}_2(\nu) &= (b_2 - \hat{b}_2)x_2(\nu) + \hat{x}_1(\nu) - x_1(\nu) \\ &= (\hat{b}_2 - b_2)\big(x_2(\tau)\,\mathrm{e}^{-\hat{b}_1(\nu-\tau)} - x_2(\nu)\big) + x_1(\tau)\big(\,\mathrm{e}^{-\hat{b}_1(\nu-\tau)} - \mathrm{e}^{-b_1(\nu-\tau)}\,\big) \\ &= \frac{d_1}{b_1 - b_2}\Big((\hat{b}_2 - b_2)\,\mathrm{e}^{-b_2\nu}(\mathrm{e}^{(\nu-\tau)(b_2-\hat{b}_1)} - 1) \\ &\qquad + (b_1 - \hat{b}_2)\,\mathrm{e}^{-b_1\nu}(\mathrm{e}^{(\nu-\tau)(b_1-\hat{b}_1)} - 1)\Big).\end{aligned}$$

Since $\dot{\hat{x}}_2(\nu) - \dot{x}_2(\nu) = 0$ for $\nu = \tau$, the sign is established by the derivative

$$\begin{aligned}&\frac{d}{d\tau}(\dot{\hat{x}}_2(\nu) - \dot{x}_2(\nu)) \\ &= \frac{d_1}{b_1 - b_2}\Big((\hat{b}_2 - b_2)(\hat{b}_1 - b_2)\,\mathrm{e}^{-\hat{b}_1(\nu-\tau) - b_2\tau} + (b_1 - \hat{b}_2)(\hat{b}_1 - b_1)\,\mathrm{e}^{-\hat{b}_1(\nu-\tau) - b_1\tau}\Big).\end{aligned}$$

Now use $\hat{b}_2 - b_2 > b_1 - \hat{b}_1$, $\hat{b}_1 - b_2 > b_1 - \hat{b}_2$ to get

$$\begin{aligned}&\frac{d}{d\tau}(\dot{\hat{x}}_2(\nu) - \dot{x}_2(\nu)) \\ &> \frac{d_1}{b_1 - b_2}\Big((b_1 - \hat{b}_1)(b_1 - \hat{b}_2)\,\mathrm{e}^{-\hat{b}_1(\nu-\tau) - b_2\tau} + (b_1 - \hat{b}_2)(\hat{b}_1 - b_1)\,\mathrm{e}^{-\hat{b}_1(\nu-\tau) - b_1\tau}\Big) \\ &= \frac{d_1}{b_1 - b_2}(b_1 - \hat{b}_1)(b_1 - \hat{b}_2)\,\mathrm{e}^{-\hat{b}_1(\nu-\tau)}\big(\,\mathrm{e}^{-\tau b_2} - \mathrm{e}^{-\tau b_1}\,\big) > 0.\end{aligned}$$

This implies that $\dot{\hat{x}}_2(\nu) - \dot{x}_2(\nu)$ is positive when $\tau > \nu$, which in turn implies that $\hat{x}_2(t) > x_2(t)$ for $t > \nu$ and close to ν. Since $x_2(t)$ and $\hat{x}_2(t)$ are continuous and there are no intersections between $x_2(t)$ and $\hat{x}_2(t)$ for $\nu < t < \tau$, this is contradictory with $\hat{x}_2(t) \leq x_2(t)$ for t in a neighborhood of τ. Since the case $\tau < \nu$ leads to a contradiction in the same way, one can conclude that if $x_2(\tau) = \hat{x}_2(\tau)$ and $\dot{x}_2(\tau) = \dot{\hat{x}}_2(\tau)$, a $\nu \neq \tau$ such that $x_2(\nu) = \hat{x}_2(\nu)$ does not exist.

Now suppose that there are more than two intersections between $x_2(t)$ and $\hat{x}_2(t)$. Since $\hat{x}_2(t)$ depends linearly on $\hat{d}_1$, it is then possible to reduce this weight until two of the intersections are reduced to one tangent point, while other intersections still exist (or possibly also are reduced to tangent points). But in the tangent case, there can be no other intersections between the curves, so there cannot be more than two intersections between $x_2(t)$ and $\hat{x}_2(t)$.

B Proof of Proposition 1

We only show the case $b_1 + b_2 > b_1^* + b_2^*$ and $b_1 > b_1^*$, as a similar technique can be used in the other case.

Let $x_i^*, i = 1, 2$ and $x_i, i = 1, 2$ respectively denote the states of the true and the estimated system. Consider the output of the estimated system, if it were driven by the same impulses as the true system. Since $x_2(t)$ depends monotonously on both $b_1 - b_2$ and b_2, it then follows that $x_2(t) < x_2^*(t)$ for all $t > t_1$. Since $x_2(t)$ depends linearly on the impulse weights, the weight of the first impulse d_1 can be increased so that $x_2(t_2) = x_2^*(t_2)$. Utilizing the asymptotic behavior of the systems and Lemma 1, it can be shown that in this case $x_2(t) < x_2^*(t)$ for $t > t_2$. Now apply the same technique for the whole optimization horizon, i.e. at every t_k, increase the impulse weight (generally from zero) so that $x_2(t_{k+1}) = x_2^*(t_{k+1})$. Since this results in a solution that is optimal, and the solution is unique (see [7]), it follows that all estimated impulses are positive.

References

[1] A. Churilov, A. Medvedev, and A. Shepeljavyi. Mathematical model of non-basal testosterone regulation in the male by pulse modulated feedback. *Automatica*, 45(1):78 – 85, 2009.

[2] N. M. Davies, J. K. Takemoto, D. R. Brocks, and J. A. Yanez. Multiple peaking phenomena in pharmacokinetic disposition. *Clinical Pharmacokinetics*, 49(6):351–377, 2010.

[3] H. Runvik and A. Medvedev. Laguerre domain estimation of an input impulse train to a continuous linear time-invariant system. In *2020 59th IEEE Conference on Decision and Control (CDC)*, pages 4622–4627, Dec. 2020.

[4] H. Runvik, A. Medvedev, and M. C. Kjellsson. Impulsive feedback modeling of levodopa pharmacokinetics subject to intermittently interrupted gastric emptying. In *2020 American Control Conference (ACC)*, pages 1323–1328, July 2020.

[5] E. Hidayat and A. Medvedev. Parameter estimation in a pulsatile hormone secretion model. Technical Report 2010-007, Department of Information Technology, Uppsala University, Mar. 2010.

[6] M. L. Johnson, L. Pipes, P. P. Veldhuis, L. S. Farhy, R. Nass, M. O. Thorner, and W. S. Evans. Chapter 15 AutoDecon: A robust numerical method for the quantification of pulsatile events. In *Methods in Enzymology*, volume 454, pages 367–404. Academic Press, Jan. 2009.

[7] P. Mattsson and A. Medvedev. Modeling of testosterone regulation by pulse-modulated feedback: An experimental data study. *AIP Conference Proceedings*, 1559(1):333–342, September 2013.

[8] R. Oberdieck, N. A. Diangelakis, I. Nascu, M. M. Papathanasiou, M. Sun, S. Avraamidou, and E. N. Pistikopoulos. On multi-parametric programming and its applications in process systems engineering. *Process Systems Engineering - A Celebration in Professor Roger Sargent's 90th Year*, 116:61–82, Dec. 2016.

[9] J. D. Veldhuis, D. M. Keenan, and S. M. Pincus. Motivations and methods for analyzing pulsatile hormone secretion. *Endocrine Reviews*, 29(7):823–864, Dec. 2008.

Paper IV

Title

Robust one-step estimation of impulsive time series

Authors

Håkan Runvik and Alexander Medvedev

Edited version of

H. Runvik and A. Medvedev. "Robust one-step estimation of impulsive time series". *arXiv preprint, arXiv:2304.13394*. 2023.

Robust one-step estimation of impulsive time series

Abstract

The paper deals with the estimation of a signal model in the form of the output of a continuous linear time-invariant system driven by a sequence of instantaneous impulses, i.e. an impulsive time series. This modeling concept arises in, e.g., endocrinology when episodic hormone secretion events and elimination rates are simultaneously estimated from sampled hormone concentration measurements. The pulsatile secretion is modeled with a train of Dirac impulses constituting the input to a linear plant, which represents stimulated hormone secretion and elimination. A previously developed one-step estimation algorithm effectively resolves the trade-off between data fit and impulsive input sparsity. The present work improves the algorithm so that it requires less manual tuning and produces more accurate results through the use of an information criterion. It is also extended to handle outliers and unknown basal levels that are commonly recognized issues in biomedical data. The algorithm performance is evaluated both theoretically and experimentally on synthetic and clinical data.

1 Introduction

Estimating the parameters of a dynamical model from measured data is a fundamental part of system identification. Typically, knowledge of both input and output signals is assumed, but in some applications, the input can neither be controlled, nor measured. In such cases, the identification is a matter of time-series estimation. The present paper considers a particular setup of this type, where the input signal consists of a sequence of impulses, and the parameters and the input signal are estimated from sampled measurements of the model output, which consequently are termed as an impulsive time series.

Impulsive time series estimation is particularly relevant in biological contexts, where systems driven by intrinsic impulsive feedback mechanisms that are hard to measure or model sometimes occur. Typical examples include gait models [14], muscle activation [9], and population models in ecology [8]. We will focus on a problem in endocrinology, where the secretion events and clearance rates of hormones are estimated from blood concentration measurements. In the traditional approach for solving this problem, each secretion event is represented by a function of a predefined shape, while a linear hormone clearance model is used. As a result, the output of the system is given by a convolution integral, and the model estimation constitutes a deconvolution problem. Software utilizing deconvolution include AutoDecon [5] and WINSTODEC [17]; see also the overview in [3]. Other methods that have been proposed include the Bayesian approach in [6] and the constrained least squares formulation in [11]. The present method builds upon the latter work where Dirac impulses, rather than continuous functions, are utilized to represent the pulsatile secretion.

Due to physiological, ethical, and experimental limitations, the sampling rate of clinical endocrine data is often low compared to the half-life times of the involved substances. Combined with uncertainties in both measurements and models, this leads to a challenging estimation problem. There is in particular a fundamental trade-off between impulsive input sparsity and fit to data that needs to be addressed, regardless of which estimation technique that is employed. For example, the deconvolution methods mentioned above implement statistical tests (AutoDecon) and regularization (WINSTODEC) to avoid overfitting.

The goal of the current work is to formulate and solve the combined parameter and input estimation problem in a way that, on the one hand, imposes minimal additional assumptions, heuristics or manual tuning, and on the other hand, is feasible when faced with the challenges related to clinical data, such as measurement outliers and unknown basal levels. A hybrid model, i.e., a model where both continuous and discrete dynamics are included, turns out to be beneficial for this goal. The model we use is based on the closed-loop model of testosterone regulation introduced in [12, 1], with the feedback mechanism disregarded in the current work. The secretion events are represented by instantaneous impulses in this model. Naturally, such impulses are mathematical constructs that do not occur in real biological systems, but when the duration of the secretion bursts is significantly shorter than the sampling time of the series, this approximation is motivated. Here it leads to a tractable mathematical formulation and enables the use of a one-step estimation method that was introduced in [16].

In statistics, one-step estimation methods refer to estimators where a preliminary estimate is improved upon by performing a single step of New-

ton's method, rather than the more common situation where this is recursively repeated until convergence. The motivation is that, under certain conditions, the asymptotic properties of the estimator do not improve by taking multiple steps (see, e.g., [20, Ch. 5.7]). Our method is also based on performing a single Newton step, but the motivation is different. Here it is employed to address the ill-posedness of the problem, by finding an initial estimate of the elimination rates such that the estimated impulsive input is guaranteed to be sparse, and then using the Newton step to refine this estimate while preserving the input sparsity.

An earlier version of the method considered here was used in [15] to estimate the elimination rates and secretion events in luteinizing hormone (LH) data sets collected from healthy males. That work showed the promise of the method, but also revealed a number of limitations when it was applied to clinical data. The main contribution of this paper is to address the shortcomings of the algorithm, by adding the following features to the estimation method:

- Point estimates for all parameters, obtained by extending the estimation algorithm with a novel regularization method and an information criterion;
- Basal level estimation through a direct generalization of the one-step algorithm;
- Robustness against measurement outliers in the data through the incorporation of a robust least squares solver;
- Detection of outlying hormone profiles.

The rest of the paper is outlined as follows. In Section 2, the model and estimation problem are introduced and the general estimation strategy and its application to a first-order system are provided. In Section 3, the implementations of the above listed features are presented. The resulting estimation algorithm is applied to synthetic and clinical data in Section 4, followed up by discussion and conclusions in Section 5.

2 Model and estimation problem

The impulsive time series is defined as the (possibly irregularly) sampled output measurements $y(t_k), k = 1, \ldots, K$ of a system of the form

$$y(t) = y_0 + G(p)\xi(t), \tag{1}$$

where $G(p)$ is a linear time-invariant single-input single-output system with p denoting the differential operator, y_0 is a constant offset, and $\xi(t)$ a sequence of time-shifted Dirac delta-impulses with positive weight, i.e.

$$\xi(t) = \sum_{n=0}^{\infty} d_n \delta\left(t - \tau_n\right),$$

where $d_n > 0$, $\tau_n > 0$. In endocrine applications, $y(t_k)$ is a hormone concentration measured in blood samples, y_0 is the basal level of this hormone, $\xi(t)$ represents the pulsatile hormone secretion, and $G(p)$ describes the linear elimination and stimulated secretion of the involved hormones. The operator $G(p)$ will thus admit a minimal state-space realization in the form of a compartmental model, and $\xi(t)$ will generally not be available for measurement. The impulsive time-series estimation problem now consists of evaluating the weights d_n, the times τ_n, y_0 and the parameters of G from $y(t_k)$.

2.1 Estimation strategy

The basis of the estimation strategy is a least squares formulation derived in [11], which assumes a second-order $G(p)$ with a particular parametrization, which we describe in Section 3. In this formulation, the linear plant parameters and the basal level form a vector ω which belongs to a set $\mathcal{D}_\omega \subseteq \mathbb{R}^m$ and is estimated by a least squares method, while the impulse times are assumed to coincide with the sampling times.

The impulse weights and initial states of the system can then be collected in a vector θ, which is estimated by

$$\begin{aligned} \hat{\theta}(\omega) = \arg\min_{\theta} ||Y(\omega) - \Phi(\omega)\theta||^2, \\ \text{s.t. } \theta \geq 0, \end{aligned} \tag{2}$$

where $Y(\omega)$ is given by

$$Y(\omega) = \begin{bmatrix} y(t_1) - y_0 & \dots & y(t_K) - y_0 \end{bmatrix}^\mathsf{T},$$

and the regressor $\Phi(\omega)$ is derived from the linear dynamics. We now concentrate out θ and consider the residual sum of squares

$$f(\omega) = \|Y(\omega) - \Phi(\omega)\hat{\theta}(\omega)\|^2.$$

It would seem like the estimation problem now could be solved by minimizing f with respect to ω. This is however not possible, as a perfect fit to any data can be obtained with a dense input and sufficiently fast linear dynamics, or

a sufficiently low basal level. In [16], the following strategy was introduced to solve this problem. Consider the function

$$f^\dagger(\omega) = \|Y(\omega) - \Phi^\dagger(\omega)\hat{\theta}^\dagger(\omega)\|^2,$$

where $\Phi^\dagger(\omega)$ and $\hat{\theta}^\dagger(\omega)$ are restricted to only include elements corresponding to the true impulse times. This implies that minimizing $f^\dagger(\omega)$ will give a least squares solution $\hat{\omega}$, but, since the impulse times are unknown, so is $f^\dagger$. However, if $f^\dagger(\omega)$ and $f(\omega)$ are approximately equal in a subset S of $\mathcal{D}_\omega$, the estimation can be performed through the following steps:

1. Find a suitable point $\bar{\omega} \in S$;
2. Approximate $f(\omega)$ by its second-order Taylor expansion around $\bar{\omega}$, denoted $f_{\mathrm{q}}(\omega)$;
3. Let $\hat{\omega} = \arg\min_{\omega \in \mathcal{D}_\omega} f_{\mathrm{q}}(\omega)$;
4. Determine the impulse times by (2) with $\omega = \hat{\omega}$.

Note that steps 2–3 correspond to a single step in Newton's method in optimization. In the case of a scalar ω, a candidate for $\bar{\omega}$ is obtained by

$$\begin{aligned} \bar{\omega} = \arg\min_{\omega \in \mathcal{D}_\omega} & N_f(\omega), \\ \text{s.t. } & df(\omega)/dx < 0, \end{aligned} \tag{3}$$

where

$$N_f(\omega) = -\frac{f(\omega)}{df(\omega)/d\omega},$$

and the constraint prevents infeasible solutions with perfect fit to the data, which corresponds to $f(\omega) = df(\omega)/d\omega = 0$. The motivation for using the point $\bar{\omega}$ is two-fold. It is firstly at a reasonable distance to $\hat{\omega}$, a property that will be elaborated upon in Section 2.2.1. Secondly, it also simplifies the minimization of f_{q}, as it removes the need of second derivatives in the calculation since

$$\left.\frac{dN_f(\omega)}{d\omega}\right|_{\omega=\bar{\omega}} = 0$$

implies

$$\left.\frac{df(\omega)/dx}{d^2 f(\omega)/dx^2}\right|_{\omega=\bar{\omega}} = \left.\frac{f(\omega)}{df(\omega)/dx}\right|_{\omega=\bar{\omega}} = N_f(\bar{\omega}),$$

which leads to the estimate

$$\hat{\omega} = \bar{\omega} + N_f(\bar{\omega}). \tag{4}$$

As a consequence, the step in Newton's method in optimization coincides with a step in Newton's root finding algorithm, see Fig. 1. The main downside with this strategy is that (3) does not generalize in a natural way to a vector-valued ω.

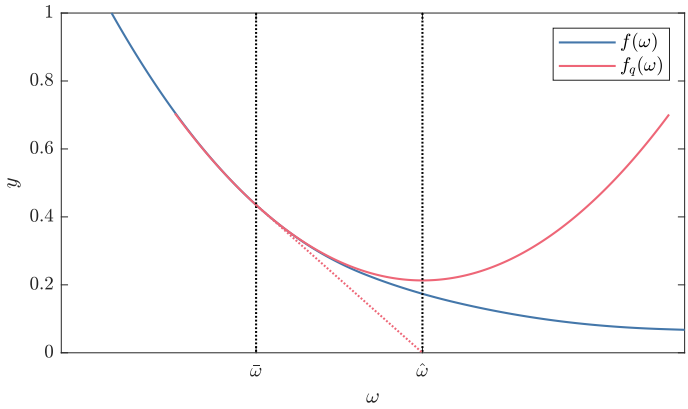

Figure 1: Residual sum of squares $f(\omega)$ decreases monotonously (blue line). Quadratic approximation at $\bar{\omega}$ gives a function $f_{\mathrm{q}}(\omega)$ (red line), whose minimum $\hat{\omega}$ is used as a parameter estimate. The tangent of $f(\omega)$ at $\bar{\omega}$ crosses zero at $\hat{\omega}$.

2.1.1 Estimating the impulses

Steps 1–3 described above follow the strategy in [15]. However, for step 4, a refinement is proposed in the present work. In the presence of noise, the solution to (2) with $\omega = \hat{\omega}$ is generally not sparse, so one has to decide which elements of $\hat{\theta}$ correspond to nonzero impulse weights. In [15], this was decided through manually chosen parameters, while an ℓ_1-regularization was used in [11] for a similar purpose. But, recalling that the input is sparse when $\omega = \bar{\omega}$, the same sparsity can be enforced when $\omega = \hat{\omega}$. However, even when $\omega = \bar{\omega}$, the determination of nonzero impulse amplitudes is not obvious, particularly since numerical solutions to (2) typically have no elements exactly equal to zero. To avoid such ambiguities, we suggest to regularize the solution at $\omega = \hat{\omega}$ so that the residual sum approximately equals $f_{\mathrm{q}}(\hat{\omega})$.

2.2 The case of first-order dynamics

As a preliminary case, the estimation of an impulsive time series with first-order continuous dynamics is considered in this section. This simplified setup is adopted mainly to enable a tractable analytical analysis of the estimation method, but versions of the methods presented here are also applied in the second-order case. The model is written in state-space form as

$$\dot{x} = -bx + \xi(t), \quad y = x, \tag{5}$$

where the parameter $b > 0$ is estimated along with the input signal. As a convention, we let ω be the estimated parameter and b denote the true

parameter value. The initial state is not included in the estimation since it can be represented by an impulse at time zero. The impulse times and amplitudes are also not uniquely identifiable, since an impulse between two sampling times can be simultaneously shifted in time and re-scaled while leaving the output unaffected. The impulse times are therefore restricted to occur at the sampling times, which leads the regressor and parameters of (2) to become

$$\Phi(\omega) = \begin{bmatrix} \mathrm{e}^{-\omega(t_1-t_1)} & 0 & \dots & 0 \\ \mathrm{e}^{-\omega(t_2-t_1)} & \mathrm{e}^{-\omega(t_2-t_2)} & \dots & 0 \\ \vdots & \vdots & & \vdots \\ \mathrm{e}^{-\omega(t_K-t_1)} & \mathrm{e}^{-\omega(t_K-t_2)} & \dots & \mathrm{e}^{-\omega(t_K-t_K)} \end{bmatrix},$$

and

$$\theta = \begin{bmatrix} d_1 & d_2 & \dots & d_K \end{bmatrix}.$$

2.2.1 The initial estimate

The initial estimate $\bar{\omega}$ should satisfy two criteria. First, it should result in a sparse estimated input signal. As shown for a second-order system in [16], this is achieved when the elimination rate is sufficiently slow. To explain this further, let $\hat{d}_n(\omega)$ denote the elements of $\hat{\theta}(\omega)$ and consider the integrals

$$Z = \int_0^\infty y(t)\ dt = \frac{1}{b}\sum_n d_n, \quad \int_0^\infty \hat{y}(t)\ dt = \frac{1}{\omega}\sum_n \hat{d}_n(\omega),$$

where $\hat{y}$ is the output corresponding to the estimated impulse weights $\hat{d}_n(\omega)$ and the number of impulses is assumed to be finite. Under the natural assumption that

$$\int_0^\infty \hat{y}(t)\ dt \approx Z,$$

the sum $\sum_n \hat{d}_n(\omega)$ is approximately proportional to ω. A low value of ω then acts as an ℓ_1-constraint, which gives rise to sparse solutions.

The second criterion is that $\hat{\omega} - \bar{\omega}$ should be small, for the quadratic approximation of f to be accurate. We thus want $\bar{\omega}$ to be as large as possible, while keeping the input sparse. The consequences of determining $\bar{\omega}$ by solving (3) are analyzed next; derivations of the results are given in Appendix A. Consider the response of a single impulse with the weight d for system (5), with the output measurements subject to i.i.d additive Gaussian noise with variance σ^2. Equation (3) then leads to the approximate relations

$$N_f(\bar{\omega}) = \hat{\omega} - \bar{\omega} \approx \sqrt{\frac{c_0}{c_2}}, \tag{6}$$

where $c_0 = (K-1)\sigma^2$ and

$$c_2 = \sum_{k=1}^{K} \left(\frac{\partial \alpha_0}{\partial \omega}\Big|_{\omega=b} - t_k d \right)^2 \mathrm{e}^{-2bt_k}, \quad \alpha_0 = d \, \frac{\sum_{k=1}^{K} \mathrm{e}^{-(b+\omega)t_k}}{\sum_{k=1}^{K} \mathrm{e}^{-2\omega t_k}}.$$

In the limit when the noise variance goes to zero, $\hat{\omega}$ approaches b and the approximation becomes strict. If equidistant sampling with a period of T now is assumed, the point

$$\tilde{\omega} = b - \sqrt{\frac{c_0}{c_2}} \frac{\mathrm{e}^{bT}\sqrt{\pi/2}}{\sqrt{(K-1)(1-\mathrm{e}^{-2bT})}} \tag{7}$$

gives an approximation of an upper limit for $\bar{\omega}$ such that multiple impulse estimates are unlikely to appear. If $\hat{\omega}$ is close to the true parameter value, the condition $\bar{\omega} < \tilde{\omega}$ corresponds to

$$K \gtrapprox \frac{\pi \, \mathrm{e}^{2bT}}{2(1-\mathrm{e}^{-2bT})} + 1.$$

In the experiments in Section 4.1.1, $T = 0.5$ and b is of the order of 1, which gives $K \gtrapprox 7.8$. The calculation of $\tilde{\omega}$ is based on several approximations and it should therefore not be interpreted as an exact bound. However, (7) still indicates that $\bar{\omega}$ is likely to give a sparse input signal if the sampling frequency is high and K is large. Also note the square root of $K-1$ in this equation, which limits the sensitivity of $\tilde{\omega}$ with respect to K. As a result, $\tilde{\omega} - \bar{\omega}$ grows relatively slowly with K, i.e. $\bar{\omega}$ is not unnecessarily far from this limit.

2.2.2 Sensitivity analysis

Sensitivity analysis of the estimation method is presented here. For detailed derivations, see Appendix A.

For simplicity, the impulse response of (5) is again considered, with sampled measurements subject to Gaussian i.i.d noise. The parameter c_2 introduced above then relates to the Fisher information $\mathcal{I}(b)$ for the parameter b and, by the Cramér-Rao bound, the variance of its estimate as

$$\mathcal{I}(b) = \frac{c_2}{\sigma^{-2}} \leq \mathrm{Var}(\hat{\omega}).$$

Combined with (6), that leads to the approximate relation

$$\mathrm{Var}(\hat{\omega}) \gtrapprox \frac{\big(N_f(\bar{\omega})\big)^2}{K-1}, \tag{8}$$

which becomes a proper inequality when the noise level approaches zero, and an equality when K furthermore tends to infinity, under the assumption that a single (correct) impulse is estimated (which the analysis in Section 2.2.1 indicates should happen when $K \to \infty$). This indicates that a short Newton step and a large K corresponds to a good estimate.

Since inequality (8) only provides a lower bound and does not take the particular estimation method given by (3), (4) into account, the accuracy of the one-step estimation method needs to be investigated. To this end, the sensitivity of the estimate with respect to higher order terms of f is determined. Consider the case

$$f(\omega) = f_{c_3}(\omega) = c_0 + c_2(\omega - b)^2 + c_3(\omega - b)^3, \tag{9}$$

i.e. a third-order term is introduced to represent deviations from the quadratic assumption that the estimation strategy builds upon. The first-order effect of this is an error that scales with c_3 as

$$E = \frac{3c_0}{2c_2^2}c_3 + O(c_3^2). \tag{10}$$

Since c_0 scales with the noise and c_2 scales with the impulse weight squared, the factor $3c_0/2c_2^2$ is typically small. For example, with $d = 0.5$, $T = 0.5$, $\sigma = 0.01$, $K = 10$, which roughly correspond to the parameter values in the experiments in Section 4.1.1, $c_0 = 9 \times 10^{-4}$, $c_2 = 0.0906$ and $3c_0/2c_2^2 = 0.165$. Deviations from the quadratic assumption and the use of the one-step estimation strategy are therefore not expected to contribute significantly to the overall uncertainty of the estimate, in particular if the noise level is low. This is also in line with the numerical experiment in Section 4.1.1.

2.3 Implementation

2.3.1 Optimization formulation

The strict constraint on the derivative in (3) cannot be implemented numerically. We therefore use the modified formulation

$$\begin{aligned} \bar{\omega} &= \arg\min_{\omega \in \mathcal{D}_\omega} N_f(\omega), \\ \text{s.t. } & df(z)/dz \leq 0, \forall z \leq \omega, \end{aligned} \tag{11}$$

which restricts the search space to the region where $f(\omega)$ is monotonously decreasing. However, experiments with synthetic data have shown that this region is not restrictive enough, in that it sometimes permits estimates with unreasonably large values of $\bar{\omega}$, compared to the true parameter value. A constraint on the total number of estimated impulses was used in [15] to

prevent this, but that requires the specification of a somewhat arbitrary threshold for counting in an impulse, which is undesirable. We instead suggest to add a small positive constant ε to f, which acts as a regularization. If it is set to be of the same order of magnitude as the noise variance, which in the endocrine case can be approximated through the measurement uncertainty, it has a negligible effect on $N_f(\omega)$ in the range of values of ω that is relevant for the estimation.

2.3.2 Optimization solution

For reasons discussed in Appendix A, the function N_f can display multiple local minima. For simplicity, we therefore suggest gridding to solve (11) and to approximate the derivative of f using finite differences over the same grid.

3 Robust endocrine estimation

We now turn to the model which was studied in [11, 16, 15] and also is the main focus of this paper. It has the form

$$\dot{x} = \begin{bmatrix} -b_1 & 0 \\ g_1 & -b_2 \end{bmatrix} x + \begin{bmatrix} 1 \\ 0 \end{bmatrix} \xi(t), \quad y = y_0 + \begin{bmatrix} 0 & 1 \end{bmatrix} x, \tag{12}$$

i.e. $G(p)$ in (1) is specialized here to a second-order system. It could represent a number of hormone axes, but has mainly been applied to hormones from the male reproductive axis, which also is the application we consider here. The states of the system then correspond to the concentrations of gonadotropin releasing hormone (GnRH) and luteinizing hormone (LH) and b_1 and b_2 represent their respective elimination rates. The coefficent g_1 describes the secretion rate at which LH is stimulated by GnRH, but, since it is not uniquely identifiable, $g_1 = 1$ is assumed without loss of generality.

Two version of the vector ω are considered:

$$\begin{aligned} \omega =& \omega_1 = \begin{bmatrix} b_1 & b_2 \end{bmatrix}, \\ \omega =& \omega_2 = \begin{bmatrix} b_1 & b_2 & y_0 \end{bmatrix}, \end{aligned}$$

respectively corresponding to a known (i.e. zero) and unknown constant basal level. The set $\mathcal{D}_\omega$ is assumed to be a hypercube in the corresponding coordinate space, i.e. the parameters are restricted to intervals $I_{b_1}, I_{b_2}, I_{y_0}$. The expressions for θ and $\Phi(\omega)$, see (2), are given by

$$\Phi(\omega) = \begin{bmatrix} \varphi(b_1, b_2, t_1) & \dots & \varphi(b_1, b_2, t_K) \end{bmatrix}^\intercal,$$

where

$$\varphi(b_1, b_2, t_i) = \begin{bmatrix} \mathrm{e}^{b_2(t_i - t_1)} & z(b_1, b_2, t_i - t_1) & \dots & z(b_1, b_2, t_i - t_{K-1}) \end{bmatrix}^\intercal,$$

$$\theta = \begin{bmatrix} x_2(t_1) & d_1 & \dots & d_{K-1} \end{bmatrix}^\intercal,$$

$$z(b_1, b_2, t) = \frac{\mathrm{e}^{-b_2 t} - \mathrm{e}^{-b_1 t}}{b_1 - b_2} H(t),$$

and H is the Heaviside step function.

A difference compared to the first-order case is that impulses that occur between sampling times can be uniquely represented by impulses at the sampling times [11]. Furthermore, with ω as a vector, it is no longer possible to use (3) directly to find an initial estimate. In [16], two approaches were presented to resolve this, when the basal level is fixed. In the case of very low measurement noise, (3) was used anyway, but with $N_f(\omega)$ defined with a partial derivative with respect to the slower elimination rate, and the minimization being performed over both parameters. With a higher noise level, gridding over one parameter and optimizing over the other produced a set of possible solutions, in the form of a curve γ in the set $\mathcal{D}_\omega$ of the parameter space. In [15], this curve was shown to coincide with the posterior distribution from a Markov-chain Monte-Carlo estimator, i.e. it represents a direction of high variance in $\mathcal{D}_\omega$. However, for practical applicability of the method, point estimates are also required when the noise level is higher.

3.1 Point estimates

A method for identifying point estimates along the curve γ is presented in this section. For simplicity, the basal level is assumed to be known, while the case of unknown constant basal level is covered in the next section. The curve γ is defined by all points $(b_1, \hat{b}_2(b_1)) \in I_{b_1} \times I_{b_2}$, where $\hat{b}_2(b_1)$ is determined by

$$\begin{aligned} \bar{b}_2(b_1) &= \underset{b_2 \in I_{b_2}}{\arg\min}\, N_f(b_1, b_2), \\ \text{s.t. } &\partial f(b_1, z)/\partial z \leq 0, \forall z \leq b_2, \\ \hat{b}_2(b_1) &= \bar{b}_2(b_1) + N_f(b_1, \bar{b}_2(b_1)), \end{aligned} \tag{13}$$

where

$$N_f(b_1, b_2) = -\frac{f(b_1, b_2)}{\partial f(b_1, b_2)/\partial b_2}.$$

Motivated by the analysis of the first-order dynamics in Section 2.2, it is expected that estimates along γ display a beneficial trade-off between input sparsity and fit to the data. To explain the method used to compare these estimates, more details on the impulse estimation procedure outlined in Section 2.1 are needed.

3.1.1 Impulse estimation

The impulses are estimated through regularization, where some estimated weights in $\hat{\theta}$ are set to zero. However, since the corresponding impulses are constrained to the sampling times, whereas in reality, impulses will almost surely occur between these, the estimated weights are not used directly. Instead, the regularization is performed based on the impulses obtained by merging consecutive impulses, according to Algorithm 1 in [11].

Let m_k denote the weight of the impulse obtained by merging impulse k and $k+1$. To determine which pairs that should be used to form each merged impulse (impulse k could be combined with either impulse $k-1$ or $k+1$), the following linear integer programming formulation, which finds the combination which minimizes the total sum of the impulse weights, is used:

$$\begin{aligned} \hat{P} &= \arg\min_{P} D^\intercal P, \\ \text{s.t. } p_{1,k} + p_{2,k-1} + p_{2,k} &= 1 \text{ for } k = 2, \dots K, \\ p_{1,1} + p_{2,1} &= 1, \\ p_{i,k} &\in \{0, 1\} \text{ for } k = 1, \dots K, i = 1, 2, \end{aligned}$$

where

$$\begin{aligned} D^\intercal &= \begin{bmatrix} d_1 & \dots & d_K & m_1 & \dots m_{K-1} \end{bmatrix}, \\ P^\intercal &= \begin{bmatrix} p_{1,1} & \dots & p_{1,K} & p_{2,1} & \dots & p_{2,K-1} \end{bmatrix}, \end{aligned}$$

and $p_{2,k}$ indicates that impulses k and $k+1$ are merged, while $p_{1,k}$ indicates that impulse k is not merged. By its construction, the minimization will tend to merge most impulses.

When the linear programming formulation is applied to the impulse estimates obtained from (2) with the parameters $b_1, \hat{b}_2(b_1)$, the nonzero elements of $\hat{P}$ define a set of impulses. We now define the function $\hat{f}_n$ as the residual sum of (2), when the n largest of these impulses are included, and let $\hat{c}_0$ denote the quadratic approximation of f evaluated at $\hat{b}_2(b_1)$, i.e.

$$\hat{c}_0(b_1) = f_{\mathrm{q}}(b_1, \hat{b}_2(b_1)) = \frac{1}{2}\big(N_f(b_1, \bar{b}_2(b_1))\big)^2 \frac{\partial^2 f(b_1, b_2)}{\partial b_2}\bigg|_{b_2 = \bar{b}_2(b_1)}. \tag{14}$$

The number of impulses to include is then given by

$$n_0(b_1) = \arg\min_{n \in \mathbb{N}} |\hat{f}_n(b_1, \hat{b}_2(b_1)) - \hat{c}_0(b_1)|, \tag{15}$$

i.e. for each b_1, the estimated input is given by the $n_0(b_1)$ largest impulses defined by $\hat{P}$, which results in the residual sum of squares $\hat{f}_{n_0(b_1)}(b_1, \hat{b}_2(b_1))$.

3.1.2 Comparing estimates

We now have parameters corresponding to the two criteria needed to evaluate the estimates along γ; $n_0(b_1)$ characterizes the input sparseness and $\hat{f}_{n_0(b_1)}(b_1, \hat{b}_2(b_1))$ the fit to data. Define the set $N = \{n \in \mathbb{N} \mid \exists b_1 \text{ s.t. } n_0(b_1) = n\}$. To obtain point estimates along γ, a first step is to determine the set of Pareto-efficient estimates

$$\hat{b}_1^{(n)} = \underset{b_1 : n_0(b_1)=n}{\arg\min} \hat{f}_n(b_1, \hat{b}_2(b_1)), \quad \hat{b}_2^{(n)} = \hat{b}_2(\hat{b}_1^{(n)}),$$

for $n \in N$. As a further refinement, an information criterion (see e.g. [18]) can be used to identify a single estimate. We use the Bayesian information criterion (BIC) for this purpose. Observing that n impulses correspond to $2(n+2)$ estimated parameters, and assuming Gaussian i.i.d. noise, the number of impulse estimates given by this criterion is

$$n^{\mathrm{BIC}} = \underset{n \in N; n \leq n_{\max}}{\arg\min} \left\{ K \log\left(\hat{f}_n\left(\hat{b}_1^{(n)}, \hat{b}_2(\hat{b}_1^{(n)})\right)\right) + 2(n+2)\log K \right\},$$

where $n_{\max} \in \mathbb{N}$ is an upper bound of the number of parameters. Finally, the corresponding estimated parameters are defined by

$$\hat{b}_1^{\mathrm{BIC}} = \hat{b}_1^{(n^{\mathrm{BIC}})}, \quad \hat{b}_2^{\mathrm{BIC}} = \hat{b}_2^{(n^{\mathrm{BIC}})}.$$

Note that the BIC requires the sample size to be much larger than the number of parameters, which generally does not hold in the present application. However, the results with the method have proven satisfactory in numerical experiments, as demonstrated in Section 4.

3.2 Basal level

The estimation of the basal level y_0 suffers from the same problem as the estimation of the elimination rates, in the sense that the fit will always increase when the basal level is lowered and, as a result, more nonzero impulses are estimated. To resolve this, we again propose a one-step estimation algorithm. So, if b_1 is assumed to be known, minimizing N_f and taking the Newton step for a range of different basal levels produces a curve γ in the b_2-y_0 plane, from which a point estimate can be obtained according to the strategy presented above. The problem is that b_1 is not known. Furthermore, the experiments with the Markov-chain Monte-Carlo estimates in [15] show that multiple parameter values can give a similar fit to data even when the basal level is fixed, so adding one more parameter may just add another dimension to the space of plausible solutions.

However, if one elimination rate is significantly faster than the other, i.e. $b_1 \gg b_2$, the situation becomes more promising. In such cases, b_1 will have a smaller effect on the output (other than a pure re-scaling) and therefore be hard to estimate. On the other hand, this also implies that estimates of b_2 and y_0 should be insensitive to the value b_1. In this situation, performing the estimation for a number of fixed values of b_1 as outlined above will therefore give similar estimates of the basal level. To choose between these, an information criterion can again be employed. This choice would also correspond to an estimate of b_1, however the uncertainty here is expected to be significant.

Fortunately, in many hormone axes, the elimination rate of the releasing hormone is significantly faster than the elimination rate of the other hormones of the axis, so the proposed method has practical relevance. For example, the elimination rate of GnRH is an order of magnitude faster than the elimination rate of LH (see [7]).

3.3 Robustness against outlying measurements

Measurement errors are often large in clinical endocrine data and the presence of outlying measurements is particularly problematic. This situation can be described statistically as a fraction of the measurement errors being drawn from a corrupting distribution, as opposed to Gaussian i.i.d. errors. It is well known that the performance of least squares estimates such as (2) can be severely degraded under such circumstances.

In biomedical applications, robust estimation techniques are the recommended way to counteract this sensitivity, as opposed to simpler strategies based on, e.g., residual analysis [4]. AutoDecon does use the latter method for robustness, but the scheme is more involved as it includes repeated estimation steps [5]. The linear least squares formulation in our estimator enables the simple strategy of replacing (2) with a robust least squares solution, if outliers in the data set are suspected. We use the robust risk minimization algorithm presented in [13] for this purpose. The algorithm produces a robust solution by reducing the effective sample size, which results in a down-weighting of the outliers and only requires the user to specify an upper bound ϵ on the fraction of corrupted data points. The method thus also offers an automatic and non-subjective method for detecting measurement errors in hormone data, as opposed to more ad hoc methods such as, e.g., the methods compared in [19].

The introduction of the robust least squares solution requires two small modifications of the one-step algorithm. First, to have consistent finite-difference approximations of derivatives, the weighting of the data points in the robust least squares solutions must be consistent. The function values

$f(b_1, b_2 - h)$ and $f(b_1, b_2 + h)$, which are used for (13) and (14), are therefore calculated with the weights of the robust least squares solution for $f(b_1, b_2)$. Second, for (15) to be consistent, the weights from $f(b_1, \bar{b}_2(b_1))$ are used in the calculation of $\hat{f}_n(b_1, \hat{b}_2(b_1))$.

3.4 Outlying hormone profiles

Hormone profiles that are inconsistent with the chosen model structure are sometimes encountered. In the case of LH measurements, there are several congenital or acquired conditions that can affect the functioning of the male reproductive axis (see, e.g., [2]), and thus disrupt the expected pulsatile behaviour. As previously mentioned, due to the ill-posedness of the estimation problem, it is in principle possible to find a good fit to the data even in such a case. But, that is typically not a relevant solution, since many other such solutions also exist and there is no way to choose one over another. Our estimation method instead indicates such cases by $\bar{b}_2$ in (13) coinciding with the lower boundary of I_{b_2}, so that the estimated elimination rate becomes very slow. An intuitive explanation of this behavior is that the variations in the measurements are interpreted by the algorithm as high-variance noise, rather than the responses to distinct impulses, and the slow elimination rate corresponds to the moving average of the signal being approximately constant.

3.5 Optimization solution

The estimation of γ according to (13) is again based on gridding. The derivative is calculated using finite differences over the grid points in the non-robust case, while the robust implementation requires additional function evaluations for the derivative. To decrease the computation time, gridding over the full range of b_1 is only performed for a sparse subset of the b_2-values, with local optimization performed in between. For further details, we refer to the code provided online.

4 Experiments

The performance of the one-step estimation method is demonstrated on synthetic and clinical data. For the former, Matlab code is available at `https://github.com/HRunvik/Robust-One-Step-Estimation-of-Impulsive-Time-Series` (clinical data experiments cannot be shared as the authors do not own the data).

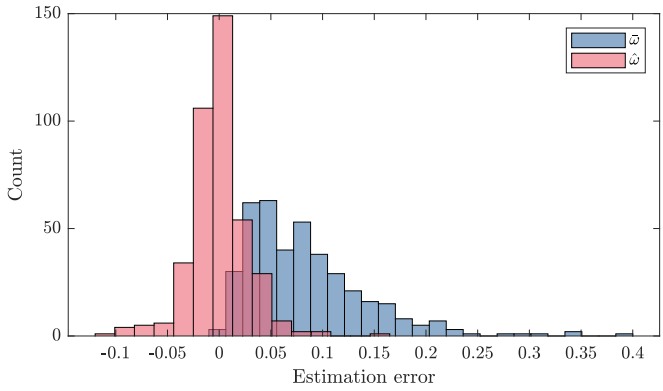

Figure 2: Histograms over $b - \bar{\omega}$ (initial estimation errors) and $b - \hat{\omega}$ (one-step estimation error) from 400 Monte Carlo runs with synthetic data with first-order dynamics.

4.1 Synthetic data experiments

Synthetic data experiments with first-order linear dynamics, defined by (5), and second-order dynamics, defined by (12), are performed. The data generation is similar for both cases and is described in Appendix B. The estimation is performed according to the descriptions above, with the parameter ε set equal to the noise variance in the experiments with second-order dynamics, while a value of four times the noise variance is used in the first-order case.

4.1.1 First-order dynamics

Estimation according to (4) and (11) is performed in 400 Monte-Carlo runs. The resulting distributions of $\bar{\omega}$ and $\hat{\omega}$ are displayed in Fig. 2; the improvement of the Newton step upon the preliminary estimate is clearly visible. In Fig. 3, the estimation errors of the one-step estimation method are plotted against the estimation error obtained when minimizing $f^{\dagger}(\omega)$ directly, i.e., when the impulse times are assumed to be known. The correlation coefficient is 0.68, which indicates a strong correlation between the errors, and the increase in root-mean-square error when the impulse times are unknown is relatively small: 0.0278 versus 0.0247. This shows that the variance of the one-step estimate mainly comes from the the uncertainty of estimating the elimination rate with a known impulse time, and that (11) is useful in determining the initial estimate.

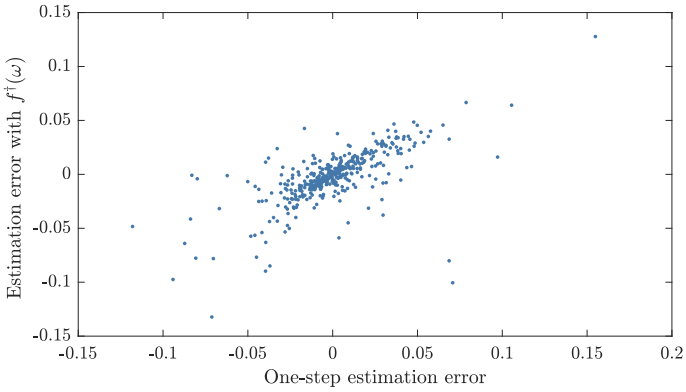

Figure 3: Time constant estimation errors for synthetic data with first-order dynamics. Errors when estimating with known impulse times are plotted against errors when time constant and elimination rate are estimated simultaneously with the one-step method.

4.1.2 Second-order dynamics: point estimates

Estimation of a second-order system with a fixed basal level is considered in this section. The estimates $(\hat{b}_1^{(n)}, \hat{b}_2^{(n)})$ and $(\hat{b}_1^{\mathrm{BIC}}, \hat{b}_2^{\mathrm{BIC}})$, calculated according to Section 3.1 are compared against estimates $(\hat{b}_1^*, \hat{b}_2^*)$ obtained by minimizing N_f over both b_1 and b_2, as suggested in [16]. The evaluation is performed through a sequence of Monte-Carlo runs where the synthetic data are subject to noise with increasing variance. A typical data set is illustrated by the data subject to Gaussian i.i.d. noise in Fig. 6.

Table 1: Estimation errors expressed as the mean Euclidean distance between the estimates and the true parameter values, and mean number of estimated impulses, for synthetic data subject to noise with standard deviation σ. Columns $(b_1^{(n)}, b_2^{(n)})$ and γ correspond to the estimates closest to the true parameters in the sets $\{(b_1^{(n)}, b_2^{(n)}) \mid n \in N\}$ and n_0 is the average number of estimated impulses.

σ	$(\hat{b}_1^{\mathrm{BIC}}, \hat{b}_2^{\mathrm{BIC}})$	$(\hat{b}_1^{(n)}, \hat{b}_2^{(n)})$	$(\hat{b}_1^*, \hat{b}_2^*)$	γ	n_0
0.002	0.090	0.030	0.060	0.0039	4.01
0.004	0.130	0.062	0.129	0.0081	3.84
0.006	0.162	0.083	0.190	0.0121	3.76
0.008	0.185	0.108	0.269	0.0159	3.71
0.010	0.218	0.132	0.349	0.0202	3.61
0.012	0.245	0.157	0.423	0.0250	3.55

The estimation errors are summarized in Table 1. Regardless of the noise variance, the best of the Pareto-efficient estimates $(\hat{b}_1^{(n)}, \hat{b}_2^{(n)})$ tends to be closer to the true parameter values than $(\hat{b}_1^*, \hat{b}_2^*)$. As the noise variance is increased, $(\hat{b}_1^{\text{BIC}}, \hat{b}_2^{\text{BIC}})$ also starts to outperform $(\hat{b}_1^*, \hat{b}_2^*)$. Note also that γ is much closer to the true parameters than any point estimate, i.e. the estimation errors are mostly caused by choosing a wrong point along γ.

Generally, the number of estimated impulses exceeds the true number of impulses, but curiously, the estimate improves when the noise level increases. The use of the BIC with many parameters compared to the amount of data is a potential cause. However, it should be noted that our method makes no assumptions about the weight of the impulses as the regularization is done implicitly. For synthetic data sets, incorporating information regarding the impulse weights in the estimation could potentially improve the performance, but for clinical data, making similar assumptions about the magnitude of secretion events may be unwarranted.

4.1.3 Second-order dynamics: basal level

Synthetic data where one elimination rate (b_2) is significantly slower than the other is used to evaluate the estimation of the basal level y_0, and the parameters b_1, b_2, according to the description in Section 3.2. Histograms of the basal level estimation error and the minimal value (compared to the basal level) of the sampled data from 200 Monte-Carlo runs are displayed in Fig. 4. It can be seen that estimating the basal level outperforms the simplistic approach of choosing the minimal value as the basal level, and they display biases in opposite directions. The bias of the latter method is expected since the impulse response of the system only approaches the basal level as time tends to infinity, while the bias of former is discussed further below. In Table 2, the performance of the estimation of basal level and elimination rates are given. As expected, the estimation performance for the slower elimination rate is significantly better than for the faster.

Table 2: Elimination rate and basal level estimation performance from synthetic data experiment.

Estimate	Bias	Variance
b_1	0.327	1.62
b_2	0.00462	0.00456
y_0, one-step est.	-0.00949	6.73×10^{-4}
y_0, $\min y_k$	0.0739	0.00425

Fig. 4 indicates that a few data sets give rise to a significant negative basal level estimation error. The synthetic and estimated parameters of the

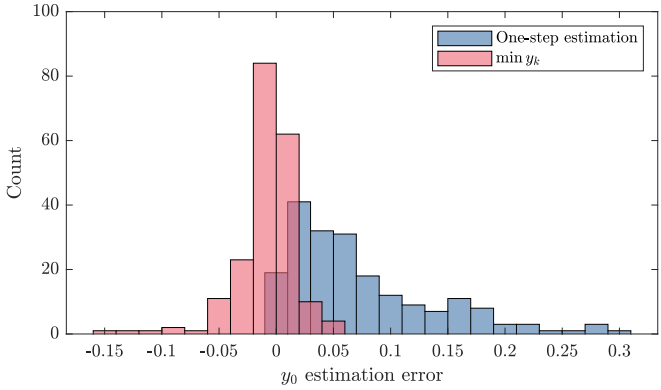

Figure 4: Histograms over one-step estimation error of basal level, and minimum value of output from 200 Markov runs with synthetic data.

most extreme case are summarized in Table 3 and the corresponding output is illustrated in Figure 5. There are clear discrepancies for all parameters, however the residual sum is lower with the estimated parameters, so the estimator apparently finds alternative solutions where additional impulses yield a better fit than for the noisy original data. Similar results can be seen for other data sets where the estimation errors are large. Imposing stricter restrictions on the number of impulse estimates would prevent these problems, but we chose to retain them in order to keep the estimation assumptions at a minimum, and to illustrate the challenging nature of this estimation problem.

Table 3: True and estimated parameter values from synthetic data with large basal level estimation error.

	b_1	b_2	y_0	n_0	Residual error
Data	4.76	0.460	0	3	1.88×10^{-3}
Estimate	7.14	0.371	-0.148	5	6.43×10^{-4}

4.1.4 Second-order dynamics: robustness against outliers

To evaluate the impact of outlying measurements on the estimation, synthetic data subject to two different types of noise are used. In the base case, Gaussian i.i.d. noise is applied to all data points. In an alternative setup, the aforementioned noise is applied to all but two data points, which instead are subject to uniformly distributed noise with significantly higher variance. In Fig. 6 one data set subject to the two noise types is illustrated.

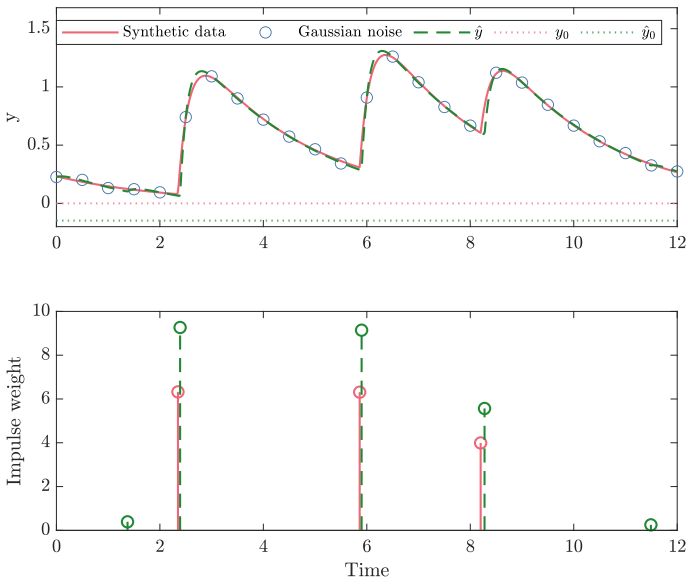

Figure 5: Top: Synthetic data and simulated output from estimated model with large basal level estimation error. Bottom: Corresponding synthetic and estimated impulses.

The estimation method is evaluated in 50 Monte-Carlo runs, where the standard one-step estimation is performed for both the i.i.d. and mixed noise cases, while robust estimation is only performed for the mixed noise case. The threshold of $\epsilon = 0.1$ is used, which corresponds to reducing the effective sample size by approximately two (depending on the size of the individual data sets). Estimated γ-curves for these cases, based on the data in Fig. 6, are displayed in Fig. 7. The distance between the curves and the true parameter values indicate that the outliers clearly deteriorate the performance of the non-robust estimation, however, when the robust algorithm is used, the performance is recovered almost fully. The discontinuities that can be observed for all three curves are caused by different local minima corresponding to to the global minimum. Local minima are typically associated with different sets of nonzero impulse estimates, which is briefly discussed in Appendix A.

In Table 4, an evaluation of both the estimated curves and point estimates are provided for the Monte-Carlo runs. The small difference between the results for the base case and the robust estimation, and the large deviation when the standard method is used on mixed noise, show the usefulness of the robust method. Also note that, in the latter case, the minimizer of N_f at times coincides with the minimal value of I_{b_1}, so if a larger parameter

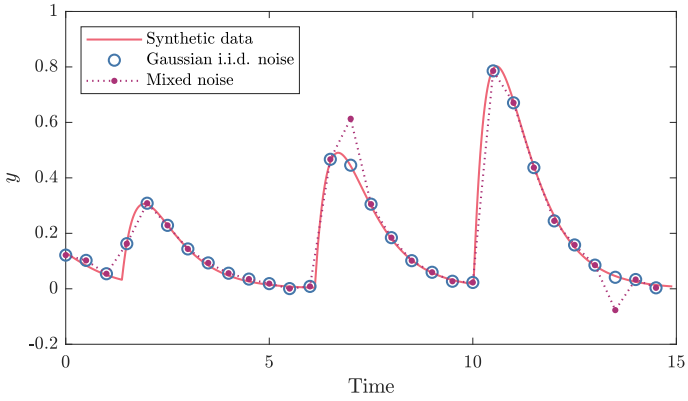

Figure 6: Example of a synthetic data set, subject to Gaussian i.i.d noise, and a mixture of Gaussian noise and uniformly distributed noise with higher variance.

range was used in the estimation, the performance could deteriorate even further.

Table 4: Mean Euclidean distance between estimated γ-curve and point estimates $(\hat{b}_1^{\text{BIC}}, \hat{b}_2^{\text{BIC}})$ from synthetic data experiments. Point estimates for the mixed noise case with standard estimator are not included as the large error in γ renders the estimates useless.

Setup	$(\hat{b}_1^{\text{BIC}}, \hat{b}_2^{\text{BIC}})$	γ
Gaussian i.i.d. noise, standard estimation	0.173	0.0134
Mixed noise, standard estimation	-	0.0739
Mixed noise, robust estimation, mixed noise	0.191	0.0160

4.2 LH data experiments

The one-step estimation method is now used on clinical data. We use a data set with LH blood concentrations collected from healthy males, which was collected in experiments described in [10]. A more rigorous analysis of this data, including the effect of a selective gonadotropin releasing hormone receptor antagonist, is included in [15]. The focus here is instead on the features of the algorithm introduced in this work, which are exemplified on individual data sets. For these experiments, we note that the elimination rates for LH and GnRH are expected to satisfy

$$0.23 \text{ min}^{-1} \leq b_1 < 0.69 \text{ min}^{-1}, \quad 0.0087 \text{ min}^{-1} < b_2 \leq 0.014 \text{ min}^{-1}, \quad (16)$$

according to [7].

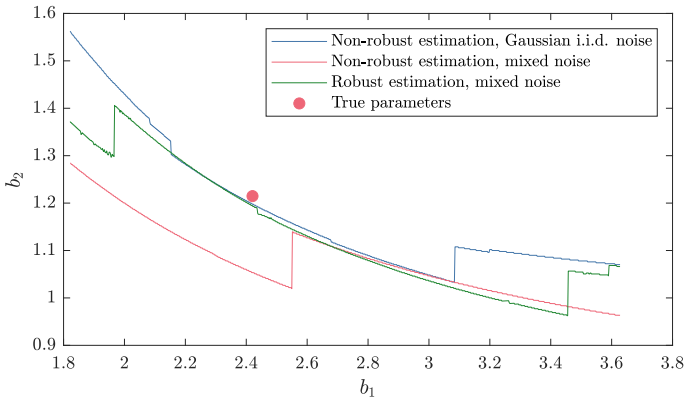

Figure 7: Non-robustly and robustly estimated γ-curve from the synthetic data sets in Fig. 6.

4.2.1 Robust basal level estimation

Estimation of the basal level, the elimination rates, and the secretion events is performed on hormone data of a 32-year old healthy male. The data set consists of 108 measurements of LH sampled every ten minutes. Since large measurement errors are suspected for several data points, robust estimation is needed. The methods described in Section 3.2 and Section 3.3 are therefore combined, with the range of b_1 values given by (16), and the parameter ϵ set to $5/108$, i.e. an effective sample size of 103 is assumed. The estimated values of b_2 and y_0, and the BIC, are plotted against b_1 in Fig. 8. As expected, the sensitivity of the estimates to b_1 is relatively low, but curiously the lowest BIC score appear at both edges of the parameter range. Also note that the estimated values of b_2 are biologically viable and satisfy (16). The simulated response of the estimated model corresponding to the lowest BIC score is illustrated in Fig. 9. There, the weights of the data points obtained from the robust estimator are also displayed and the most down-weighted points are highlighted.

4.2.2 Outlying hormone profile

The hormone profile of a 68-year old healthy male that appears inconsistent with the assumed model is now analyzed. For simplicity, the basal level is assumed to coincide with the lowest measured LH concentration and $b_1 = 0.5$ is fixed; very similar results are obtained with other parameter values. Standard and robust estimations of b_2, with different values of ϵ, are performed. The corresponding functions N_f are displayed in Fig. 10. Three observations can be made from this plot. First, the effect of the robust estimation is to

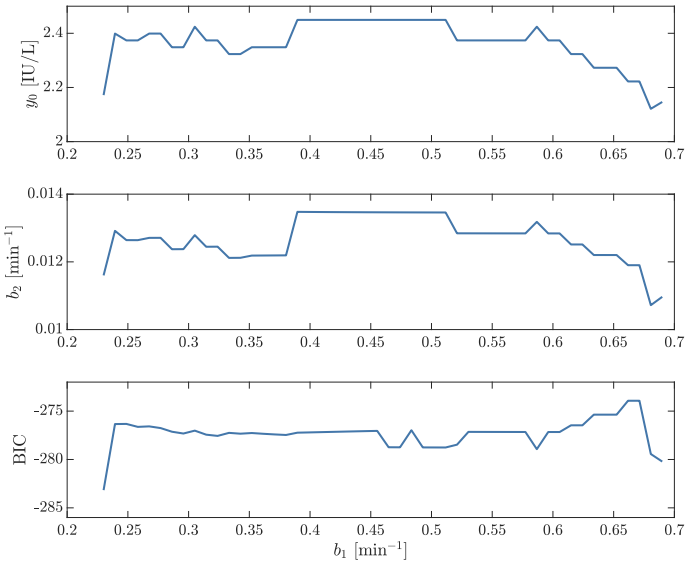

Figure 8: Estimated basal level (top), LH elimination rate (middle) and BIC (bottom) depending on GnRH elimination rate for LH data shown in Fig. 9.

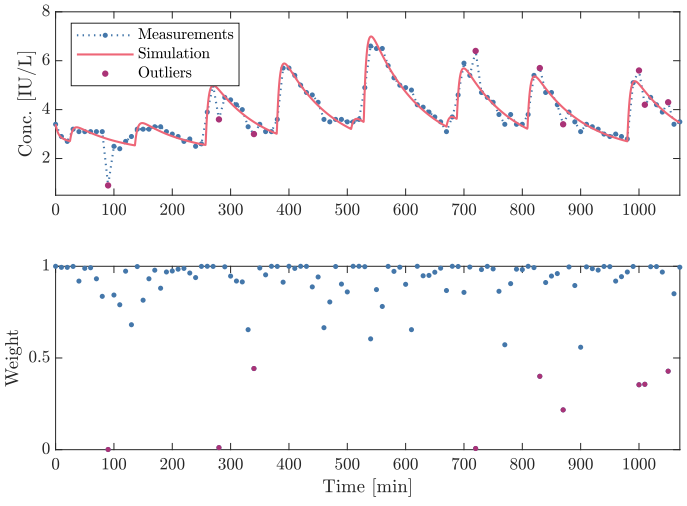

Figure 9: Top: LH measurements from a 32-year old male, and simulated output from estimated system. Bottom: weighting of data points from robust least squares solver. Points weighted below 0.5 are highlighted in red in both plots.

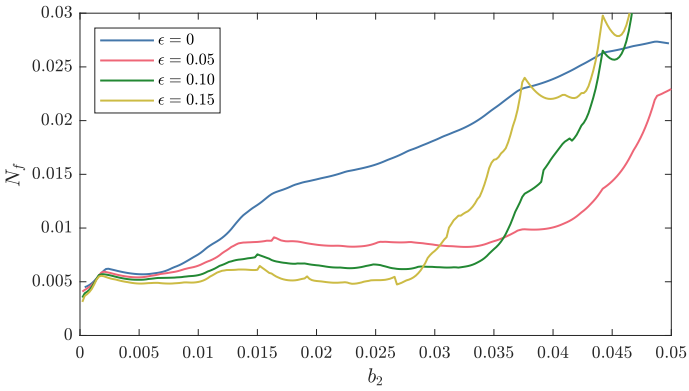

Figure 10: N_f-curves for standard ($\epsilon = 0$) and robust estimation ($\epsilon > 0$) for LH data shown in Fig. 11.

decrease N_f for larger values of b_2. This behavior is generally seen for data sets with outliers, and is the same mechanism by which robust estimation moves the γ-curve closer to the true parameters in the presence of outliers in Fig. 7. Second, depending on which interval I_{b_2} and value of ϵ that are chosen, local minima of N_f could be identified as solutions to (13). The simulated output for such an estimate of the system with $I_{b_2} = [0.003, 0.01]$ and $\epsilon = 0.01$ is shown together with the weights of the robust estimator in Fig. 11. Third, the global minimizer of N_f is in fact $b_2 = 0$ for all ϵ, which indicates that the data are inconsistent with the assumed model according to the discussion in Section 3.4. The reliability of estimates such as the one illustrated in Fig. 11 is therefore questionable, something that is also indicated by the large number of outliers. It is known that GnRH pulses appear at higher frequency in older males, so increasing the sampling rate of the measurements is probably a better strategy to recognize the impulsive events for this individual.

5 Discussion and conclusions

There are many possible approaches to analyzing hormone concentration time-series data. The aim of the present work has been to develop a method involving minimal assumptions or manual tuning, which also is well-motivated mathematically. However, achieving these goals simultaneously is challenging, particularly when the algorithm is adapted for clinical data. We have here only attempted a theoretical analysis of the first-order case, but as the model and data depart from this situation, the algorithm becomes more involved and less tractable.

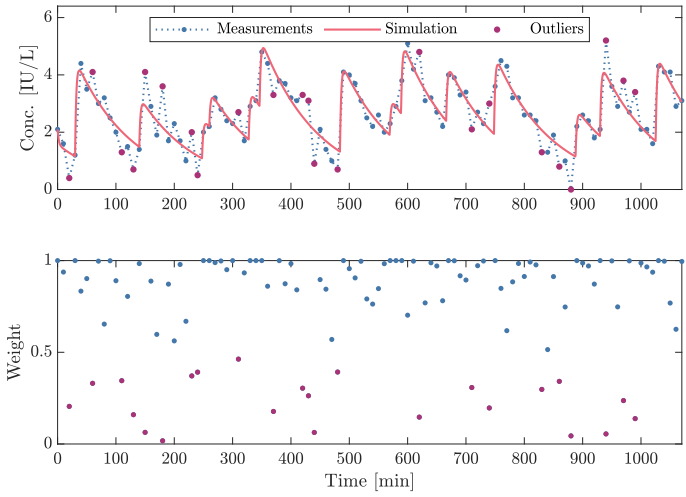

Figure 11: Top: LH measurements from a 68-year old healthy male, and simulated output from estimated model. Bottom: weighting of data points from robust least squares solver. Points weighted below 0.5 are highlighted in red in both plots.

An advantage of the presented method is that estimates with different resolutions can be obtained. Keeping the uncertainties in model and measurements and the inherent ill-posedness of the estimation problem in mind, the reliability of any point estimate from clinical data is probably low. All estimates produced along a section of the curve γ might therefore be a better representation of the range of possible parameters and secretion events of a given data set. Such lower resolution estimates have the additional advantage of a more transparent mathematical derivation.

Possible future research directions include the application of the one-step estimation method under other modeling assumption. Generalization of the method has already been presented in this work, in the form of applying it to estimate the basal level and incorporating a robust estimator. This indicates that other generalizations may also be possible.

A Sensitivity of estimation of a first-order system

We wish to analyze the estimation performance from the response of system (5) to a series of impulses. But, as the response of each impulse can be viewed as a separate least squares problem, the analysis is restricted to consider a single impulse with amplitude d at $t = 0$. By summing over all impulses, corresponding formulas for the general case are obtained.

A.1 Residual sum for impulse response

Consider first the noise-free impulse response. If the impulse time is known, the residual sum of squares is given by

$$f_0^\dagger(\omega) = \sum_{k=1}^{K} (\alpha_0(\omega)\,\mathrm{e}^{-\omega t_k} - d\,\mathrm{e}^{-bt_k})^2,$$

where the impulse weight $\alpha_0(\omega)$ which minimizes the squared error is given by

$$\alpha_0(\omega) = d\,\frac{\sum_{k=1}^{K} \mathrm{e}^{-(\omega+b)t_k}}{\sum_{k=1}^{K} \mathrm{e}^{-2\omega t_k}}.$$

If the measurements are corrupted by additive zero-mean i.i.d. noise with (finite) variance σ^2, i.e. $y(t_k) = x(t_k) + \epsilon_k$, the corresponding residual sum becomes

$$\begin{aligned} f^\dagger(\omega) = f_0^\dagger(\omega) &+ \sum_{k=1}^{K} (2\eta\alpha_0(\omega) + \eta^2)\,\mathrm{e}^{-2bt_k} \\ &+ \sum_{k=1}^{K} (2d\,\mathrm{e}^{bt_k}\,\epsilon_k + \epsilon_k^2 - 2(\alpha_0(\omega)\,\mathrm{e}^{-\omega t_k}\,\epsilon_k + \eta\,\mathrm{e}^{-\omega t_k}(d\,\mathrm{e}^{-\omega^* t_k} + \epsilon_k))), \end{aligned}$$

where

$$\alpha(\omega) = \alpha_0(\omega) + \eta(\omega), \quad \eta(\omega) = \frac{\sum_{k=1}^{K} \mathrm{e}^{-bt_k}\,\epsilon_k}{\sum_{k=1}^{K} \mathrm{e}^{-2bt_k}}.$$

The expected value of $f^\dagger(\omega)$ is given by

$$\mathbb{E} f^\dagger(\omega) = f_0^\dagger(\omega) + c_0,$$

where $c_0 = (K-1)\sigma^2$. In the following, we suppress the argument of α_0, α, η and their derivatives.

The estimation is based on approximating $f^\dagger(\omega)$ as a quadratic function. In the noise-free case, the derivatives are

$$\frac{\partial f_0^\dagger}{\partial \omega} = 2\sum_{k=1}^{K} (\alpha_0\,\mathrm{e}^{-\omega t_k} - d\,\mathrm{e}^{-bt_k}) \left(\frac{\partial \alpha_0}{\partial \omega} - t_k \alpha_0 \right) \mathrm{e}^{-bt_k},$$

$$\frac{\partial^2 f_0^\dagger}{\partial \omega^2} = 2\sum_{k=1}^{K} \left(\left(\frac{\partial \alpha_0}{\partial \omega} - t_k \alpha_0 \right)^2 \mathrm{e}^{-2bt_k} + (\alpha_0 \,\mathrm{e}^{-\omega t_k} - d\,\mathrm{e}^{-bt_k}) \left(\frac{\partial^2 \alpha_0}{\partial \omega^2} - 2t_k \frac{\partial \alpha_0}{\partial \omega} + t_k^2 \alpha_0 \right) \right) \mathrm{e}^{-bt_k}.$$

When evaluated at the minimum $\omega = b$, $\alpha_0 = d$, which leads to

$$\left.\frac{\partial f_0^\dagger}{\partial \omega}\right|_{\omega=b} = 0, \quad \left.\frac{\partial^2 f_0^\dagger}{\partial \omega^2}\right|_{\omega=b} = 2c_2,$$

where

$$c_2 = \sum_{k=1}^{K} \left(\left.\frac{\partial \alpha_0}{\partial \omega}\right|_{\omega=b} - t_k d \right)^2 \mathrm{e}^{-2bt_k},$$

so

$$f_0^\dagger(\omega) = c_2(\omega - b)^2 + O((\omega - b)^3).$$

By dominated convergence and boundedness of moments of the noise, expectations and derivatives can be interchanged, so

$$\mathbb{E} f^\dagger(\omega) = c_0 + c_2(\omega - b)^2 + O((\omega - b)^3).$$

In this construction, $c_2\sigma^{-2}$ can be identified as the Fisher information for the parameter b.

A.2 Multiple impulse estimates

The formula in (7), which approximates the transition between one and multiple impulses being estimated from a noisy impulse response, is derived here. Due to the challenging combinatorial nature of the problem, a number of approximations are made.

As an auxiliary step, note that the sum that defines c_2 also can be interpreted using a discrete random variable X, given by

$$P(X = t_k) = \frac{\mathrm{e}^{-2bt_k}}{\sum_{k=1}^{K} \mathrm{e}^{-2bt_k}}, \quad k = 1, \dots K.$$

The mean and variance of X then satisfy

$$d\ \mathbb{E}X = \left.\frac{\partial \alpha_0}{\partial \omega}\right|_{\omega=b},$$
$$d^2\ \mathrm{Var}X = \sum_{k=1}^{K} \left(\left.\frac{\partial \alpha_0}{\partial \omega}\right|_{\omega=b} - t_k d \right)^2 \mathrm{e}^{-2bt_k} \left(\sum_{k=1}^{K} \mathrm{e}^{-2bt_k} \right)^{-1} = c_2 \left(\sum_{k=1}^{K} \mathrm{e}^{-2bt_k} \right)^{-1}.$$

Now consider the transition between one (located at time t_1) and two (at t_1 and t_{m+1}) nonzero impulse estimates. The setup with two nonzero impulses can be viewed as two separate least squares estimation problems so the total residual sum of squares is the sum of the residuals from the two. That implies that c_0 decreases from $(K-1)\sigma^2$ to $(K-2)\sigma^2$ when transitioning from one to two impulses. Now consider the interpretation of c_2 as

$$c_2 = d^2 \sum_{k=1}^{K} \mathrm{e}^{-2bt_k} \ \mathrm{Var}X,$$

in the single impulse case. With two impulses, the corresponding parameter $c_{2,2}$ is given by

$$c_{2,2} = d^2 \sum_{k=1}^{m} \mathrm{e}^{-2bt_k} \ \mathrm{Var}X_1 + d^2 \sum_{k=m+1}^{K} \mathrm{e}^{-2bt_k} \ \mathrm{Var}X_2,$$

where X_1 and X_2 are defined analogously to X above. It is not hard to see that $c_{2,2} \leq c_2$, however the degree reduction depends on m. The extreme case $m = 2$ leads to $\mathrm{Var}X_1 = 0$ and $\mathrm{Var}X_2 \approx \mathrm{Var}X$, under the assumption that X is well-approximated by a geometric distribution. That leads to

$$\frac{c_{2,2}}{c_2} \approx \frac{\sum_{k=2}^{K} \mathrm{e}^{-2bt_k}}{\sum_{k=1}^{K} \mathrm{e}^{-2bt_k}} \leq \frac{K-1}{K}.$$

On the other hand, if $m = K$, the effect on either the sums or the variances is negligible, so in particular we have

$$\frac{c_{2,2}}{c_2} \geq \frac{K-2}{K-1}.$$

We can now conclude that $\min_\omega N_f(\omega)$, which is approximated by $\sqrt{c_0/c_2}$, may either increase or decrease when two impulses are estimated rather than one and that the effect will depend on the location of the second impulse. More general transitions of this kind are changes between different sets of nonzero impulse estimates, which can result in different local minima for N_f.

To estimate $\tilde{\omega}$, we consider only the case $m = 1$ and estimate the probability of d_2 being nonzero. Assume $t_1 = 0$, $\omega \leq b$ and that the estimated state of the system satisfies

$$\hat{x}(t_k) = \alpha_0 \, \mathrm{e}^{-bt_k} \tag{17}$$

for $k \geq 2$, i.e. $\alpha(b)$ is approximated by its expected value $\alpha_0(b)$, when only the indices $k = 2, 3, \ldots K$ are considered. This results in two cases depending on the first noise term ϵ_1:

- If $\epsilon_1 \geq \alpha_0(\omega) - d$, d_2 is estimated to be zero to minimize the residual error at t_1;
- If $\epsilon_1 < \alpha_0(\omega) - d$, d_1 can be chosen to give zero error at t_1, while a positive d_2 can be chosen to keep (17) satisfied.

We are therefore interested in the probability

$$P(\epsilon_k) \geq \alpha_0(\omega) - d,$$

i.e. the probability of one impulse being used rather than two, and for which b this probability is significantly larger than zero. Assuming Gaussian noise, the probability distribution is linearized around $\epsilon_k = 0$, i.e. $\omega = b$, and the value $\bar{\omega}$ where zero is crossed is derived. That gives

$$b - \bar{\omega} = \frac{\sigma}{\partial\alpha_0/\partial\omega}\sqrt{\pi/2}$$

Now assume equidistant sampling, so $t_{k+1} - t_k = T$, and approximate X as a geometric distribution, scaled to take values $kT, k = 0, 1, \ldots$. The expected value and variance of X then satisfy the relation

$$\mathrm{Var}X \approx (\mathbb{E}X)^2\, \mathrm{e}^{2bT},$$

which implies

$$\frac{\partial\alpha_0}{\partial\omega} \approx \mathrm{e}^{-bT}\sqrt{c_2(1 - \mathrm{e}^{-2bT})},$$

which in turn leads to (7).

A.3 Deviations from quadratic approximation

We consider the residual sum f_{c_3} on the form (9) and investigate the sensitivity with respect to c_3 of the estimation method. The analysis is done through linearization and includes the terms $\bar{\omega}$ and $N_{f_{c_3}}(\bar{\omega})$. The first is characterized by the derivative being zero, which implies

$$\left(\frac{\partial f}{\partial\omega}\Big|_{\omega=\bar{\omega}}\right)^2 = \left(f(\omega)\frac{\partial^2 f}{\partial\omega^2}\right)\Big|_{\omega=\bar{\omega}},$$

which yields

$$2c_0c_2 + 6c_0c_3z - 2c_2^2z^2 - 4c_2c_3z^3 - 3c_3^2z^4 = 0,$$

where $z = \bar{\omega} - b$. Differentiating with respect to c_3 and solving for the derivative results in the sensitivity

$$\frac{\partial z}{\partial c_3}\Big|_{c_3=0} = \frac{c_0}{2c_2^2}.$$

The sensitivity of the second term is calculated similarly and yields

$$\frac{dN_{f_{c_3}}(\bar{\omega})}{dc_3}\Big|_{c_3=0} = \frac{c_0}{c_2^2},$$

which leads to error term (10).

B Synthetic data generation

Let $\mathcal{U}_{[a,b]}$ denote the uniform distribution in the interval $[a, b]$. In all experiments, the data set is generated as the uniformly sampled (period 0.5) response to 4 impulses. The time separation between the impulses, and the time from the last impulse to the end of the time horizon, have distribution $\mathcal{U}_{[2,5]}$. To obtain nonzero initial conditions, the impulse train is shifted so that time zero is situated at the midpoint between the first two impulses, and only the last 3 impulses are included in the time series. The remaining parameters have distributions according to Table 5.

Table 5: Distributions for impulse weights d_k and elimination rates b, b_1, b_2 and standard deviations σ of Gaussian additive noise. σ_o is standard deviation of uniform noise representing outlying data points. Experiments are numbered according to the section they appear in.

Experiment	d_k	b_2 or b	$b_1 - b_2$	σ	σ_o
4.1.1	$\mathcal{U}_{[0.1,1]}$	$\mathcal{U}_{[0.4,1.4]}$		0.01	
4.1.2	$\mathcal{U}_{[0.4,4]}$	$\mathcal{U}_{[0.4,1.4]}$	$\mathcal{U}_{[0.3,1.3]}$	See Table 1	
4.1.3	$\mathcal{U}_{[2,7]}$	$\mathcal{U}_{[0.4,1]}$	$\mathcal{U}_{[4,5]}$	0.008	
4.1.4	$\mathcal{U}_{[0.4,4]}$	$\mathcal{U}_{[0.4,1.4]}$	$\mathcal{U}_{[0.3,1.3]}$	0.006	0.289

References

[1] A. Churilov, A. Medvedev, and A. Shepeljavyi. Mathematical model of non-basal testosterone regulation in the male by pulse modulated feedback. *Automatica*, 45(1):78 – 85, 2009.

[2] P. F. Corradi, R. B. Corradi, and L. W. Greene. Physiology of the hypothalamic pituitary gonadal axis in the male. *Urologic Clinics*, 43(2):151–162, 2016.

[3] G. De Nicolao and D. Liberati. Linear and nonlinear techniques for the deconvolution of hormone time-series. *IEEE Transactions on Biomedical Engineering*, 40(5):440–455, 1993.

[4] A. Farcomeni and L. Ventura. An overview of robust methods in medical research. *Statistical Methods in Medical Research*, 21(2):111–133, 2012.

[5] M. L. Johnson, L. Pipes, P. P. Veldhuis, L. S. Farhy, R. Nass, M. O. Thorner, and W. S. Evans. AutoDecon: A robust numerical method for the quantification of pulsatile events. *Methods in enzymology*, 454:367–404, 2009.

[6] T. D. Johnson. Bayesian deconvolution analysis of pulsatile hormone concentration profiles. *Biometrics*, 59(3):650–660, Sept. 2003. Publisher: John Wiley & Sons, Ltd.

[7] D. M. Keenan and J. D. Veldhuis. A biomathematical model of time-delayed feedback in the human male hypothalamic-pituitary-Leydig cell axis. *American Journal of Physiology-Endocrinology and Metabolism*, 275(1):E157–E176, July 1998. Publisher: American Physiological Society.

[8] Y. Li and X. Liu. An impulsive model for wolbachia infection control of mosquito-borne diseases with general birth and death rate functions. *Nonlinear Analysis: Real World Applications*, 37:412–432, 2017.

[9] J. Z. Liu, R. W. Brown, and G. H. Yue. A dynamical model of muscle activation, fatigue, and recovery. *Biophysical journal*, 82(5):2344–2359, 2002.

[10] P. Y. Liu, P. Y. Takahashi, P. D. Roebuck, A. Iranmanesh, and J. D. Veldhuis. Age-specific changes in the regulation of LH-dependent testosterone secretion: assessing responsiveness to varying endogenous gonadotropin output in normal men. *American Journal of Physiology-Regulatory, Integrative and Comparative Physiology*, 289(3):R721–R728, Sept. 2005. Publisher: American Physiological Society.

[11] P. Mattsson and A. Medvedev. Modeling of testosterone regulation by pulse-modulated feedback: An experimental data study. *AIP Conference Proceedings*, 1559(1):333–342, September 2013.

[12] A. Medvedev, A. Churilov, and A. Shepeljavyi. Mathematical models of testosterone regulation. In *Stochastic optimization in informatics*, number 2, pages 147–158. Saint Petersburg State University, 2006. in Russian.

[13] M. Osama, D. Zachariah, and P. Stoica. Robust risk minimization for statistical learning from corrupted data. *IEEE Open Journal of Signal Processing*, 1:287–294, 2020.

[14] I. P. Pappas, M. R. Popovic, T. Keller, V. Dietz, and M. Morari. A reliable gait phase detection system. *IEEE Transactions on neural systems and rehabilitation engineering*, 9(2):113–125, 2001.

[15] H. Runvik and A. Medvedev. Impulsive time series modeling with application to luteinizing hormone data. *Frontiers in Endocrinology*, 13, 2022.

[16] H. Runvik and A. Medvedev. Input sequence and parameter estimation in impulsive biomedical models. In *2022 European Control Conference (ECC)*, pages 253–258. IEEE, 2022.

[17] G. Sparacino, G. Pillonetto, M. Capello, G. De Nicolao, and C. Cobelli. WINSTODEC: A stochastic deconvolution interactive program for physiological and pharmacokinetic systems. *Computer methods and programs in biomedicine*, 67(1):67–77, 2002.

[18] P. Stoica and Y. Selen. Model-order selection: A review of information criterion rules. *IEEE Signal Processing Magazine*, 21(4):36–47, 2004.

[19] E. van der Spoel, J. Choi, F. Roelfsema, S. l. Cessie, D. van Heemst, and O. M. Dekkers. Comparing methods for measurement error detection in serial 24-h hormonal data. *Journal of biological rhythms*, 34(4):347–363, 2019.

[20] A. W. van der Vaart. *Asymptotic statistics*. Cambridge series on statistical and probabilistic mathematics ; 3. Cambridge University Press, Cambridge, 1998.

Recent licentiate theses from the Department of Information Technology

2022-002 Gustaf Borgström: *Making Sampled Simulations Faster by Minimizing Warming Time*

2022-001 Sam Hylamia: *Secure In-body Communication and Sensing*

2021-002 Karl Bengtsson Bernander: *Improving Training of Deep Learning for Biomedical Image Analysis and Computational Physics*

2021-001 Niklas Gunnarsson: *On the Registration and Modeling of Sequential Medical Images*

2020-006 David Widmann: *Calibration of Probabilistic Predictive Models*

2020-005 Anna Wigren: *Exploiting Conjugacy in State-Space Models with Sequential Monte Carlo*

2020-004 Muhammad Osama: *Machine Learning for Spatially Varying Data*

2020-003 Christos Sakalis: *Securing the Memory Hierarchy from Speculative Side-Channel Attacks*

2020-002 Ulrika Sundin: *Global Radial Basis Function Collocation Methods for PDEs*

2019-007 Carl Andersson: *Deep Learning Applied to System Identification: A Probabilistic Approach*

2019-006 Kristiina Ausmees: *Efficient Computational Methods for Applications in Genomics*

2019-005 Carl Jidling: *Tailoring Gaussian Processes for Tomographic Reconstruction*

UPPSALA
UNIVERSITET

Department of Information Technology, Uppsala University, Sweden